UDK 621.3:(53+54+621+66)(05)(497.1)=00 ISSN 0352-9045

INFORMACIJE MIDEM 3 ◦ 1996

Strokovno društvo za mikroelektroniko elektronske sestavne dele in materiale

Časopis za mikroelektroniko, elektronske sestavne dele in materiale
Časopis za mikroelektroniku, elektronske sastavne dijelove i materijale
Journal of Microelectronics, Electronic Components and Materials

INFORMACIJE MIDEM, LETNIK 26, ŠT. 3(79), LJUBLJANA, september 1996

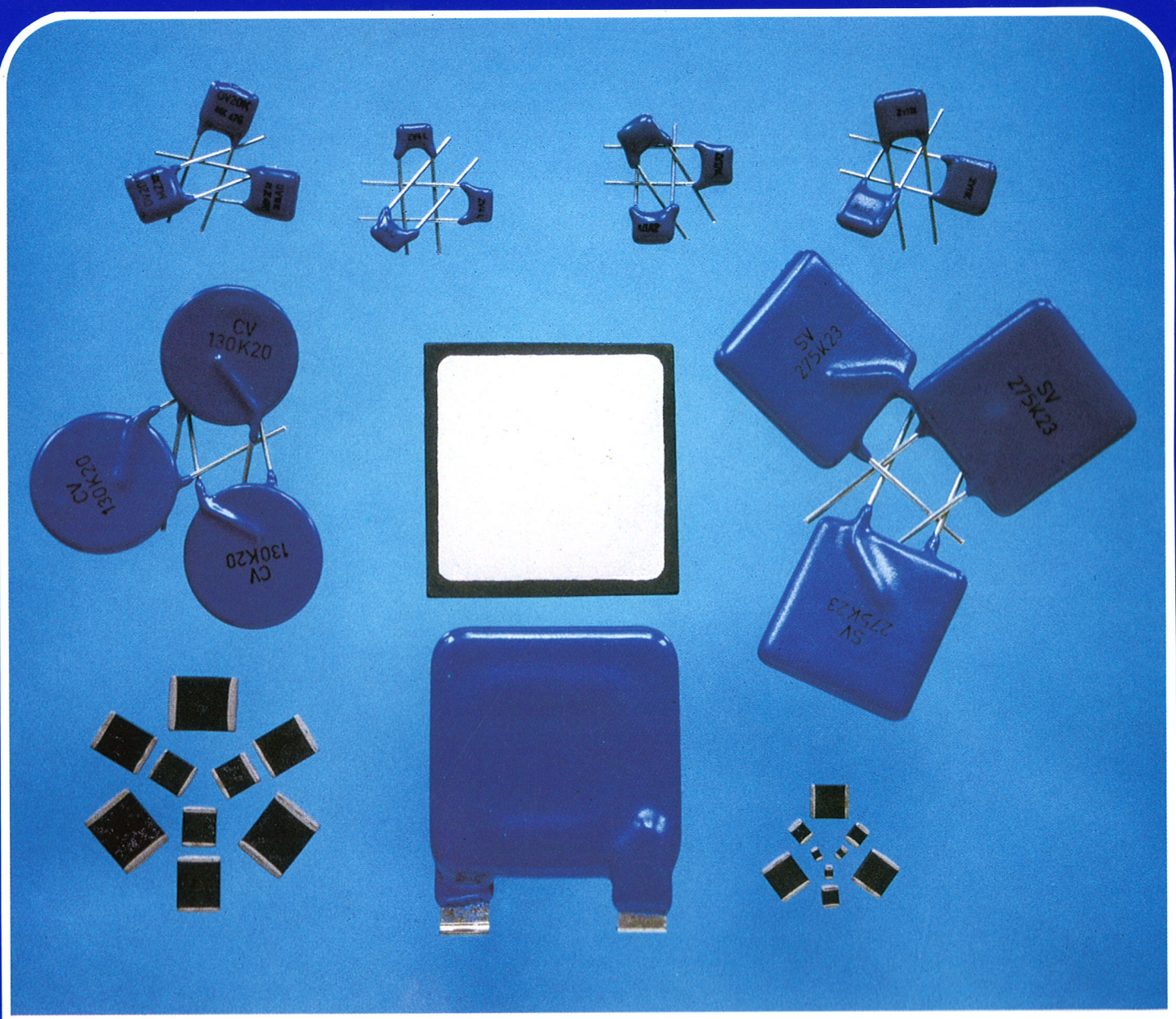

INFORMACIJE MIDEM 3 ° 1996

INFORMACIJE MIDEM	LETNIK 26, ŠT. 3(79), LJUBLJANA,	SEPTEMBER 1996
INFORMACIJE MIDEM	GODINA 26, BR. 3(79), LJUBLJANA,	SEPTEMBAR 1996
INFORMACIJE MIDEM	VOLUME 26, NO. 3(79), LJUBLJANA,	SEPTEMBRE 1996

Izdaja trimesečno (marec, junij, september, december) Strokovno društvo za mikroelektroniko, elektronske sestavne dele in materiale.
Izdaja tromjesečno (mart, jun, septembar, decembar) Stručno društvo za mikroelektroniku, elektronske sastavne dijelove i materiale.
Published quarterly (march, june, september, december) by Society for Microelectronics, Electronic Components and Materials - MIDEM.

Naslov uredništva
Adresa redakcije
Headquarters
Uredništvo Informacije MIDEM
Elektrotehniška zveza Slovenije
Dunajska 10, 1000 Ljubljana, Slovenija
(0)61 - 316 886

Letna naročnina znaša 12.000,00 SIT, cena posamezne številke je 3000,00 SIT. Člani in sponzorji MIDEM prejemajo Informacije MIDEM brezplačno.
Godišnja pretplata iznosi 12.000,00 SIT, cijena pojedinog broja je 3000,00 SIT. Članovi i sponzori MIDEM primaju Informacije MIDEM besplatno.
Annual subscription rate is DEM 200, separate issue is DEM 50. MIDEM members and Society sponsors receive Informacije MIDEM for free.

Znanstveni svet za tehnične vede I je podal pozitivno mnenje o časopisu kot znanstveno strokovni reviji za mikroelektroniko, elektronske sestavne dele in materiale. Izdajo revije sofinanci rajo Ministrstvo za znanost in tehnologijo in sponzorji društva.
Scientific Council for Technical Sciences of Slovene Ministry of Science and Technology has recognized Informacije MIDEM as scientific Journal for microelectronics, electronic components and materials.
Publishing of the Journal is financed by Slovene Ministry of Science and Technology and by Society sponsors.

Znanstveno strokovne prispevke objavljene v Informacijah MIDEM zajemamo v:
* domačo bazo podatkov ISKRA SAIDC-el, kakor tudi
* v tujo bazo podatkov INSPEC

Prispevke iz revije zajema ISI® v naslednje svoje produkte: Sci Search®, Research Alert® in Materials Science Citation Index™

Scientific and professional papers published in Informacije MIDEM are assessed into:
* domestic data base ISKRA SAIDC-el and
* foreign data base INSPEC

The Journal is indexed by ISI® for Sci Search®, Research Alert® and Material Science Citation Index™

Po mnenju Ministrstva za informiranje št.23/300-92 šteje glasilo Informacije MIDEM med proizvode informativnega značaja, za katere se plačuje davek od prometa proizvodov po stopnji 5 %.

Grafična priprava in tisk
Grafička priprema i štampa
Printed by
BIRO M, Ljubljana

Naklada
Tiraž
Circulation
1000 izvodov
1000 primjeraka
1000 issues

UDK621.3:(53+54+621+66), ISSN0352-9045 Informacije MIDEM 26(1996)3, Ljubljana

DRUŠTVO MIDEM IN KONFERENCA MIEL-SD NA INTERNETU

Dragi člani društva in bralci revije!

Predstavitev društva MIDEM in poročilo o minuli, oz. predstavitev naslednje konference MIEL-SD lahko poiščete na INTERNETU in sicer:

1. Predstavitev društva MIDEM in revije "Informacije MIDEM" na naslovu **http://pollux.fer.uni-lj.si/MIEL/MIDEM.htm**
2. Predstavitev konference MIEL-SD'96 na naslovu **http://pollux.fer.uni-lj.si/MIEL/miel96.htm**
3. Elektronsko pošto lahko pošiljate na naslov: **Iztok.Sorli@guest.arnes.si**

Pri vpisu pazite na velike in male črke!!

Vse člane vljudno prosimo, da poravnajo članarino za leto 1996.

MIDEM SOCIETY AND MIEL-SD CONFERENCE ON INTERNET

Dear readers and Society members!

Presentation of MIDEM Society and report on passed, as well info on next MIEL-SD Conference can be found on INTERNET as follows:

1. Presentation of MIDEM Society and Journal "Informacije MIDEM", address **http://pollux.fer.uni-lj.si/MIEL/MIDEM.htm**
2. Presentation of the Conference MIEL-SD'96, address **http://pollux.fer.uni-lj.si/MIEL/miel96.htm**
3. Email can be sent to: **Iztok.Sorli@guest.arnes.si**

Please, use exact lower and upper case letters as indicated.

We kindly ask all our members to pay the membership fee for 1996.

SIMPLE SIMULATION OF a-Si:H SOLAR CELLS AND THE COMPARISON WITH SPECTRAL RESPONSE

W. Kusian
Siemens AG, Corporate Research and Development, München, Germany

Keywords: semiconductors, photovoltaic applications, solar cells, description of operation, a-Si, amorphous silicon, a-Si:H, hydrogenated amorphous silicon, physical understanding, elementary models, solar cell models, solar cell simulations, PIN structures, positive-intrinsic-negative structures, PECVD, plasma enhanced chemical vapour deposition, SiH_4 silane, efficiency measurement, efficiency calculation, experimental results

Abstract: Solar cells and modules made from hydrogenated amorphous silicon (a-Si:H) have been developed for more than fifteen years. A physical understanding in simple terms of a-Si:H solar cells is made possible with the *elementary model* that uses the uniform-field approximation and neglects bulk recombination. This will be demonstrated by a qualitative discussion of dark and especially of spectral-response characteristics. Simple notions as surface recombination and flat-band voltage will be elucidated with respect to cell degradation under prolonged illumination.

Enostavna simulacija a-Si:H sončne celice in primerjava s spektralno občutljivostjo

Ključne besede: polprevodniki, aplikacije fotonapetostne, celice sončne, opis delovanja, a-Si silicij amorfni, a-Si:H silicij amorfni hidrogeniziran, razumevanje fizikalno, modeli osnovni, modeli celic sončnih, simulacije celic sončnih, PIN strukture pozitivno-notranje-negativno, PECVD nanašanje kemično s paro, izboljšano s plazmo, SiH_4 silan, merjenje izkoristka, izračun izkoristka, rezultati eksperimentalni

Povzetek: Sončne celice in moduli iz hidrogeniranega amorfnega silicija (a-Si:H) so prisotni že več kot petnajst let. Vpogled v enostavno fizikalno dogajanje znotraj a-Si:H sončnih celic nam omogočajo analitični modeli. Razviti *elementarni model* uporablja pribli'ek konstantnega električnega polja in zanemarja rekombinacije v substratu. Povedano bomo prikazali ob kvalitativni diskusiji o temni tokovnonapetostni karakteristiki in tudi karakteristiki spektralne občutljivosti. Obrazlo'ili bomo enostavna pojma, kot sta površinska rekombinacija in napetost ravnih nivojev glede na degradacijo celice pod dolgotrajno osvetlitvijo.

Introduction

Hydrogenated amorphous silicon (a-Si:H) films having electronic properties suitable for photovoltaic applications are mostly deposited by decomposition of silane (SiH_4) in a plasma enhanced chemical vapour deposition (PECVD) process. This procedure was already invented in 1969 by Chittick, Alexander and Sterling /1/, and several authors demonstrated that this material can have good electronic properties /2,3,4/. In 1975 Spear and LeComber demonstrated the doping possibility of a-Si:H that opened the way for device fabrication /5/.

Solar cells made from a-Si:H have the structure pin. For the conversion of light power into electrical power the light enters the solar cell normally through the p-layer. The photons will be absorbed within the i-layer and generate charge carriers which will then be separated by the electric field across the absorption region. Although the device quality improved very rapidly it was difficult to understand the underlying technology processes in detail and the physics of these devices. The latter can be put forward by simple or otherwise by more comprehensive solar-cell models and simulations. It is preferred here to try it with a simple analytical model first. The formulation and exemplary application of the *elementary model* will be given.

Solar Cell Operation

The understanding of a-Si:H solar cells is based on the material properties (mobilities of electrons and holes, density of localized states through the mobility gap, capture cross sections of these states) and the physics of the pin diode (drift and diffusion of mobile carriers, space charges given by the occupation of the localized states, recombination via these states). The working conditions of the solar cell are set by carrier generation under light and the external voltage. The exact simulation of the dark and light characteristics requires the numerical solution of the classical semiconductor equations (Poisson's equation, continuity equations of electrons and holes) in one dimension /6,7/.

An *exact* simulation embraces the more or less complete knowledge about the semiconductor and the pin structure. Simplifications enable *approximate* simulations or even analytical models. Simple concepts indeed helped to explain typical experiments already before the advent of exact simulations. The uniform-field concept especially has become quite useful. It assumes a spatially constant electric field right through the i-layer of a pin cell /8/. Furthermore, the i-layer alone is thought to collect photogenerated carriers, while the carriers generated within the p- and n-contact layers are immediately lost by recombination (*dead* layers). The uniform-field assumption substitutes for Poisson's equation. Thus only two of the three semiconductor equations remain active by definition, the continuity equations of electrons and holes.

The real field distribution through a pin structure becomes indeed uniform amidst the i-layer /9/. Field spikes develop towards the p-i and i-n interfaces indi-

cating partial p-i and i-n junctions. The corresponding space-charge layers near the boundaries of the i-layer depend on the high density of localized *tail states* near the valence- and conduction-band edges. The uniform-field concept now disregards the extension of the field spikes. Rather, the spikes are considered as delta functions. The associated space-charge double layers lead to potential steps through the p-i and i-n interfaces.

The uniform-field approximation considers mobile electrons and holes in the i-layer, but no trapped carriers at all. The electrons and holes remain coupled by a non-linear bulk-recombination law, after Shockley-Read-Hall for example. The electron and hole equations therefore have yet to be solved numerically. Further approximations can help to avoid that. It is most simple to neglect bulk recombination at all. The question is only whether the resulting *elementary model* /10/ has any value. Therefore the model is checked against experiments.

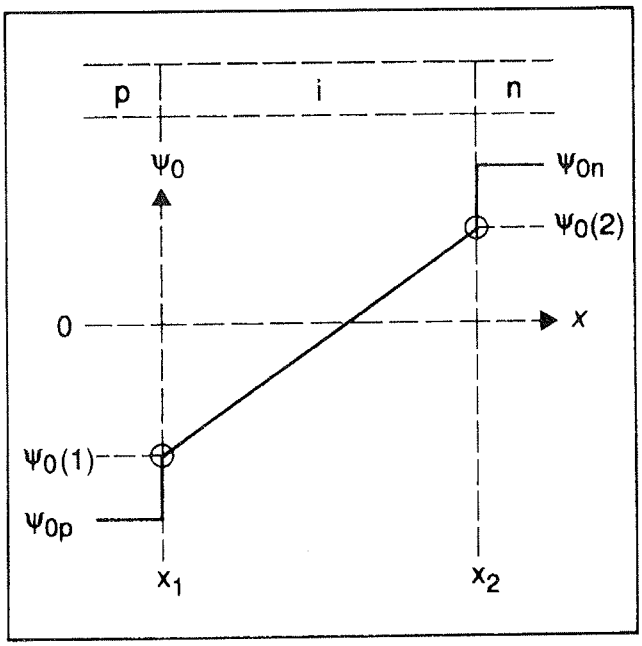

Fig. 1 *Schematic potential distribution due to the uniform-field assumption across the i-layer of an a-Si:H pin solar cell.*

The neglection of bulk recombination decouples the continuity equations of electrons and holes. The recombination then is restricted to the boundaries of the i-layer with the p- and n-layers, the p-i and i-n junctions, simply called *surfaces*. Collection of photoelectrons (photoholes) from the i-layer by the i-n (p-i) junction maintains primary photocurrents, and recombination of electrons (holes) from the i-layer with holes (electrons) from the p-(n-) layer at the p-i (i-n) junction maintains forward currents, especially secondary photocurrents. *Surface collection* and *surface recombination* are quite general notions. The elementary model (uniform-field without bulk recombination) only puts them into the foreground. So these notions alone were already helpful to interpret experimental trends /11,12/.

Elementary model

Now a formal outline of our model is presented /10,13/. The potential through a cell's pin structure according to the uniform-field assumption is sketched in Fig. 1. The electron and hole concentrations in the p- and n-layers are given by

$$n_n = n_i \exp\left(\frac{\psi_{0n}}{V_0}\right), \quad p_p = n_i \exp\left(\frac{\psi_{0p}}{V_0}\right) \tag{1}$$

with intrinsic concentration n_i, temperature voltage V_0, and "doping potentials" ψ_{0n} and ψ_{0p}. The x coordinate runs through the i-layer. The boundaries are at x_1 and x_2. The thermal equilibrium potential $\psi_0(x)$ has boundary values $\psi_0(x1)=\psi_0(1)$ and $\psi_0(x2)=\psi_0(2)$. The built-in and flat-band voltages are

$$U_B = \psi_{0n} - \psi_{0p}, \quad U_F = \psi_0(2) - \psi_0(1) \tag{2}$$

The uniform field in the i-layer without and with external voltage U is

$$E_0 = -\frac{\psi_0(2)-\psi_0(1)}{x_2-x_1} \equiv k_0 V_0, \quad E = \frac{U-U_F}{x_2-x_1} \equiv kV_0 \tag{3}$$

The field constants k_0 and k are reciprocal lengths. The potentials without and with U become

$$\psi_0(x) = \psi_0(1) - (x-x_1)E_0, \quad \psi(x) = \psi(1) - (x-x_1)E \tag{4}$$

The flat-band condition is imposed by $U=U_F$ and means $E=k=0$. The electron and hole concentrations in thermal equilibrium are

$$n_0(x) = n_i \exp\left(\frac{\psi_0(x)}{V_0}\right) = n_0(1)\exp\left[-k_0(x-x_1)\right] \tag{5}$$

$$p_0(x) = n_i \exp\left(-\frac{\psi_0(x)}{V_0}\right) = p_0(1)\exp\left[k_0(x-x_1)\right]$$

and depend on the parameters $\psi_0(1)$ and $\psi_0(2)$. The differences ψ_{0n} - $\psi_0(2)$ and $\psi_0(1)$ - ψ_{0p} are consistent with δ-like field spikes. The nonequlibrium electron and hole concentrations n and p are to be determined from the continuity equations in connection with boundary conditions. The electron and hole current densities are

$$j_n = e(D_n n' + \mu_n E n) = eD_n(n' + kn) \tag{6}$$

$$j_p = e(-D_p p' + \mu_p E p) = eD_p(-p' + kp)$$

with diffusion constants D_n and D_p, mobilities μ_n and μ_p, and $n' = dn/dx$, $p' = dp/dx$. The relations (5) let the currents (6) vanish in thermal equilibrium. The continuity equations become

$$\begin{aligned} j_n' / e &= D_n(n'' + kn') = -(g - r) \\ -j_p' / e &= D_p(p'' - kp') = -(g - r) \end{aligned} \tag{7}$$

The photocarrier generation rate $g(x)$ has to be inferred from optical modelling. The recombination rate $r(x)$ couples the relations (7) in a nonlinear fashion. These relations imply the uniformity of the total current

$$j = j_n + j_p = constant \tag{8}$$

and represent the general uniform-field equations. The elementary model puts

$$r=0 \tag{9}$$

Our boundary conditions express surface collection and recombination of excess electrons and holes, and furthermore photocarrier replenishment. The conditions are

$$\begin{aligned} j_n(1) / e &= s_n\big(n(1) - n_0(1)\big) \\ \big(j_n(2) - \beta_n j_n(1)\big) / e &= -c_n\big(n(2) - n_0(2)\big) \\ \big(j_p(1) - \beta_p j_p(2)\big) / e &= -c_p\big(p(1) - p_0(1)\big) \\ j_p(2) / e &= s_p\big(p(2) - p_0(2)\big) \end{aligned} \tag{10}$$

with boundary values $j_n(1)=j_n(x_1)$ and $j_n(2)=j_n(x_2)$, for example, to the left and right, recombination velocities s_n, s_p and collection velocities c_n, c_p. These velocities represent the two faces of a *transport velocity* /14/. The replenishment factors β_n and β_p are confined to the interval between 0 and 1. The value $\beta_n = 1$ ($\beta_n = 0$) in particular means perfect (absent) replenishment of electrons. The recombination current of electrons from the i-layer into the p-layer will be reinjected through the n-layer by virtue of the factor $\beta_n = 1$ and spares this current from being collected. A factor $\beta_n < 1$ enforces partial replenishment only. This imagined mechanism, controlled likewise via β_p for the holes, operates through the conditions (10). Replenishment hardly affects (may amplify) primary (secondary) photocurrents. The boundary value problem (7) with (9) and (10) holds for electrons and holes separately. With a function $y(x)$, representing $n(x)$ or $p(x)$, the equations (7) have the common form

$$y'' + Py' = R \tag{11}$$

with

$$P = k,\ R(x) = -g(x)/Dn$$

for the electrons and

$$P = -k,\ R(x) = -g(x)/Dp$$

for the holes. The general solution can be put together as

$$y(x) = C_1 f(x) + C_2 + \frac{1}{P}\left(\int_{x_1}^{x} R(\xi)\partial\xi - f(x) \int_{x_1}^{x} f^{-1}(\xi) R(\xi)\partial\xi \right) \tag{12}$$

with growth function $f(x)=exp(-P(x-x_1))$. The coordinate $x=x_1$ represents the left i-layer boundary, i.e. the p-i interface. The boundary conditions (10) determine the integration constants C_1 and C_2. For the flat-band case $P = 0$ the growth function becomes $f(x) = x-x_1$ and we can write

$$y(x) = C_1 f(x) + C_2 + x \int_{x_1}^{x} R(\xi)\partial\xi - \int_{x_1}^{x} \xi R(\xi)\partial\xi \tag{13}$$

The functions (12) and (13) solve the linear boundary value problem (10) and (11). The carrier concentrations in the dark and the dark characteristics stem from the inhomogeneities of the boundary conditions (10), while the right side R of the continuity equation (11) puts forth photocarriers and photocharacteristics. This remark concludes the presentation of the elementary formalism.

Dark characteristics

The comparison of the elementary model with experiments begins with the dark charcteristics. The model yields separately uniform dark currents of electrons and holes. The explicit form of the electron dark-current density is

$$j_{nD} = \frac{e n_0(1)\big(exp(U / V_0) - 1\big)}{\frac{1}{s_n} + \frac{1-\beta_n}{c_n} exp(kd) + \frac{exp(kd)-2}{D_n k}} \tag{14}$$

with $d=x_2 - x_1$ and $kd = (U-U_F)/V_0$. The flat-band case $U=U_F$ and $k=0$ yields

$$\begin{aligned} j_{nD} &= e \frac{n_0(2) - n_0(1)}{\frac{1}{s_n} + \frac{1-\beta_n}{c_n} + \frac{d}{D_n}}, \\ \frac{n_0(2)}{n_0(1)} &= \frac{p_0(1)}{p_0(2)} = exp(U_F / V_0) \end{aligned} \tag{15}$$

Similar expressions represent the hole current density, and the total dark current density becomes

$$j_D = j_{nD} + j_{pD} \tag{16}$$

as a special case of (8). Under reverse voltage $U < 0$ the current approaches the saturation value

$$j_D = -e(n_0(1)s_n + p_0(2)s_p) \quad (17)$$

or tends to the ohmic characteristic

$$j_D = \sigma_{min} E\,, \quad \sigma_{min} = e\left(\mu_n n_0(1) + \mu_p p_0(2)\right) \quad (18)$$

in case of $s_n = s_p = \infty$. Under forward voltage $U - U_F > 0$, on the other hand, and in case $c_n = c_p = \infty$ or $\beta_n = \beta_p = 1$, the dark current tends to

$$j_D = \sigma_{max} E\,, \quad \sigma_{max} = e\left(\mu_n n_0(2) + \mu_p p_0(1)\right) \quad (19)$$

It is to be understood that field $E < 0$ in (18) and $E > 0$ in (19). The current (the field) vanishes at $U = 0$ $(U = U_F)$. Current and field have opposite directions through the interval $0 < U < U_F$. Decreasing drift against diffusion lets the diode current exponentially rise through this interval. The associated quality factor is $n_Q = 1$. The field $E = 0$ at $U = U_F$ leaves a diffusion current. With $U > U_F$ the current is resistive and the characteristic bends over towards (19). Low values of the surface recombination velocities s_n and s_p retard the transition from the diode regime to the ohmic regime of the characteristic. In any case, the flat-band voltage

$$U_F = V_0 \log(\sigma_{max} / \sigma_{min}) \quad (20)$$

limits the diode regime. Fig. 2 illustrates this formal discussion. It shows forward and reverse branches of j_D after (16) assuming a *symmetric* cell (equal properties of electrons and holes, e.g. $\mu_n = \mu_p = \mu$) with the parameters of Table 1 (column A). As a check we compared with measured characteristics (see Fig. 4). The comparison indicates the following peculiarities of the elementary model: The reverse current and the factor $n_Q = 1$ are both too low (missing bulk recombination), and the characteristic becomes ohmic for $U > U_F$ (no double injection).

Table 1: Standard parameters for elementary model. Flat-band voltage U_F, potentials $\psi_0(1)$ and $\psi_0(2)$ at both sides of the i-layer in thermal equilibrium, i-layer thickness d, intrinsic carrier concentration n_i. Symmetric cells A and B with mobilities $\mu_n = \mu_p$, recombination velocities $s_n = s_p$, collection velocities $c_n = c_p$, replenishment factors $\beta_n = \beta_p$. These parameters are always used if not stated otherwise.

		A	B
U_F	[V]	0.7	0.5
$\psi_0(1)$	[V]	-0.35	-0.25
$\psi_0(2)$	[V]	0.35	0.25
d	[μm]	0.5	0.5
n_i	[1/cm^3]	10^5	10^5
μ_n, μ_p	[cm^2/Vs]	10	10
s_n, s_p	[cm/s]	10^4	10^5
c_n, c_p	[cm/s]	10^7	10^7
β_n, β_p		1	1

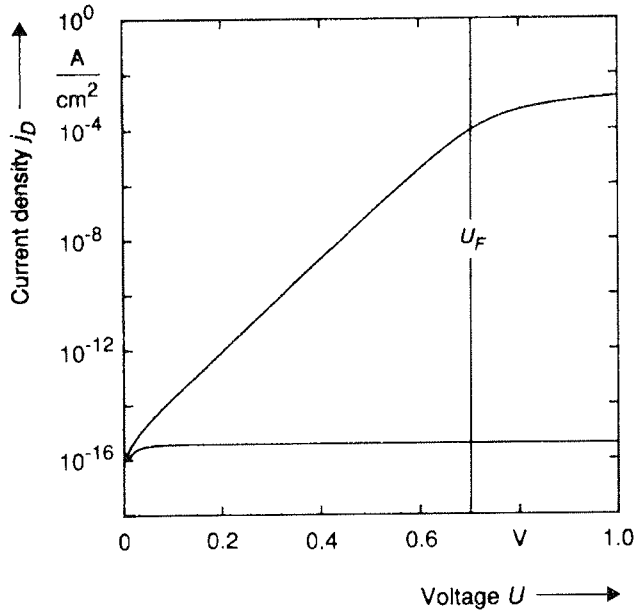

Fig. 2: Calculated dark current j_D versus voltage U, forward and reverse branches, calculated with the elementary model, parameters of table 1(column A).

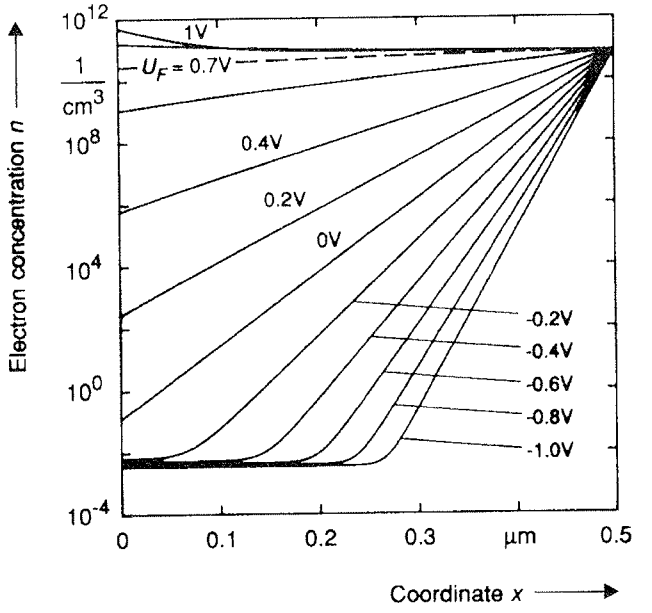

Fig. 3: Electron concentration n(x) in the dark calculated with the elementary model, parameters of table 1(column A).

The concentrations $n(x)$ of electrons and $p(x)$ of holes directly define the internal state of a pin cell. Fig. 3 shows the electron concentration associated to Fig. 2. The electrons are majority carriers in the n-layer to the right and minority carriers in the p-layer to the left. In thermal equilibrium for $U = 0$ the concentration $n(x) = n_0(x)$ follows (5). The elementary model confines itself to the I- layer. The function $n(x)$ becomes flat for $U > U_F$ and approaches the limit $n_0(x2)$ at the right side. According to Fig. 3 the electrons pile up at the left side for $U = 1$V. This behavior stems from *reverse drift* against a slowly recombining surface. Under reverse voltage $U < 0$ the electrons are pulled to the right and leave behind them a minimum concentration. The hole concentrations behave similarly as the electron concentrations.

A critical property of a-Si:H cells is *light degradation:* The efficiency comes down in the course of prolonged illumination. An anneal treatment can restore the degradation. The undegraded and degraded states are termed "A" and "B". The degradation process or the A→B transition changes the efficiency and other cell properties, including the dark currents. Fig. 4 shows as an example the measured dark characteristics of a pin cell in states A and B. Degradation increases the reverse current and the quality factor n_Q. The forward branches hence cross. The degradation process enhances bulk and surface recombination. The elementary model only offers an increase of s_n and s_p. Fig. 5 shows two modelled characteristics, one for a state A, and the other for state B. A crossing is only obtainable by a reduction of the flat-band voltage U_F for state B because $n_Q = 1$ is invariant. The observed values $n_Q > 1$ refer to bulk recombination, and the enhancement of n_Q during the degradation indicates enhancement of bulk recombination. The reduction of U_F can *simulate* enhanced bulk recombination to a certain degree. The far too low reverse currents of the modelled cell are again due to the total neglect of bulk recombination.

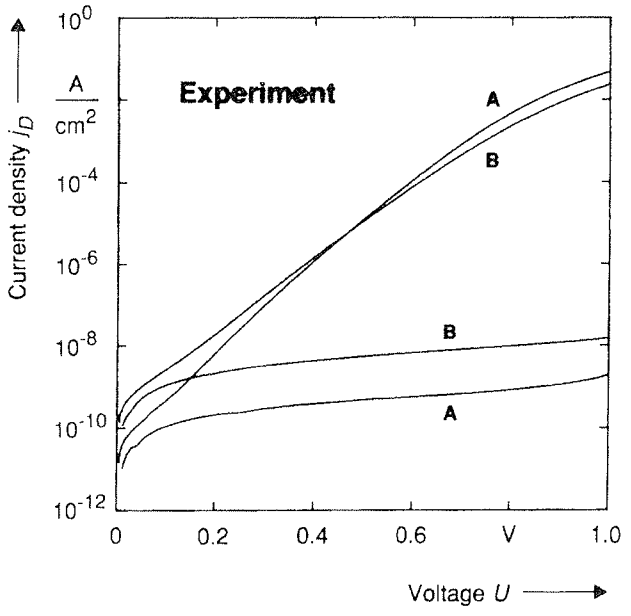

Fig. 4: Measured dark characteristics $j_D(U)$ in the undegraded state A and degraded state B.

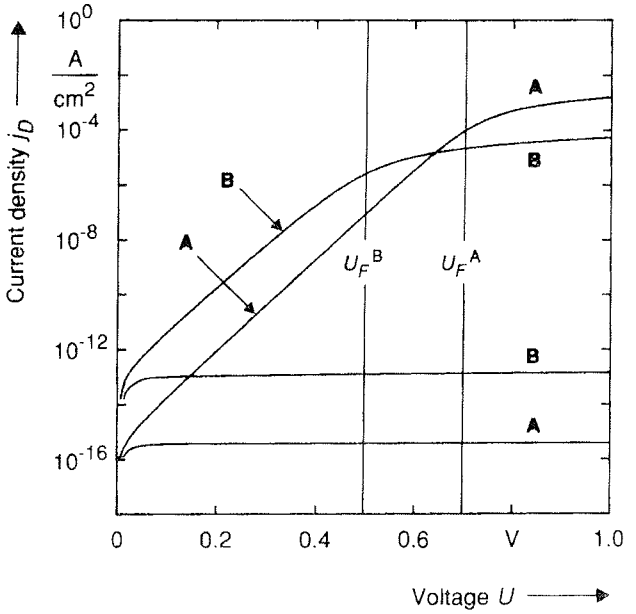

Fig. 5: Calculated characteristics $j_D(U)$ in states A and B (parameters from table 1, column A and B).

Spectral characteristics

The characteristics of a pin cell under light and in the dark are designated as $j(U)$ and $j_D(U)$. Both characteristics are measurable, and the photocharacteristic has to be derived as $j_P(U) = j(U) - j_D(U)$. A photocurrent tends under reverse voltage to a saturation current j_S, and the internal collection efficiency is by definition $q(U) = -j_P(U)/j_S$. This efficiency represents nothing else than a normalized photocurrent. It is primary (secondary) with $q < 0$ ($q > 0$). The minimum value $q = -1$ corresponds to perfect collection and $q > -1$ measures recombination losses of primary photocurrents. Values $q > 1$ are possible because the replenishment of photocarriers may amplify secondary photocurrents. The efficiency q is measurable for any illumination and may depend on light intensity. The condition $q = 0$ defines a transition voltage U_T. It generally depends on spectral composition and intensity of the respective illumination. Quite common are weak spectral illuminations, eventually in combination with a stronger background illumination. Fig. 6 shows measured $q(U)$ characteristics for a cell in the state A and a state B, found with weak spectral light of different wavelengths λ. The measurements were made with chopped signal light and without any background illumination /10/. Lock-in technique allowed to directly detect the photocurrents. Weak light should not disturb the field through a pin cell in the dark. With this condition granted the photocharacteristics probe the dark state.

The curves q-versus-U of Fig. 6 for a λ-set could be replotted as q-versus-λ curves for an U-set. A definite voltage U_P then would trace a plateau just where the A- and B-characteristics of Fig. 6 cross. The condition $q(\lambda, U_T) = 0$ defines $U_T(\lambda)$. A λ-set of $q(U)$-curves ex-

pands between the intersections $q(\lambda,0)$ with the q-axis and $U_T(\lambda)$ with the U-axis and exhibits the cross point U_P,q_P with $q_P = q(U_P)$. Degradation A→B decreases the q_P modulus and U_P, spreads the sections $q(\lambda,0)$ and $UT(\lambda)$, and decreases the section moduli. Furthermore, the "fill factor" degrades considerably, and the B-set develops two peculiarities: The "red" characteristics to the higher λ's surpass the crossing and the curved "blue" characteristic to the lowest λ shows two inflection points shortly below the crossing. Both peculiarities are in fact already present with the A-set, although in a rudimentary fashion only.

The q-sets of Fig. 6 represent an example. Its typical features pertain to any customary pin cell. The magnitudes of $q(\lambda,0)$, q_P, U_P, U_T and their degradations are quite distinguishing properties of individual cells. Is there a simple explanation for the bewildering q-phenomena? The elementary model provides it! It will be demonstrated step by step.

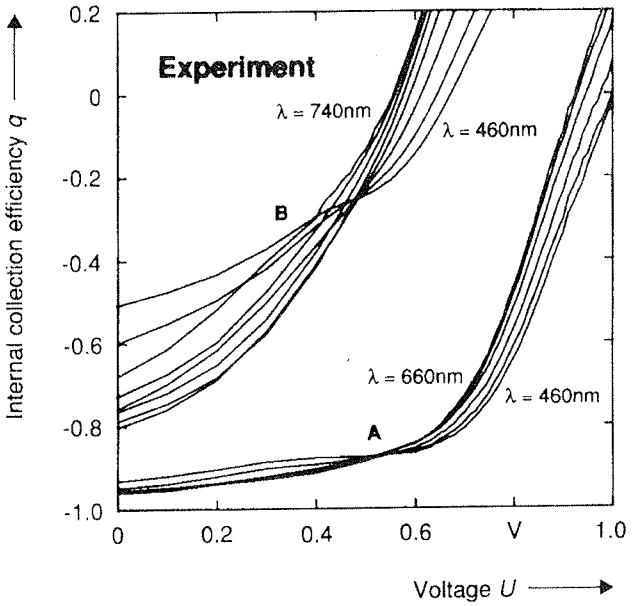

Fig. 6: Measured efficiencies q(U) at different wavelength λ of a pin diode in states A and B.

The model predicts sharp q-crossings for symmetric cells. Fig. 7 gives an example. Plotted there are two modelled q-sets designated A and B based on the parameters of Table 1. The plateau efficiency is generally given as

$$q(\lambda,U_F)=\frac{-c+(1+\beta)s}{c+(1-\beta)s+dsc/D} \qquad (21)$$

for any symmetric cell under spectral illumination /10,13/, with $s(c)$ recombination (collection) velocities, D diffusion constants and β replenishment factors of electrons and holes, and i-layer thickness d. It is only and just for $U = U_F$ that q becomes independent of the light absorption constant and λ. Thus the q-sets of Fig. 7 cross at $U_P = U_F$ through $q_P = q(U_F)$. The A→B transition was obtained by decreasing the parameters s and U_F. (The assumed degradation of U_F is exaggerated.) Let's have a short look at (21). The nominator determines the sign of $q(U_F)$. The choice $c > (1 + \beta)s$ guaranties $q(U_F) < 0$, and $s = 0$ leaves $q(U_F) = -1$. Thus a variation of s is able to shift $q(U_F)$ through the primary photocurrent regime $-1 < q < 0$. The photocurrent at $U = U_F$ is generally diffusive. Therefore $D = 0$ correctly implies $q = 0$.

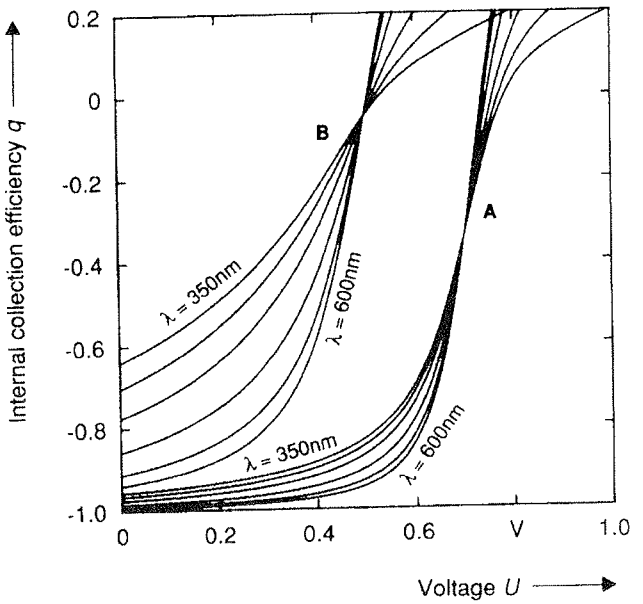

Fig. 7: Calculated efficiencies q(U) at different wavelength λ (parameters from table 1, column A and B).

The q-crossing reveals the flat-band voltage U_F. This derivation from the elementary model sticks to an ideal case, a symmetric cell. Customary pin cells are asymmetric according to $s_p > s_n$. With increasing λ the light penetrates deeper into the i-layer and just touches the back side for a certain threshold wavelength λ_t. Thus with $\lambda > \lambda_t$ the stronger back-side recombination sets in. As a consequence, the crossing is restricted to $\lambda < \lambda_t$ and the curves with $\lambda > \lambda_t$ surpass it as in Fig. 6. Just this behavior also follows from the elementary model applied to a cell /13/, and $U_P < U_F$ in addition. A measured U_P therefore indicates at best that U_F is not far away. This precaution is also necessary because the model has its own validity limits.

The unsymmetry in the junction properties of a pin diode can experimentally be pronounced by making a slightly doping of the i-layer. A doping with phosphorus ($p \nu n$) shifts the Fermi level towards the conduction band. Thus, the field spike at the p-i junction is enhanced and at the i-n junction reduced. A boron doping ($p \pi n$) acts contrarily. Theoretically, the i-layer doping influences s_n and s_p. The photocurrent behavior in such diodes strongly depends on the illumination direction. An illu-

mination through the strong field spike (i.e. low surface recombination velocity) leads to a high blue efficiency. On the other hand, an illumination through the low field spike (high surface recombination velocity) reduces the blue response and increases secondary photocurrents under forward bias. The red efficiency is in both illumination modi relatively poor.

The internal collection efficiency of *pvn* and *pπn* diodes is shown in Fig. 8 versus voltage for different wavelengths. The figure comprises both illumination modi. For illumination through the high filed spike (*pvn*) the short-circuit efficiency *q(U=0)* decreases with increasing wavelength. That means, the deeper the light penetrates into the i-layer, the stronger acts the junction with the low field spike. For illumination through the low field spike (*pπn*) *q(U=0)* increases with wavelength, because the influence of the surface recombination velocity decreases with increasing light penetration.

With the *elementary model* such characteristics are calculated and shown in Fig. 9. The parameter values are $s_n=10^3$ (10^4) cm/s and $s_p=10^4$ (10^3) cm/s for the *pvn* (*pπn*) diode. One can see, that with changing the values for s_n and s_p the overall behavior is obtained. Thus, also the slight doping of the i-layer can be described with this model.

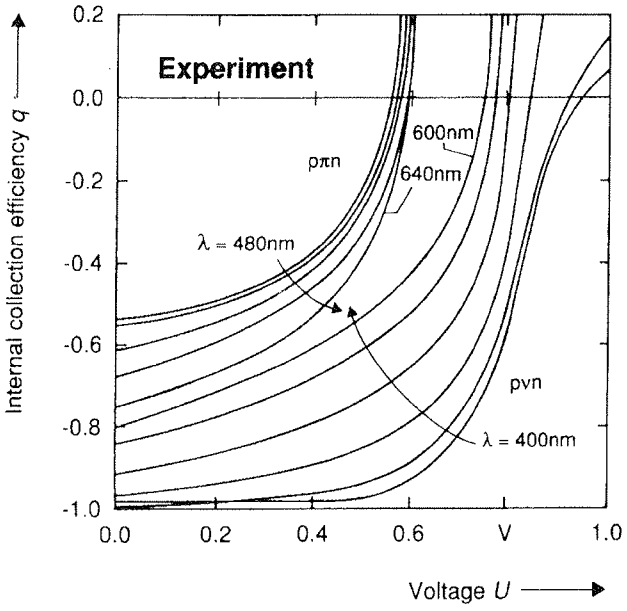

Fig. 8: Measured efficiencies q(U) for different wavelength λ of a pvn and pπn diode illuminated through the p-side.

For the following the symmetric case is regarded. An increase of s shifts any *q*-curves (of Fig. 6) upwards and broadens the short-circuit spread $\delta q = q(\lambda_2,0) - q(\lambda_1,0)$. (The relation $\lambda_2 - \lambda_1 > 0$ implies $\delta q < 0$.) This broadening effect of *s* is plausible. The penetration depth of blue (red) light is short (long) and the front-side recombination loss of electrons is high (low). The short-circuit blue efficiency will be limited by the front-side recombination velocity, whether a cell is symmetric or not. The red

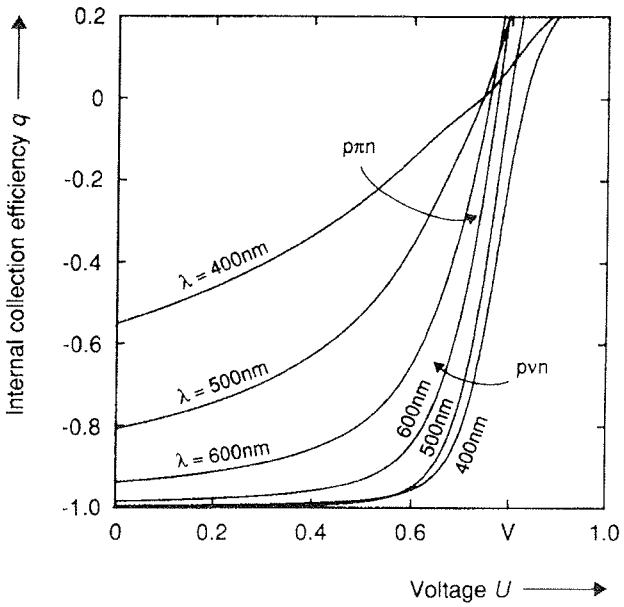

Fig. 9: Calculated efficiencies q(U) at different wavelength λ for different s_n and s_p values.

efficiency, on the other hand, will be limited by the recombination of both carriers, electrons and holes, at either side. So both velocities count. On the whole now the $q(\lambda,0)$ moduli will increase in the case $s_p > s_n$ with λ up to λ_t, because more and more electrons are collected, but with $\lambda > \lambda_t$ they again decrease, because more and more holes do recombine. This behavior is observed, e.g. with Fig. 6, and the elementary model predicts it /13/.

The measured and modelled *q*-plots of Figs. 6 and 7 are more or less similar to each other. The (exaggerated) U_F degradation indirectly simulates enhanced bulk recombination. The most conspicuous discrepancy concerns the cross or plateau efficiencies q_P. The modelled q_P are too high up (their moduli being too small). Is it possible to improve the plateau collection (to bring down the q_P-values) and leave the short-circuit spread δ_q untouched? A falling function $s_n(U)$ can do both, e.g. the one of Fig. 10 in connection with $s_p = s_n(-\infty)$. This measure transforms the *q*-sets of Fig. 7 into the sets of Fig. 11. The function $s_n(U)$ represents an arbitrary guess. It falls near a voltage U_S that is smaller than U_F, improves the collection and makes the cell asymmetric. Flat plateaus and sharp crossings do no longer exist, but a rough relation $U_P < U_F$ is to be recognized. The measured and modelled A-sets of Figs. 6 and 11 show a sharp knee near U_P. The turn-up is caused by the field reversal at $U = U_F$. Photocarriers are collected by drift and diffusion for $U < U_F$, but diffusion is dominant. Otherwise the characteristics could not be as flat. Back diffusion against drift feeds surface recombination. For $U > U_F$ collection occurs by diffusion against drift, and the surface recombination is now supported by drift. The turn-up of the characteristics indicates collection break down. The recombination is low (rising) along the flat (rising) part of the characteristics. It is the field

direction that controls surface recombination. Similar explanations apply to the B-sets. Good collection is delimited to the diode regime of the dark characteristic.

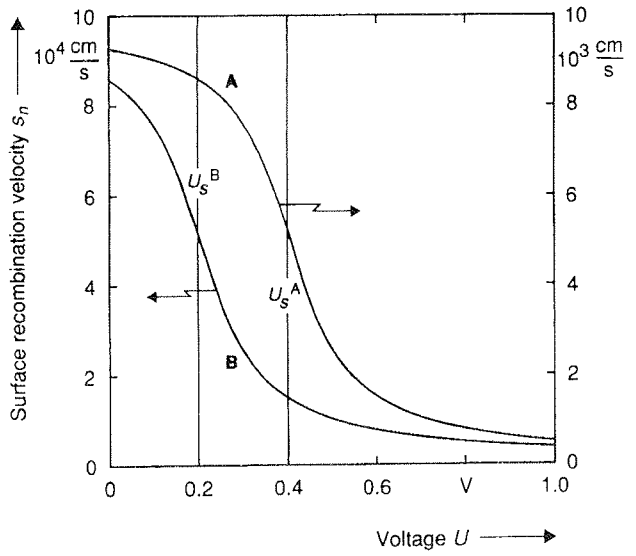

Fig. 10: Two functions $s_n(U)$ to model states A and B, U_S is the inflection voltage.

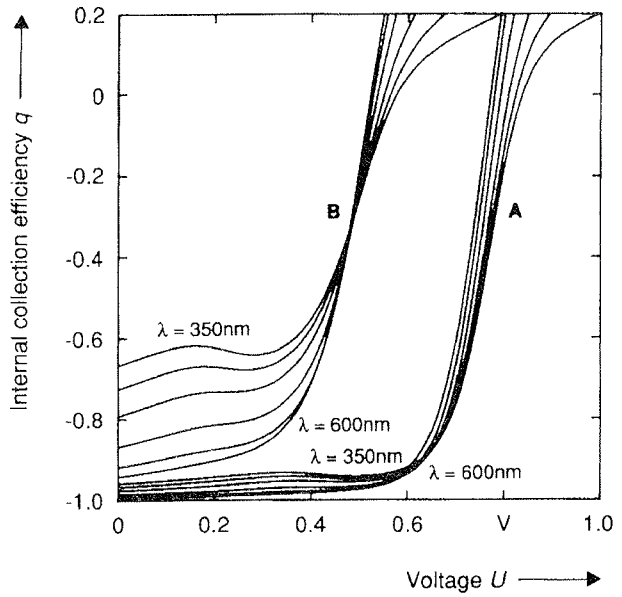

Fig. 11: Calculated efficiencies q(U) at different wavelength λ and with voltage-dependent s_n (parameters from table 1, column A and B).

The measured inflection of the B-characteristic to the shortest λ (Fig. 6) is deliberately exaggerated by our calculation (Fig. 11). The modelled "blue" characteristics even decline over a certain interval $U_S < U < U_F$ and are curved like a snake. This "blue-snake" anomaly by the way can appear also in experiments. We speak of "blue snakes" whether it comes to a slope reversal or not. The $s_n(U)$ downfall of Fig. 10 creates the blue snake of Fig. 11 and therefore simulates a real process. Customary cells have buffered p(C)-i heterojunctions. We once measured an unbuffered cell and found A- and B-sets of q without any trace of a blue snake /15/ and quite similar to Fig. 7 . Hence the blue snake is the trademark of a buffered heterojunction. Numerical simulations corroborate this conclusion /16,17/.

Discrepancies between Figs. 6 (observed) and 11 (modelled) remain: The modelled q-curves rise too steeply beyond U_F and the "fill factor" of the modelled B-set is too low. Responsible for these deficiencies are the uniform-field assumption and the neglect of bulk recombination, respectively. We have to remark that the full consideration of bulk recombination in (7) lets blue snakes appear quite naturally with constant recombination velocities s_n. So a blue snake indicates in reality a conspicuous interaction of bulk and surface recombination in the case of low-level spectral illumination!

Conclusion

The foregoing demonstrations and discussions indicate the value and the limits of the quite simple elementary model. It allows to interpret experimental characteristics and offers a first understanding of a-Si:H solar cells with respect to the most important characteristics. This comprises also the light characteristic under simulated AM1-light /18/. In order to incorporate bulk recombination a two-region model was introduced /8,19,20,21/. This two-region concept simplifies the consideration of bulk recombination. The artificial inner region boundary has to be found iteratively /19,20,21,22/, except for the simplest case (diffusion and surface recombination neglected) /8/. The neglection of bulk recombination lets the double-carrier model /22/ degenerate to our one-region elementary model /23/. The photocarrier collection occurs by drift and diffusion, and at flat-bands by diffusion alone. The distinction between minority and majority carriers becomes uncertain therefore under flat-bands, and a two-region simulation of photocharacteristics runs into serious difficulties. The flat-band situation is quite important, on the other hand. The elementary model now has no difficulty with this situation at all. Only the degenerate solution (13) has to be used. In order to fully exploit the uniform-field concept, Shockley-Hall-Read recombination rate r for example has to be considered in (7) without any further simplification. The boundary-value problem then is to be solved numerically /24/. The general uniform-field model has the potentiality to meet the experiments better than the elementary model, has also no difficulty with flat-bands, and simulates *blue snakes* without effort, as mentioned above. Simple solar cell models can in connection with experiments provide key explanations, as demonstrated here by means of our *elementary model*. The complete description of a solar cell remains the domain of *exact* simulation.

The amorphous structure and the continuously distributed density of defects has made the thorough under-

standing of a-Si:H pin solar cells very complicate. Fortunately, simple cell concepts have been proven as quite useful for the practitioner. We presented the *elementary model* as an example here. The model indentifies the significance of *flat-band voltage* and *surface recombination*, also in connection with light degradation.

References

/1/ R.C. Chittick, J.H. Alexander, H.F. Sterling, J. Electrochem. Soc. Solid State Science, Vol. 119, No. 1 (1969) 77

/2/ P.G. LeComber, W.E. Spear, Phys. Rev. Lett., Vol. 25, No. 8 (1970) 509

/3/ R.C. Chittick, Journ. of Non-Cryst. Solids 3 (1970) 255

/4/ W.E. Spear, P.G. LeComber, Journ. of Non-Cryst. Solids 8-10 (1972) 727

/5/ W.E. Spear, P.G. LeComber, Solid State Communications, Vol. 17 (1975) 1193

/6/ M. Hack and M. Shur, J. Appl. Phys. 58 (1985)997

/7/ J.L. Gray, IEEE-ED 36 (1989) 906

/8/ R.S. Crandall, J. Appl. Phys., vol.53 (1982) 3350

/9/ W. Kusian, H. Pfleiderer, AIP Conference Proceedings 234 (1991) 290

/10/ W. Kusian, H. Pfleiderer and B. Bullemer, Mat. Res. Soc. Symp. Proc., vol.118 (1988) 183

/11/ W. Kusian, H. Pfleiderer and B. Bullemer, Solar Cells, vol.22 (1987) 239

/12/ W. Kusian, H. Pfleiderer and B. Bullemer, J. Appl. Phys., vol.64 (1988) 5220

/13/ H. Pfleiderer, W. Kusian, E. Günzel and J. Grabmaier, 20th IEEE PVSC (1988) 180

/14/ M.Wolf, IEEE-ED, vol.28 (1981) 566

/15/ W. Kusian, H. Pfleiderer and W. Juergens, 9th European Photovoltaic Solar Energy Conference (1989) 52

/16/ W. Kopetzky, H. Pfleiderer and R. Schwarz, Journal of Non-Crystalline Solids, vol.137&138 (1991) 1201

/17/ H. Pfleiderer, Mat. Res. Soc. Symp. Proc. vol. 297 (1993) 791

/18/ W. Kusian, K.-D. Ufert, H. Pfleiderer, Solid State Phenomena Vols. 44-46 (1995) 823

/19/ R.S. Crandall, J.Appl.Phys., vol.54 (1983) 7176

/20/ H. Okamoto, H. Kida, S. Nonomura and Y. Hamakawa, Solar Cells, vol.8 (1983) 114

/21/ D.A. Aronov, R. Kabulov, and Yu.M. Yuabov, phys. stat. sol. (a) 118 (1990) 577

/22/ F. Irrera and F. Palma, Solid-State Electronics, vol.34 (1991) 801

/23/ W. Kusian and H. Pfleiderer, Journ. of Non-Cryst. Solids 164 - 166 (1993) 713

/24/ M. Ohnishi, T. Takahama, and Y. Kuwano, Mat. Res. Soc. Symp. Vol. 219 (1991) 421

Dr. Ing. habil. Wilhelm Kusian
Siemens AG
Corporate Research and Development
Otto-Hahn Ring 6
D-81739 München
tel.: +49 89 636 44682
fax: +49 89 636 49164
Email: wilhelm.kusian@zfe.siemens.de

Prispelo (Arrived): 12.8.1996 *Sprejeto (Accepted): 20.8.1996*

DEFECT POOL DENSITY-OF-STATES MODEL IN NUMERICAL MODELLING OF a-Si:H STRUCTURES

M. Topič, F. Smole and J. Furlan
Faculty of Electrical Engineering, University of Ljubljana, Slovenia

Keywords: semiconductors, a-Si, amorphous silicon, a-Si:H, hydrogenated amorphous silicon, PIN structures, positive-intrinsic-negative structures, solar cells, DOS, density-of-states,DP-DOS model, defect pool density-of-states, density if states, defect states, tail states, numerical simulators, potential barriers, ST-DOS model, standard density-of-states model, DB defect states, dangling bond defect states

Abstract: Defect pool density-of-states (DP-DOS) model in a-Si:H is presented. The calculation of defect states in a-Si:H based on the defect pool model has been successfully implemented in the ASPIN simulation program. Additionally, variable slopes of band tail states - as a function of doping concentration - have been included in the DP-DOS model. The effect of a leaky Schottky barrier at the front contact on the p-i-n a-Si:H solar cell performance has been analysed. The results of the model with the variable band tail state slopes agree better with the experimental results.

"Defect pool" model gostote stanj pri numeričnem modeliranju amorfnosilicijevih struktur

Ključne besede: polprevodniki, a-Si silicij amorfni, a-Si:H silicij amorfni hidrogeniziran, PIN strukture pozitivno-notranje-negativno, celice sončne, DOS gostota stanj,DP-DOS model gostote stanj "defect pool", gostota stanj, stanja defektna, stanja repov, simulatorji numerični, bariere potencialne, ST-DOS model gostote stanj standardni, DB vezi viseče stanj defektnih

Povzetek: Izračun gostote defektnih stanj znotraj mobilnostne reže, ki temelji na "defect pool" modelu, smo uspešno vključili v ASPIN simulator. Pri izračunu gostote stanj smo upoštevali tudi spremenljiv naklon stanj repov kot funkcijo tipa in koncentracije dopiranja. Obravnavali smo vpliv Schottkyjeve bariere na sprednjem kontaktu na zmogljivost p-i-n amorfnosilicijevih sončnih celic. Rezultati modela s spremenljivim naklonom stanj repov izkazuje boljše ujemanje z eksperimentalnimi rezultati.

1. Introduction

The increasing complexity of heterostructures based on hydrogenated amorphous silicon (a-Si:H) and its alloys demand permanent upgrading of computer models, which are used for their simulation. In contrast to a modelling of monocrystalline devices, in a-Si:H devices one of the key issues is a correct modelling of recombination-generation mechanism and with it connected density of states (DOS) in the mobility gap. States within the mobility gap in a-Si:H can be classified to the valence band tail states, conduction band tail states and between them to the defect states with three possible charges (+, o, -), the so-called dangling bond (DB) defect states. Electrons or holes can be trapped or recombined in these states and the charged states contribute to the space charge affecting the device electrical properties.

Most existing simulation models use for a-Si:H a standard DOS model (ST-DOS) /1/, in which DB defect states are modelled by Gaussian-shaped $D^{+/o}$ and $D^{o/-}$ states placed near the midgap and separated by the effective correlation energy U_{eff}, which was experimentally measured to be positive (Fig. 1). The density of DB states are taken to be constant in the individual layers of the multi-layer a-Si:H structure.

The ST-DOS model (as seen in Fig. 1) leads to positively charged defects in p-type amorphous silicon having a lower energy than negatively charged defects in n-type amorphous silicon, since the U_{eff} is positive. But this energetic position of charged defect states in doped

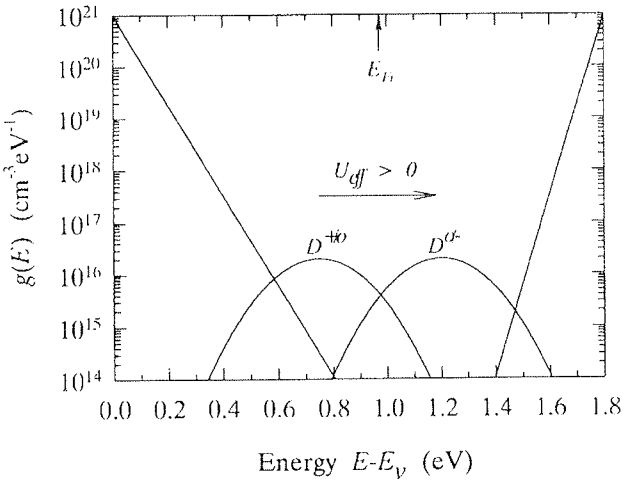

Fig. 1 One-electron density of states distribution according to the standard model (E_F indicated by an arrow).

a-Si:H is not consistent with results found in many experiments /2,3,4/.

A recent theory of defect formation in a-Si:H based on weak-bond dangling-bond reaction determined by a chemical equilibrium process explains most of the a-Si:H behaviour and it is known as the defect pool (DP) concept /5,6,7/. We have implemented this concept into

our simulator ASPIN /8,9/ and the results of this implementation are presented and discussed.

2. Defect pool model and its properties

Thermodynamic approach of defect formation is based on a chemical equilibrium reaction between silicon weak *Si-Si* bonds (the exponential valence band tail) and dangling bonds. In reaction *i* hydrogen atoms can be involved, where *i*= 0, 1, 2 /6/. This approach also postulates a possible distribution of available dangling bond energies due to the inherent disorder of the amorphous network. This is the so-called defect pool, which is assumed to be Gaussian-shaped and centered at the defect pool position E_p. For a sufficiently wide pool, the model leads to negatively charged defects in n-type a-Si:H having a lower energy than positively charged defects in p-type a-Si:H, even when the correlation energy is positive, a previously puzzling result found in many experiments /2,3,4/. The inclusion of the occupancy statistics predicts the formation of three different defect states regarding their charge state and position in the mobility gap. Furthermore, the density of charged dangling bond defects (D^- and D^+) is in thermal equilibrium higher than density of neutral defects (D^0) even in undoped a-Si:H /6/. The equilibrium density of DB defect states depends on the Fermi energy, which leads to a higher density of dangling bonds in doped a-Si:H than undoped a-Si:H.

Our numerical defect pool DOS (DP-DOS) model consists of a standard tail of donor-like states above the valence band edge, a standard tail of acceptor-like states below the conduction band edge, and three Gaussian-shaped DB defect state densities D_n, D_i, D_p, whose density depends on the Fermi energy level E_F according to the derived analytical dependencies, which are in good agreement with measured results /10/. Each Gaussian-shaped DB defect state density is approximated with an exponential dependence on E_F (for values see Table 1) as:

$$g_{D_n}(E,E_F) = gM_{D_n} \cdot e^{-\frac{(E-E_{Dn})^2}{2\sigma_p^2}} \cdot e^{\frac{E_{Fi}-E_F}{kT_n}} \quad (1)$$

$$g_{D_i}(E,E_F) = gM_{D_i} \cdot e^{-\frac{(E-E_{Di})^2}{2\sigma_p^2}} \cdot e^{\frac{E_{Fi}-E_F}{kT_i}} \quad (2)$$

$$g_{D_p}(E,E_F) = gM_{D_p} \cdot e^{-\frac{(E-E_{Dp})^2}{2\sigma_p^2}} \cdot e^{-\frac{E_{Fi}-E_F}{kT_p}} \quad (3)$$

Taking into account a positive correlation energy for doubly occupied state, each dangling bond defect state (D_n, D_i, D_p) is divided into two further peaks (+/0, 0/-), since each defect state can be occupied by zero (+), one (0) or two electrons (-) (Fig. 1). Thus, we can duplicate Eqs. 1-3 for six Gaussian-shaped DB defect states with their peaks at:

$$E_{D_n^{+/0}} = E_p - \frac{2\sigma_p^2}{E_{0v}} \qquad E_{D_n^{0/-}} = E_p - \frac{2\sigma_p^2}{E_{0v}} + U_{eff} \quad (4)$$

$$E_{D_i^{+/0}} = E_p - \frac{\sigma_p^2}{E_{0v}} \qquad E_{D_i^{0/-}} = E_p - \frac{\sigma_p^2}{E_{0v}} + U_{eff} \quad (5)$$

$$E_{D_p^{+/0}} = E_p \qquad E_{D_p^{0/-}} = E_p + U_{eff} \quad (6)$$

In thermal equilibrium, the D_n, D_i, D_p states correspond to doubly occupied (D^-), singly occupied (D^0) and un-

Table 1: Defect pool DOS model input parameters

Parameter	p	i	n
Tail States Parameters:			
Density at E_c, E_v ($cm^{-3}eV^{-1}$)	2.10^{21}	2.10^{21}	2.10^{21}
E_{v0} (meV)	50/90	50	50/80
E_{c0} (meV)	25/45	25	25/40
$\sigma_C v_{th}$ (cm^3/s)	5.10^{-11}	5.10^{-11}	5.10^{-11}
$\sigma_N v_{th}$ (cm^3/s)	5.10^{-9}	5.10^{-9}	5.10^{-9}
Defect States Parameters:			
Concentration (cm^{-3})	10^{18}	10^{16}	10^{18}
U_{eff} (eV)	+0.2	+0.2	+0.2
E_p-E_v (eV)	1.2	1.2	1.2
σ_p (eV)	0.125	0.125	0.125
$\sigma_C v_{th}$ (cm^3/s)	5.10^{-11}	5.10^{-11}	5.10^{-11}
$\sigma_N v_{th}$ (cm^3/s)	5.10^{-9}	5.10^{-9}	5.10^{-9}

	D_n	D_i	D_p
gM_D ($cm^{-3}eV^{-1}$)	2.10^{16}	4.10^{15}	2.10^{16}
$E_D^{+/0}$-E_v (eV)	0.55	0.85	1.20
U_{eff} (eV)	+0.2	+0.2	+0.2
σ_p (eV)	0.125	0.125	0.125
kT (eV)	0.103	10^{12}	0.107

occupied (D^+) dangling bond defect states, respectively.

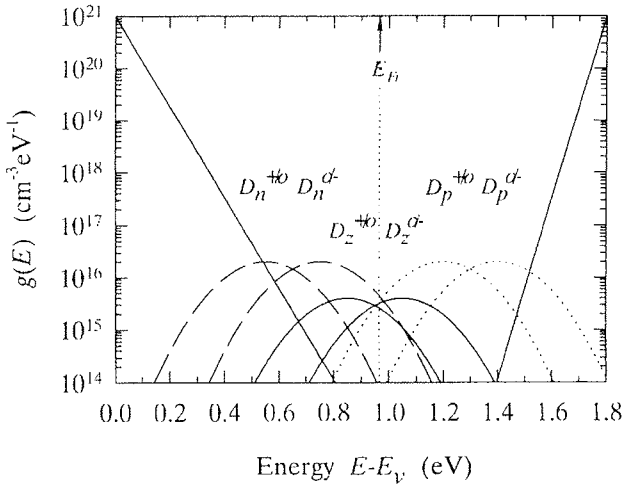

Fig. 2: One-electron density of states distribution according to the defect pool model for intrinsic a-Si:H in thermal equilibrium (E_F indicated by an arrow).

Since the defect pool model implies that the position of the Fermi energy determines the defect distribution, in the p-i-n structure the spatial-dependent defect states density is calculated self consistently from the Poisson's and continuity equations at the equilibration temperature T* (500 K) together with the derived analytical dependencies on E_F (see Eqs. 1-3).

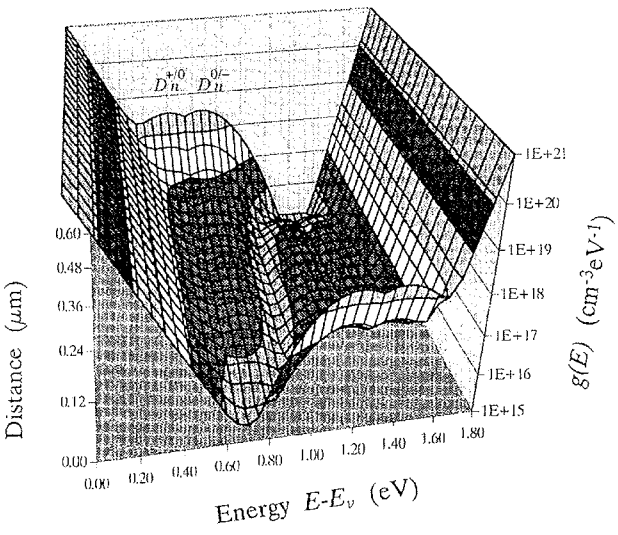

Fig. 3: One-electron density of states throughout the p-i-n structure - calculated from the defect pool model.

The "frozen" gap states distribution profile (Figs. 3, 4) is used to calculate the behaviour of the device at the operational temperature. Out of thermal equilibrium, the charge state of defects becomes a function of the electron and hole concentration.

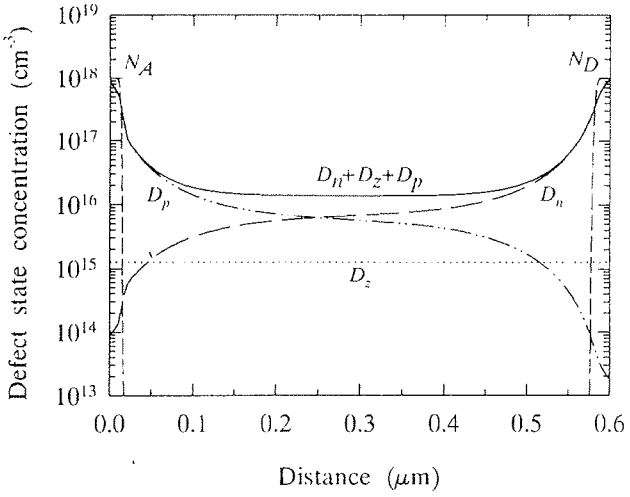

Fig. 4: Defect pool in the p-i-n structure: calculated distribution of defects D_n, D_i, D_p and the doping profile.

3. Results

A lot of scientific attention has been paid to a leaky Schottky barrier at the TCO/p interface /11,12/. Using defect pool DOS model we have analysed how the barrier affects the solar cell performance. Results under AM 1.5 illumination are seen in Fig. 5 (full line). Surface potential barrier V_B ranges from 0.0 V, i.e. the thermal equilibrium value as in the bulk of the p layer, to 0.24 V. Bigger potential barrier increases the diffusion of electrons into the front contact and thus decreasing the J_{SC}. Bigger barrier affects most strongly the V_{OC}. Consequently, the efficiency drops significantly with increasing the barrier.

Recent CPM measurements /13,14/ revealed that the slopes of the band tail states (E_{V0}, E_{C0}) are affected by the doping concentration, especially by boron atoms in a p layer. Based on experimental results, we included a linear fit of this dependence to the DP-DOS model (DP*-DOS) and it is seen in Fig. 6.

The effects of the improved DP*-DOS model on the cell performance are presented in Fig. 5 (dashed line). The J_{SC} is surprisingly bigger. Fig. 7 reveals the difference in the built-in electric field, which is at the bias of 0.0 V in case of variable slopes slightly lower in the i layer, but higher near the surface of the p layer, so that it mitigates the harmful diffusion of electrons into the front contact and improves the collection efficiency in the short wavelength region. Consequently, the J_{SC} increases. On the other hand, the increased tail states in the doped layers contribute to an increase of the recombination rate and thus reducing V_{OC} and FF. In DP*-DOS model, the V_{OC} and FF values seem to be in better agreement with experimental results.

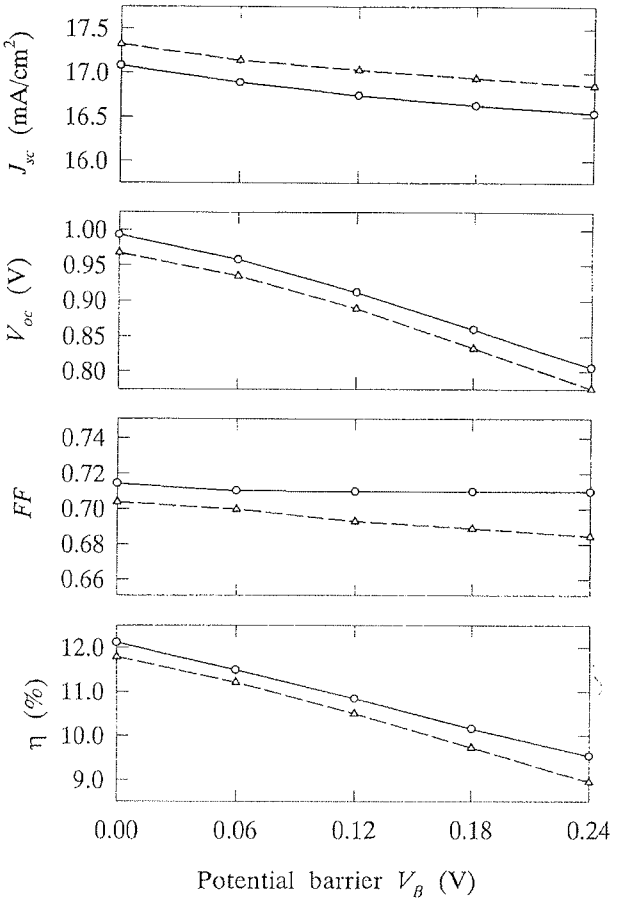

Fig. 5: Photoelectric properties of a p-i-n a-Si:H solar cell as a function of potential barrier at the TCO/p contact interface (full line - constant band tail state slopes; dashed line - variable band tail state slopes).

Another inspection tool is the dark current-voltage characteristic. In Fig. 8 we can see the difference in calculated characteristics for DP-DOS model and DP*-DOS model with the barrier of 0.0 V and 0.12 V. The main difference occurs at applied voltages above 0.5 V, where in case of variable band tail slopes the electric field in the p and i layer drops with applied voltage faster and the recombination rate in the p layer increases strongly.

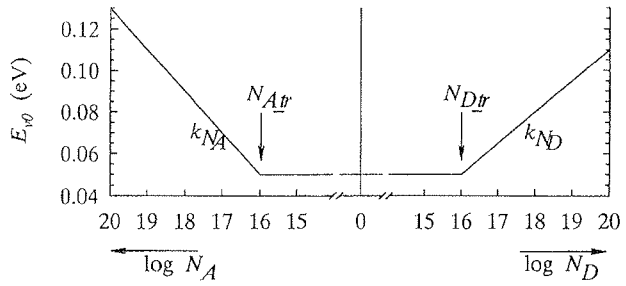

Fig. 6: A model of E_{V0} dependency on doping concentration. Similar dependency holds also for E_{C0} - only initial value E_{C00} is smaller (25 meV).

The electric field profile in dark calculated from a defect pool DOS models differs significantly from a profile using a ST-DOS model. However, under AM1.5 illumination both approaches give similar profiles. This phenomenon leads to the conclusion that - assuming the DP-DOS models are correct and more exact - the electric field profile is very sensitive to the illumination intensity. By measuring collection efficiency under different

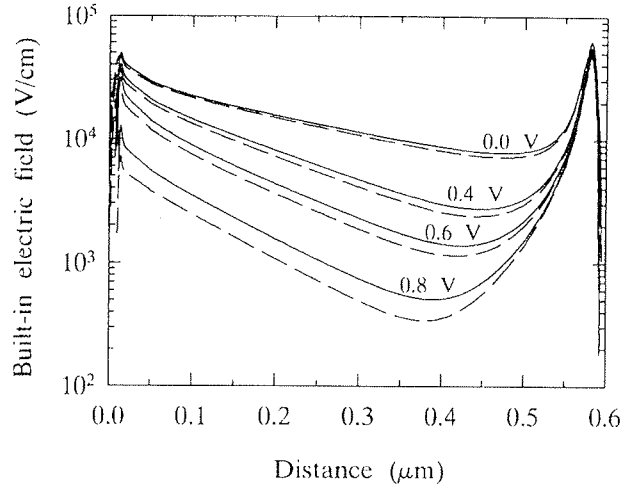

Fig. 7: Calculated electric field profiles under AM1.5 for the surface potential of 0.12 V using DP-DOS model with constant (full line) and DP-DOS model with variable band tail slope (dashed line).

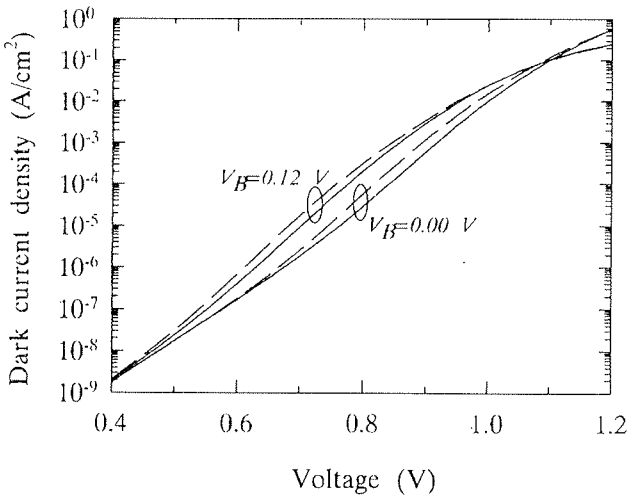

Fig. 8: Calculated dark current-voltage characteristics for DP-DOS model with constant (full lines) and with variable band tail slope (dashed lines) throughout the structure for two surface potential barrier values.

intensities and accompanied with numerical simulations, this could be verified.

4. Conclusions

According to the defect pool concept, we have formed a numerical defect pool model and successfully implemented the calculation of the defect state distribution in the device simulator ASPIN. The possibility of varying the slopes of band tail states as a function of doping concentration has been added. Based on experimental results from literature, a model for variable slopes was proposed. For both, constant and variable slope cases, the validity of the defect pool model for modelling a-Si:H devices was verified for p-i-n solar cells. The model with the variable slopes of band tail states exhibits better agreement with the experimental results and it is certainly more realistic. However, further work, predominantly experimental is necessary to obtain better fit for band tail slope dependence on doping concentration.

References

/1/ N. F. Mott, E. A. Davis, Processes in Non-Crystalline Materials (Oxford: Clarendon, 1979).

/2/ J. Kocka, M. Vanecek, F. Schauer, J. Non-Cryst. Solids 97&98 (1987) 715.

/3/ K. Winer, I. Hirabayashi, L. Ley, Phys. Rev. B 38 (1988) 7680.

/4/ K. Pierz, W. Fuhs, H. Mell, Philos. Mag. B 63 (1991) 123.

/5/ K. Winer, Phys. Rev. B 41 (1990) 12150.

/6/ M. J. Powell and S. C. Deane, Phys. Rev. B 48 (1993) 10815.

/7/ G. Schumm, Phys. Rev. B 49 (1994) 2427.

/8/ F. Smole, J. Furlan, J. Appl. Phys. 72 (1992) 5964.

/9/ M. Topic, Ph.D. Thesis, University of Ljubljana, 1996.

/10/ K.Pierz, W.Fuhs and H.Mell, Phil. Mag. B 63 (1991) 123.

/11/ F. S. Sinencio and R. Williams, J. Appl. Phys. 54 (1983) 2757.

/12/ K. Itoh, H. Matsumoto, T. Kobata and A. Fujishima, Appl. Phys. Lett. 51 (1987) 1685.

/13/ H. Stiebig and F. Siebke, Materials Reserach Society Symposium Proceedings, Vol. 377 (1995) 287.

/14/ H. Stiebig and F. Siebke, Phil. Mag. B 72 (1995) 489.

dr. Marko Topič, dipl. ing.
prof. dr. Franc Smole, dipl. ing.
prof. dr. Jože Furlan, dipl. ing.
Fakulteta za elektrotehniko
Tržaška c. 25
Ljubljana, Slovenia
Tel.: +386 61 176 83 03
Fax: +386 61 346 087

Prispelo (Arrived): 16.8.1996 *Sprejeto (Accepted): 20.8.1996*

BASE TRANSPORT PROPERTIES OF *npn* SiGe HETEROJUNCTION BIPOLAR TRANSISTORS: PHYSICS AND MODELLING

Saša Sokolić and Slavko Amon
Faculty of Electrical Engineering, University of Ljubljana, Slovenia

Keywords: semiconductors, bipolar transistors, HBT, heterojunction bipolar transistors, BJT, bipolar junction transistors, physical properties, comparison of properties, SiGe HBT, SiGe heterojunction bipolar transistors, base transport properties, base transit times, bandgap narrowing, effective mass, collector current, base transit time, Fermi-Dirac statistics,analitical modelling.

Abstract: The base transport properties of *npn* SiGe heterojunction bipolar transistors (HBTs) are analyzed. Physical effects influencing the electron current in the base and the base transit time are discussed, and the modelling of these effects is described. The results of modelling demonstrate that the improvement of SiGe HBTs compared to Si BJTs increases with cooling and decreases with increasing doping concentration in the base, and that Fermi-Dirac statistics influence significantly the electron current in the base. The analytical approach to the modelling of base transport properties is presented, rendering simple and accurate evaluation of the electron current in the base and the base transit time in the wide range of doping concentrations at 77*K* and 300*K*.

Transportne lastnosti baze v *npn* SiGe heterospojnih bipolarnih tranzistorjih: fizikalna slika in modeliranje

Ključne besede: polprevodniki, transistorji bipolarni, HBT transistorji bipolarni heterospojni, BJT transistorji s spojem bipolarnim, lastnosti fizikalne, primerjava lastnosti, SiGe HBT transistorji bipolarni heterospojni, lastnosti transportne baze transistorja, časi tranzitni baze transistorjev, oženje pasu prepovedanega, masa efektivna, tok kolektorski, čas tranzitni baze, Fermi-Dirac statistika, modeliranje analitično

Povzetek: V delu so analizirane transportne lastnosti baze v *npn* SiGe heterospojnih bipolarnih tranzistorjih (HBT). Razloženi so fizikalni efekti, ki vplivajo na tok elektronov v bazi in na tranzitni čas baze. Opisano je modeliranje teh efektov. Rezultati modeliranja kažejo, da se izboljšanje lastnosti SiGe HBT-jev v primerjavi s silicijevimi bipolarnimi tranzistorji povečuje z nižanjem temperature in znižuje z višanjem koncentracije primesi v bazi, ter da Fermi-Diracova statistika bistveno vpliva na tok elektronov v bazi. Predstavljen je pristop k analitičnemu modeliranju transportnih lastnosti baze, ki pripelje do enostavnega in natančnega izračuna toka elektronov v bazi in tranzitnega časa baze v širokem območju koncentracij primesi pri 77*K* in 300*K*.

1. Introduction

Heterojunction bipolar transistors (HBTs) with strained SiGe layers in the base have been the subject of intensive research in the last few years /1-7/. Compared to Si BJTs, SiGe HBTs with better current gain and greatly improved cutoff frequencies have been reported /1-3/. Moreover, SiGe BiCMOS technology has been presented, combining unique capabilities of SiGe HBTs with the advantages of CMOS devices /4/. It has been also demonstrated that SiGe HBTs are well suited for low temperature operation and that their performances improve naturally with cooling /5,6/. SiGe HBTs optimized for 77*K* operation have been recently reported /7/, exhibiting better performances than those of the same technology operating at 300*K*. In addition to the superior performances of SiGe HBTs, their compatibility with existing silicon technology represent an important advantage for these devices to find wide use in the semiconductor market.

The improvement of SiGe HBTs compared to Si BJTs is closely related to the transport properties of the SiGe base /1/. As a consequence of germanium and compressive strain, several effects influencing carrier transport appear in the base. The most important effect - bandgap reduction due to strain and alloying in the base - results in increased electron injection from the emitter to the base and, consequently, increased electron current in the base /1/. Further, graded germanium profile in the base introduces graded energy gap in the base and, consequently, a beneficial effective electrical field in the base, improving the high frequency characteristics of SiGe HBTs /1/. Beside the bandgap reduction, several other effects in the base additionally influence the device characteristics.

The insight into the physics of the base transport mechanisms and related effects is inevitable for an understanding of the possibilities for further improvement of SiGe HBTs. Besides, the modelling of these effects is important for accurate analysis and optimization of SiGe HBTs. Since the current gain and the base transit time are controlled by the Ge profile in the base rather than by the doping profile, doping profile in the base can be optimized, resulting in additional freedom for device designers. Bearing in mind also the possibilities for low-temperature operation of SiGe HBTs, it is obvious that the germanium, doping and temperature dependence of mechanisms related to the base transport properties should be known for adequate modelling of SiGe HBTs.

The purpose of this paper is to discuss the physical effects in the base related to the transport of carriers, and to suggest the models which are required for evaluation of the electron current in the base and the base transit time. In the following, the physics of SiGe base is examined and corresponding models are reviewed. The device performance issues such as SiGe HBT vs. Si BJT improvement, 77*K* vs. 300*K* operation, and the importance of Fermi-Dirac statistics for the carrier transport in the base are analyzed. Finally, an approach to the accurate analytical modelling of the electron current in the base and the base transit time is presented.

2. Physics of the SiGe base

Due to the presence of germanium, the physics of carrier transport in the SiGe base differs from that in the conventional Si base. In this section we analyze the electron current in the base, which is the main contributor to the collector current in SiGe HBT. We examine the base transit time which is a parameter influencing significantly the high frequency performance of SiGe HBTs. Finally, we address the evaluation of *pn* product in the base which is an important base transport parameter.

2.1 Electron current in the base

The electron current in the SiGe base can be described by the generalized Moll-Ross relation /8/, which takes into account the influence of nonuniform doping and energy gap grading in the base:

$$j_n = \frac{qn_{i,Si}^2\left(exp\left(\frac{qV_{BE}}{kT}\right)-1\right)}{\int_0^{W_b} exp\left(-\frac{\Delta D_{SiGe}(x)}{kT}\right)\frac{N_A(x)dx}{D_{n,SiGe}(x)}}, \qquad (1)$$

where N_A is the acceptor concentration in the base, $n_{i,Si}$ is intrinsic carrier concentration in silicon, $D_{n,SiGe}$ is electron diffusion constant in the SiGe base, ΔG_{SiGe} is an apparent bandgap narrowing in the base which accounts for the deviation of *pn* product in SiGe from that in intrinsic silicon; the other symbols have their usual meaning.

In contrast to most GaAs based heterojunction devices -where the carrier transport is controlled by the heterojunction barriers - the electron current in SiGe HBTs is determined by drift and diffusion and depends almost entirely on the bulk base properties. This is a consequence of the small conduction band discontinuity (approximately 10 *meV* /9/) which appears on the Si/SiGe heterojunction. It has been shown recently that even if thermionic emission of electrons over the conduction band discontinuity is taken into account, the small barrier does not influence the electron transport unless the temperature is extremely low ($T < 50$ *K*) /10/. The minority electron diffusion constant and the apparent bandgap narrowing are thus the most important parameters determining the stationary electron transport in the base. Beside the effects related to the apparent bandgap narrowing, which will be addressed in more detail in the following, it is necessary to stress the Ge-dependence of electron diffusion constant in the base. It has been observed experimentally that the minority carrier mobility in SiGe is higher than that in silicon as a consequence of germanium and strain /11/. A simple empirical model for diffusion constant enhancement due to strain and germanium has been recently presented /12/, where it has been assumed that the temperature and doping dependence of electron mobility in SiGe is the same as that in silicon.

2.2 Base transit time

Taking into account the influence of nonuniform energy gap in the base, the base transit time (τ_B) can be described as proposed in /8/:

$$\tau_B = \int_0^{W_B}\left[exp\left(\frac{\Delta G_{SiGe}(z)}{kT}\right)\int_z^{W_B} exp\left(-\frac{\Delta G_{SiGe}(x)}{kT}\right)\frac{N_A(x)dx}{D_{n,SiGe}(x)}\right]dz \qquad (2)$$

The base transit time is controlled by the same physical effects as the electron current. However, in contrast to the electron current, which is influenced mostly by bandgap narrowing at the base side of the emitter-base depletion region, the base transit time is affected mainly by the grade of the apparent bandgap narrowing in the base.

2.3 *pn* product in the base

The *pn* product in the SiGe base is an important parameter which influences significantly the electron current in the base and the base transit time. It is affected by the structure of conduction and the valence band in SiGe, which is modified as a result of compressive strain and alloying /9,13/. The conduction band of strained SiGe splits into fourfold degenerate and twofold degenerate states, influencing the effective density of states in the conduction band ($N_{C,SiGe}$) /13/. In the valence band of SiGe the heavy hole and the light hole bands split, with the heavy hole band moving up and the light hole band moving down in the energy diagram /9,13/. Both bands, together with the split-off band, are highly distorted and non-parabolic. As a result, the energy gap in SiGe is reduced compared to the energy gap in silicon /9,13,14/. Furthermore, the effective density of states in the valence band ($N_{V,SiGe}$) is changed owing to the lower hole effective mass (m_p*) in SiGe /15-17/. Besides, the high doping concentration causes additional bandgap reduction ($\Delta E_{g,hd}$), which appears to be of the same origin as a corresponding bandgap reduction in silicon /18,19/.

An apparent bandgap narrowing (ΔG_{SiGe}) can be defined to account for the difference between *pn* product in the SiGe base and the intrinsic carrier concentration in silicon:

$$(pn)_{SiGe} = n_{i,Si}^2 \exp\left(\frac{\Delta G_{SiGe}}{kT}\right), \quad (3)$$

Under the assumption of space charge neutrality, quasi-equilibrium and reparabolization of nonparabolic energy bands in the *p*-type SiGe base, a relation between Fermi level and the doping concentration in the base can be defined by the Fermi integral:

$$p_{SiGe} = N_A = N_{V,SiGe} \frac{2}{\sqrt{\pi}} F_{1/2}\left(\frac{E_{V,SiGe} - E_F}{kT}\right), \quad (4)$$

where E_F is equilibrium Fermi level and $E_{V,SiGe}$ is the edge of reparabolized and shifted valence band. E_F can be expressed by minority electron concentration:

$$E_F = E_{C,SiGe} + kT\, ln\left(\frac{n_{SiGe}}{N_{C,SiGe}}\right). \quad (5)$$

If n_{SiGe} is expressed by ΔG_{SiGe} (3), and the difference between the energy gap in intrinsic silicon and the energy gap in SiGe is expressed by $\Delta E_{g,SiGe} + \Delta E_{g,hd}$, where $\Delta E_{g,SiGe}$ corresponds to the bandgap reduction due to strain and germanium and $\Delta E_{g,hd}$ corresponds to the bandgap narrowing due to high doping concentration, we arrive at the expression:

$$N_A = N_{V,SiGe} \frac{2}{\sqrt{\pi}} F_{1/2}\left(\frac{\Delta E_{g,Ge} + \Delta E_{g,hd} - \Delta G_{SiGe}}{kT} - ln\left(\frac{N_{C,Si,i} N_{V,Si,i}}{N_{C,SiGe} N_A}\right)\right), \quad (6)$$

where $N_{C,Si,i}$ and $N_{V,Si,i}$ represent effective densities of states in the conduction and the valence band in intrinsic silicon. By applying the inverse Fermi integral to (6), a closed form expression for ΔG_{SiGe} can be found:

$$\Delta G_{SiGe} = \underbrace{[\Delta E_{g,hd}]}_{A} + \underbrace{[\Delta E_{g,Ge}]}_{B} + \underbrace{\left[kT\, ln\left(\frac{N_{C,SiGe} N_{V,SiGe}}{N_{C,Si,i} N_{V,Si,i}}\right)\right]}_{C} + \underbrace{\left[kT\, ln\left(\frac{N_A}{N_{V,SiGe}}\right) - kTG_{1/2}\left(\frac{N_A}{N_{V,SiGe}}\right)\right]}_{D}, \quad (7)$$

where contributions denoted A-D have clear physical meaning: A represents the doping induced actual bandgap reduction, B represents the bandgap narrowing due to strain and alloying, C represents an effective bandgap reduction due to lower effective densities of states in SiGe compared to effective densities of states in intrinsic silicon, and D corresponds to the Fermi level shift due to Fermi-Dirac statistics (degeneracy). Careful analysis of (7) indicates that for the evaluation of ΔG_{SiGe} at an arbitrary temperature, doping level and germanium content, several parameters should be known: $\Delta E_{g,hd}$, $\Delta E_{g,Ge}$, $N_{C,SiGe}$ and $N_{V,SiGe}$.

A. Effective densities of states

Since the lowest conduction band edge is fourfold degenerate and the character of the conduction band in SiGe is the same as that of silicon /13/, the effective density of states in the conduction band of SiGe is approximately 2/3 of that in silicon. For low Ge-fractions, where it is taken into account that also the twofold degenerate upper conduction band states contribute to the electron concentration, $N_{C,SiGe}/N_{C,Si,i}$ can be described by the model from /20/. Since the electron effective mass in silicon, which determines $N_{C,Si,i}$, is a weak function of temperature /21/, it can be assumed that its doping dependence in the degenerate regime is negligible.

In contrast to $N_{C,SiGe}$, the modelling of $N_{V,SiGe}$ is more complicated due to the distortion and nonparabolicity of the valence band /15,16/. However, by means of properly defined hole effective mass (m_p*), the correct relationship between Fermi level and the majority carrier concentration can be accomplished without loss of validity of the Fermi integral /15,16/. The hole effective mass in SiGe is severely influenced by distortion and nonparabolicity of the valence band, and is lower than that in silicon. Moreover, it depends on temperature (T), doping concentration and Ge content (x_{Ge}) /15-17/, thus influencing the effective density of states in the valence band ($N_{V,SiGe}$).

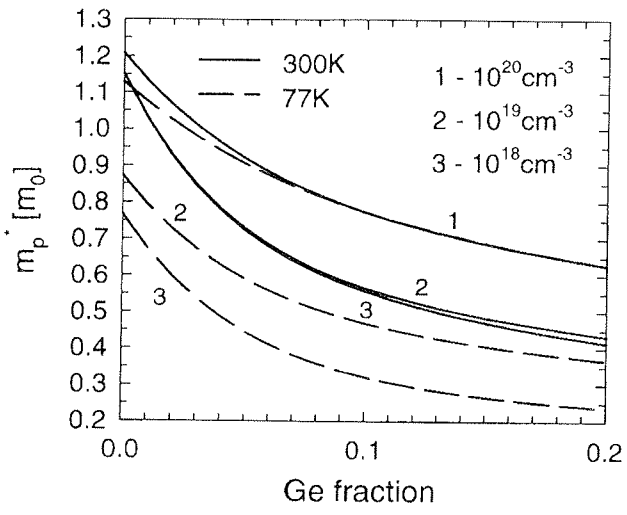

Fig. 1: The hole effective mass calculated with the model proposed in /17/.

A model for $m_p^*(N_A,T,x_{Ge})$ for $77\,K \le T \le 300$ K, $N_A \le 10^{20}$ cm^{-3} and $x_{Ge} \le 0.2$ - taking into consideration both the available experimental data and the theoretical studies of the valence band structure /15,16/ -has been recently proposed /17/. Fig. 1 indicates the most important features of m_p^* in SiGe: strong doping dependence at low temperatures, low temperature dependence at high doping concentrations and strong Ge dependence. The ratio of densities of states between SiGe and intrinsic silicon is presented in Fig. 2, indicating that N_CN_V in SiGe is considerably lower than that in silicon.

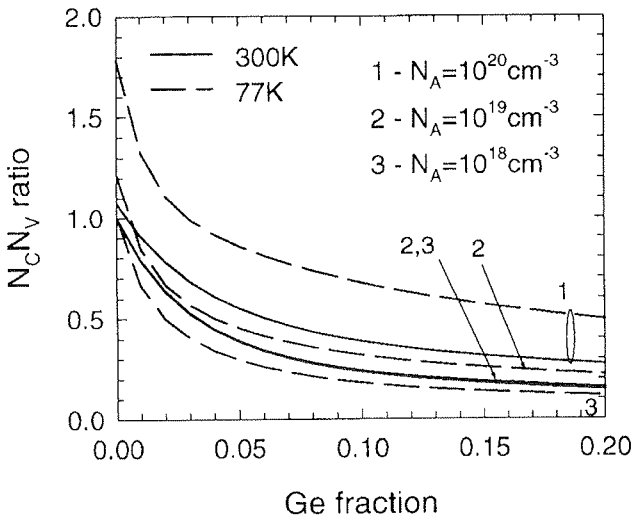

Fig. 2: The ratio of the product of effective densities of states in doped SiGe (including doped Si) and intrinsic Si.

B. Bandgap narrowing due to doping

For doping concentrations higher than $10^{18} cm^{-3}$, the interactions of carriers and dopant atoms cause reduction of the energy gap ($\Delta E_{g,hd}$). Based on the assumption that the doping induced bandgap narrowing in SiGe is of the same origin as, and of the comparable magnitude to the doping induced bandgap reduction in silicon /18,19/, $\Delta E_{g,hd}$ in p-type silicon can be regarded as a measure of doping induced bandgap narrowing in SiGe. A model for $\Delta E_{g,hd}$ in p-type silicon has been recently determined /22/ from measured characteristics of Si BJTs, where it has been assumed that the contribution of Fermi-Dirac statistics can be accounted for by means of the model for $m_p^*(N_A,T,x_{Ge}=0)$ from /17/ (see Fig. 3):

$$\Delta E_{g,hd} = \left(\left(6.76 \cdot 10^{-11} N_A^{0.5}\right)^{-4} + \left(3.58 \cdot 10^{-7} N_A^{0.28}\right)^{-4}\right)^{-1/4} [eV]. \quad (8)$$

Bearing in mind that the doping concentration in the base of an optimized SiGe HBT exceeds $10^{18}\,cm^{-3}$ /1,2/, and in some cases approaches $10^{20}\,cm^{-3}$ /3/, the doping induced bandgap narrowing is an important effect that should be taken into account for analysis and optimization of the base transport properties of SiGe HBTs.

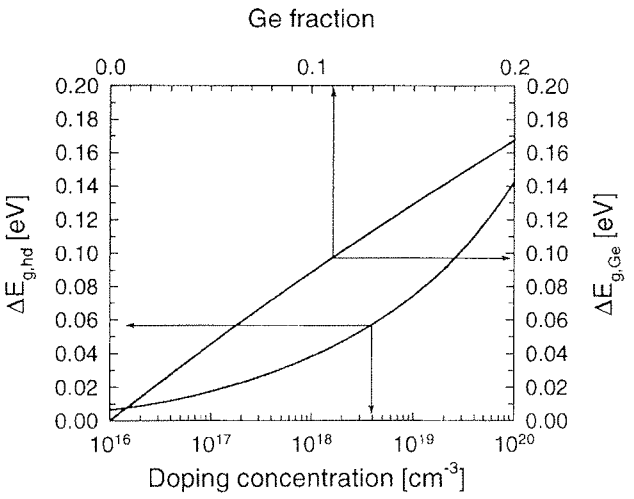

Fig. 3: $\Delta E_{g,hd}$ and $\Delta E_{g,Ge}$ as a function of doping and Ge-fraction, respectively.

C. Bandgap narrowing due to strain and alloying

Compressive strain and alloying cause the energy gap reduction in SiGe base ($\Delta E_{g,Ge}$). Based on a comprehensive analysis of experimental data of SiGe HBTs, and on the assumption that the model for $m_p^*(N_A,T,x_{Ge})$ from /22/ determines the Fermi level shift and $N_{V,SiGe}$ reduction in SiGe, a model for $\Delta E_{g,Ge}$ has been recently proposed /17/ (see Fig.3):

$$\Delta E_{g,Ge} = 0.937 x_{Ge} - 0.5 x_{Ge}^2 \quad [eV]. \quad (9)$$

As can be seen from Fig. 4, even a few percents of germanium result in influential bandgap reduction in the base, consequently influencing the base transport properties of SiGe HBTs. It is worth mentioning that this effect is the most important consequence of germanium in the base, which is basically responsible for the improved properties of SiGe HBTs compared to Si BJTs.

D. Apparent bandgap narrowing

Apparent bandgap narrowing, calculated according to (7) with the models described above, is presented in Fig.4. As expected, ΔG_{SiGe} increases with increasing doping concentration and Ge content. However, eq. (7) indicates that it is generally difficult to isolate the doping effects from those caused by germanium and alloying in ΔG_{SiGe} due to doping and Ge dependence of $N_{V,SiGe}$. An important qualitative difference between apparent

bandgap narrowing in SiGe and Si is temperature dependence /25/. While apparent bandgap narrowing in silicon is temperature independent in the most conditions of interest, ΔG_{SiGe} decreases with increasing temperature even at moderate doping concentrations. This temperature dependence is a result of lower densities of states in SiGe than in silicon, and at very low temperatures or at very high doping concentrations a consequence of Fermi-Dirac statistics. However, as discussed in /23/, the influence of this temperature dependence on transistor characteristics is significant, consequently affecting the interpretation of corresponding experimental data.

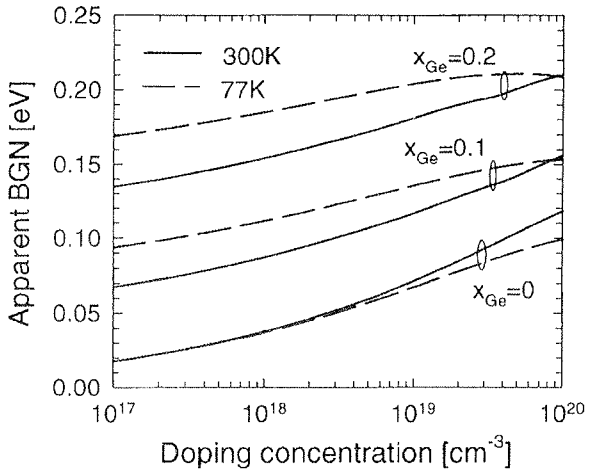

Fig. 4: Apparent bandgap narrowing as a function of doping calculated according to (7).

The model for apparent bandgap narrowing in silicon proposed by Klaassen *et al.* /24/, which is frequently used to account for $\Delta E_{g,hd}$ or even for the complete doping effects ($\Delta E_{g,hd}$ + Fermi-Dirac statistics) in the SiGe base, generally does not correspond to $\Delta E_{g,hd}$. For the doping concentrations higher than 10^{19} cm^{-3} it accounts also for the influence of Fermi-Dirac statistics, which is different in silicon than in SiGe due to lower hole effective mass in SiGe. This difference should be carefully taken into account when Si data are used for modelling doping effects in SiGe devices.

3. Modelling results

It is well known that one of the main advantages of SiGe HBTs compared to Si BJTs - in cases where both devices differ only by the presence of germanium in the base - is increased collector current due to reduced energy gap in the base, resulting in increased current gain (base current of SiGe HBT is comparable to the base current of Si BJT) /1/. Further, the base transit time in SiGe HBTs is decreased due to increased minority carrier mobility and due to energy gap grading which induces an effective electrical field in the base /1/. In this section we analyze several issues related to the base transport properties of SiGe HBTs. In addition to the model for apparent bandgap narrowing in the base and the model for Ge-induced mobility enhancement described above, we also use the model for minority electron mobility in silicon proposed by Klaassen /26/, and the model for intrinsic carrier concentration in silicon suggested by Green /21/.

3.1 SiGe HBT vs. Si BJT performance

The ratio of the current gain between SiGe HBT and Si BJT is presented in Fig. 5. As can be seen, the box Ge profile in the base with 6% of germanium generates almost 3 times higher current gain at 300 *K* than that in Si BJT. The current gain improvement is slightly lower for trapezoidal Ge profile with the same Ge dose, because the electron current in the base is influenced significantly by the bandgap narrowing at the base side of the emitter-base depletion region. As can be seen from Fig. 5, the current gain ratio decreases with increasing doping concentration. This is a consequence of the lower hole effective mass in SiGe, which induces a higher Fermi level shift due to Fermi-Dirac statistics in the SiGe base at high doping concentrations and, consequently, a decrease of electron concentration in SiGe compared to that in Si.

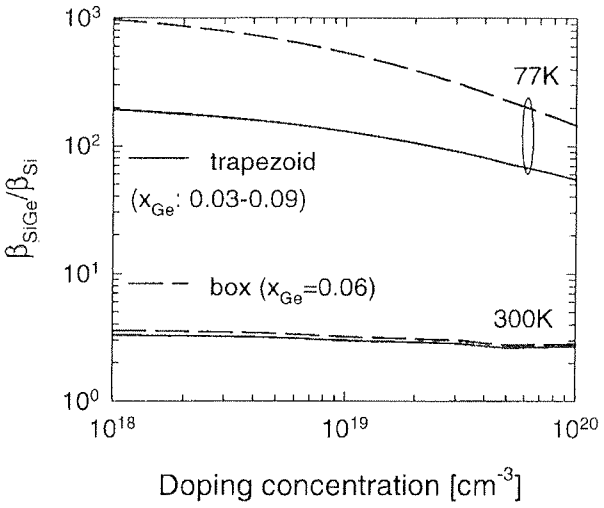

Fig. 5: The ratio of the current gain between SiGe HBT and Si BJT where both devices have the same doping profile.

The base transit time ratio (SiGe HBT vs Si BJT) is presented in Fig.6. While box Ge profile introduces only a minor decrease of τ_B (Ge dependence of minority electron mobility), the trapezoidal Ge profile results in significant improvement of the base transit time. As in the case of base current gain, the base transit time improvement is lowered at high doping concentrations. This result can again be explained by the higher influence of Fermi-Dirac statistics at high doping concentrations, which effectively lowers the grade of germanium in the base.

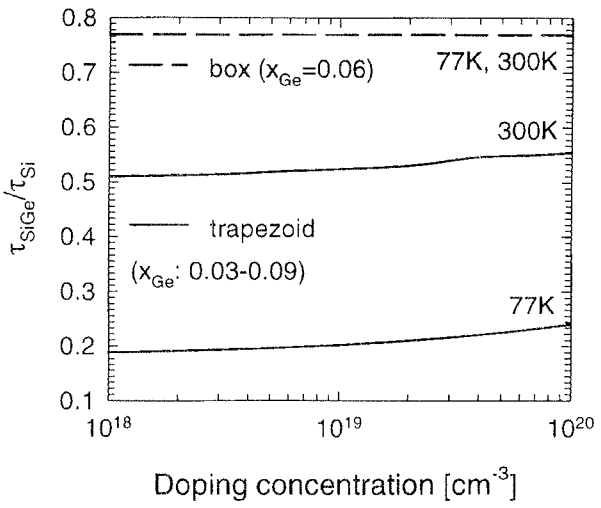

Fig. 6: The ratio of the base transit time between SiGe HBT and Si BJT where both devices have the same doping profile.

3.2 77 *K* vs. 300 *K* operation

It has been demonstrated that SiGe HBTs exhibit completely different behaviour at 77*K* than Si BJTs /5,6/. The current gain of Si BJTs decreases exponentially with decreasing temperature and the current gain degradation of Si BJT is the main reason for these devices being considered as useless for low temperature electronics. In contrast to Si BJTs, the current gain increases with decreasing temperature in SiGe HBTs, resulting in an important achievement for low temperature electronics. In first order approximation this behaviour can be explained by observing apparent bandgap narrowing, because the current gain is proportional to the difference between apparent bandgap narrowing in the base and in the emitter, which is thermally activated ($\beta \propto \exp(\Delta G(BASE) - \Delta G(EMITTER))$; since, in the case of SiGe HBTs $\Delta G(BASE) > \Delta G(EMITTER)$, the current gain naturally improves with cooling. Thermal activation of the apparent bandgap narrowing in the base is also responsible for the improvement of the base transit time at low temperatures. The improvement of SiGe HBTs at 77 *K* is evident from a comparison of 300 *K* and 77 *K* characteristics presented in Fig. 5 and Fig. 6.

3.3 Influence of Fermi-Dirac statistics

The importance of Fermi-Dirac statistics has been traditionally related to the operation of heavily doped emitters of Si BJTs. However, due to the lower hole effective mass in SiGe than in Si, lower possible temperature of operation, and higher doping concentrations in the base, it is expected that the Fermi-Dirac statistics will influence the base transport properties of SiGe HBTs.

The influence of Fermi-Dirac statistics on the collector current of SiGe HBTs at low temperatures has been recently analyzed /27/. It has been shown that Fermi-Dirac statistics is responsible for two effects: the Fermi level shift, which lowers the collector current (a contribution of term D in (7)) and is a major effect of Fermi-Dirac statistics, and an increase of $N_{V,SiGe}$ which attenuates the Fermi level shift (a contribution of term C in (7)) and is a minor effect of Fermi-Dirac statistics. The ratio of the collector current and the base transit time calculated by Fermi-Dirac and Boltzmann statistics is presented in Fig. 7 and Fig. 8, respectively. As can be seen, the Fermi-Dirac statistics influence the collector current more than the base transit time, especially if the temperature is low. In the case of collector current, the box Ge profile is more sensitive to the Fermi-Dirac statistics due to the increased importance of Fermi-Dirac statistics at higher Ge content (lower hole effective mass). It is clear that Fermi-Dirac statistics significantly influences the collector current of SiGe HBTs at 77*K* for all doping concentrations in the base of interest, and

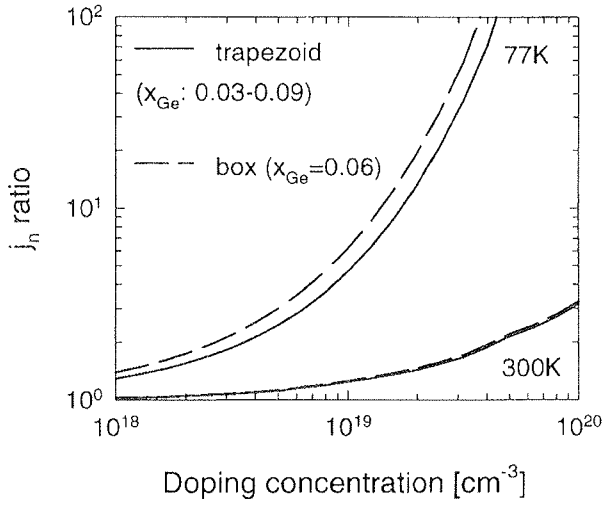

Fig. 7: The ratio of the electron current in the base calculated with Boltzmann and Fermi-Dirac statistics.

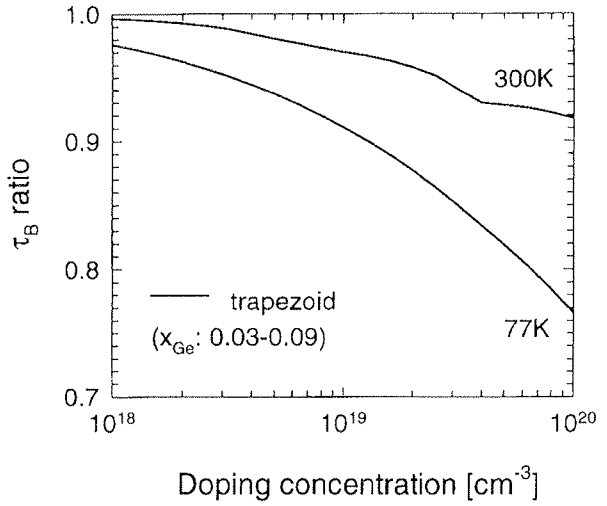

Fig. 8: The ratio of the base transit time calculated with Boltzmann and Fermi-Dirac statistics.

should be taken into account for optimization of these devices. If doping concentration in the base exceeds $4 \cdot 10^{18} cm^{-3}$, the Fermi-Dirac statistics are important for the collector current also at 300 *K*. The base transit time is affected by Fermi-Dirac statistics only if the base doping concentration is very high and operating temperature approaches 77 *K*.

4. Analytical modelling of base transport properties

The analytical model describing carrier transport in the base with uniform impurity profile doped up to $10^{20} cm^3$ and trapezoidal Ge profile with arbitrary grade is important for efficient analysis of the current gain and the base transit time of SiGe HBTs at both 77*K* and 300*K*. Present approaches to the analytical modelling of base transport properties are restricted to the exact consideration of $\Delta E_{g,Ge}$ /1/. Although fundamental insight into the influence of Ge profile on collector current or base transit time can be obtained in this way, accurate modelling and optimization also requires the consideration of Fermi-Dirac statistics as well as the Ge dependence of effective densities of states and diffusion constant.

An approach to the analytical modelling of collector current at 77*K* has been recently presented in /27/. This idea has been further extended for 300*K* analysis and for the modelling of base transit time in /28/. The analytical approach here presented is based on effective Ge induced bandgap narrowing ($\Delta E_{g,Ge,eff}$) /27,28/, which takes into account all Ge dependent effects responsible for minority electron current in the base:

$$\Delta E_{g,Ge,eff} = \Delta E_{g,Ge} + kT\, ln\left(\frac{N_{C,SiGe} N_{V,SiGe}}{N_{C,Si,i} N_{V,Si,i}}\right) + \tag{10}$$

$$+kT\, ln\left(\frac{N_A}{N_{V,SiGe}}\right) - kT\, G_{1/2}\left(\frac{N_A}{N_{V,SiGe}}\right) + kT\, ln(\eta),$$

where η is $D_{n,SiGe}/D_{n,Si}$. Since $\Delta E_{g,Ge,eff}$ is nearly a linear function of Ge fraction at both 300 *K* and 77 *K* (see Fig. 9), an effective trapezoidal Ge profile can be found for every grown trapezoidal Ge profile. By means of an effective trapezoidal Ge profile, analytical expressions for $I_{C,SiGe}$ and $\tau_{B,SiGe}$ can be derived:

$$j_n = \frac{q n_{i,Si}^2 D_{n,Si}}{W_B N_A} exp\left(\frac{qV_{BE}}{kT}\right) \tag{11}$$

$$\frac{\left(\Delta E_{g,Ge,eff}(W_B) - \Delta E_{g,Ge,eff}(0)\right) exp\left(\frac{\Delta E_{g,Ge,eff}(0) + \Delta E_{g,hd}}{kT}\right)}{kT\left(1 - exp\left(\frac{\Delta E_{g,Ge,eff}(W_B) - \Delta E_{g,Ge,eff}(0)}{kT}\right)\right)},$$

$$\tau_B = \frac{W_B^2}{D_{n,Si}\tilde{\eta}} \frac{kT}{\Delta E_{g,Ge,eff}(W_B) - \Delta E_{g,Ge,eff}(0)} \tag{12}$$

$$\left(1 - \frac{kT\left(1 - exp\left(\frac{\Delta E_{g,Ge,eff}(0) - \Delta E_{g,Ge,eff}(W_B)}{kT}\right)\right)}{\Delta E_{g,Ge,eff}(W_B) - \Delta E_{g,Ge,eff}(0)}\right)$$

where $\tilde{\eta}$ represents a position-averaged quantity of $D_{n,SiGe}/D_{n,Si}$. Since η does not significantly depend on x_{Ge}, its averaging appears not to be serious limitation of the model. To complete the model, accurate analytical expressions for $\Delta E_{g,Ge,eff}$ for both 300*K* and 77*K* should be found and these are presented in /28/. Expression (11) clearly demonstrates that the electron current in the base depends significantly on $\Delta E_{g,Ge,eff}(0) + \Delta E_{g,hd}$, which represent the apparent bandgap narrowing and the Ge enhancement of diffusion constant at the base side of the emitter-base depletion region. On the other hand, eq. (12) indicates that the base transit time depends only on the grade of $\Delta E_{g,Ge,eff}$ in the base $(\Delta E_{g,Ge,eff}(W_B) - \Delta E_{g,Ge,eff}(0))$.

5. Conclusions

The electron current in the base and the base transit time are analyzed. The physical mechanisms in the base influencing the base transport properties are described. It is shown that the bandgap narrowing due to strain and alloying, as well as hole effective mass reduction due to distortion and nonparabolicity of the valence

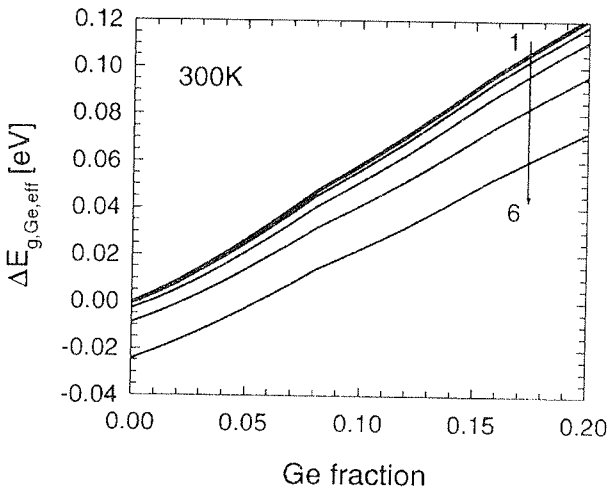

(a)

Fig. 9: Effective Ge-induced bandgap narrowing as a function of Ge fraction. Curves 1-6 correspond to different doping concentrations: $10^{17} cm^{-3}$, $10^{18} cm^{-3}$, $3.2 \cdot 10^{18} cm^{-3}$, $10^{19} cm^{-3}$ $3.2 \cdot 10^{19} cm^{-3}$ and $10^{20} cm^{-3}$. (a) 300 K.

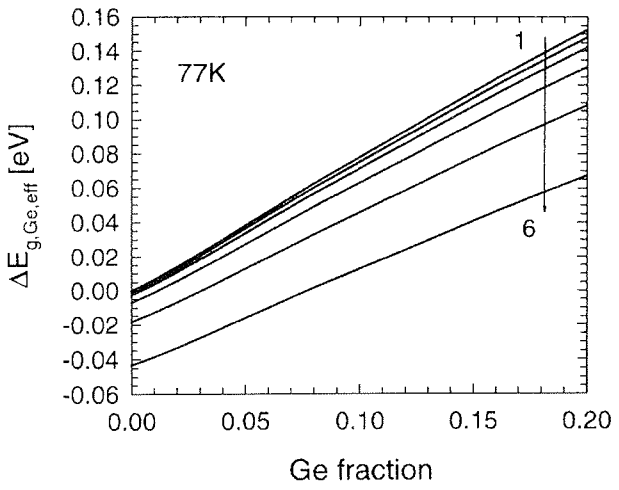

(b)

Fig. 9: Effective Ge-induced bandgap narrowing as a function of Ge fraction. Curves 1-6 correspond to different doping concentrations: $10^{17}cm^{-3}$, $10^{18}cm^{-3}$, $3.2\cdot10^{18}cm^{-3}$, $10^{19}cm^{-3}$ $3.2\cdot10^{19}cm^{-3}$ and $10^{20}cm^{-3}$. (b) 77 K.

band are the most important effects induced by Ge in the base. A set of required models is suggested, and an analytical approach to the modelling of electron current in the base and the base transit time is presented. It has been demonstrated that the improvement of SiGe HBTs compared to Si BJTs decreases slightly with increased doping concentration, and increases significantly with cooling. It has been shown that Fermi-Dirac statistics significantly influence the electron current in the base and should be taken into account for accurate analysis and optimization of SiGe HBTs.

Acknowledgement

This work has been partially sponsored by the Ministry of Science and Technology of the Republic of Slovenia.

References:

/1/ D. L. Harame, J. H. Comfort, J. D. Cressler, E. F. Crabbé, J. Y.-C. Sun, B. S. Meyerson, and T. Tice, *IEEE Trans. Electron Devices.* **42**, 455 (1995), and the references therein.

/2/ D. L. Harame, J. H. Comfort, J. D. Cressler, E. F. Crabbé, J. Y.-C. Sun, B. S. Meyerson, and T. Tice, *IEEE Trans. Electron Devices.* **42**, 469 (1995), and the references therein.

/3/ A. Gruhle, H. Kibbel, U. König, U. Erben, and E. Kasper, *IEEE Electron Dev. Lett.* **13**, 206 (1992).

/4/ D. L. Harame, E. F. Crabbé, J. D. Cressler, J. H. Comfort, J. Y.-C. Sun, S. R. Stiffer, E. Kobeda, J. N. Burghartz, M. M. Gilbert, J. C. Malinowski, and A. J. Dally, *IEDM Tech. Dig.* p. 19 (1992).

/5/ J. D. Cressler, J. H. Comfort, E. F. Crabbé, G. L. Patton, J. M. C. Stork, J. Y.-C. Sun, and B. S. Meyerson, *IEEE Trans. Electron Devices* **40**, 525 (1993).

/6/ J. D. Cressler, *J. Phys. IV* **4**, C6-101 (1994).

/7/ J. D. Cressler, E. F. Crabbé, J. H. Comfort, J. Y.-C. Sun, and J. M. C. Stork, *IEEE Electron Dev. Lett.* **15**, 472 (1994).

/8/ H. Kroemer, *Solid-State Electron.* **28**, 1101 (1985).

/9/ J. C. Bean, *Proc. IEEE* **80**, 571 (1992).

/10/ S. Sokolić, and S. Amon, *Proc. MIEL'95*, p. 385, Čatež, Slovenia (1995).

/11/ J. Poortmans, M. Caymax, A. Van Ammel, M. Libezny, K. Werner, S. C. Jain, J. Nijs, and R. Mertens, *Proc. ESSDERC'93*, p. 317, Grenoble, France (1993).

/12/ S. Decoutere, J. Poortmans, L. Deferm, and J. Nijs, *Solid-State Electron.* **38**, 157 (1995).

/13/ R. People, *IEEE J. Quantum Electron.* **QE-22**, 1696 (1986).

/14/ D. J. Robins, L. T. Canham, S. J. Barnett, A. D. Pitt, and P. Calcott, *J. Appl. Phys.* **71**, 1407 (1992).

/15/ T. Manku, and A. Nathan, *J. Appl. Phys.* **69**, 8414 (1991).

/16/ Y. Fu, S. C. Jain, M. Willander, and J. J. Loferski, *J. Appl. Phys.* **74**, 402 (1993).

/17/ S. Sokolić, and S. Amon, *J. Phys. IV* **6**, C3-137 (1996).

/18/ J. Poortmans, S. C. Jain, D. H. J. Totterdell, M. Caymax, J. Nijs, R. Mertens, and R. Van Overstraeten, *Solid-State Electron.* **36**, 1763 (1993).

/19/ A. Souifi, G. Brémond, T. Benyattou, and G. Guillot, *Appl. Phys. Lett.* **62**, 2986 (1993).

/20/ B. Pejčinović, L. E. Kay, T.-W. Tang, and D. H. Navon, *IEEE Trans. Electron Dev.* **36**, 2129 (1989).

/21/ M. A. Green, *J. Appl. Phys.* **67**, 2944 (1990).

/22/ S. Sokolić, and S. Amon, to be published in *Proc. ESSDERC'96*, Bologna, Italy (1996).

/23/ S. Sokolić, and S. Amon, submitted for publication.

/24/ D. B. M. Klaassen, J. W. Slotboom, and H. C. de Graaff, *Solid-State Electron.* **35**, 125 (1992).

/25/ S. Sokolić, and S. Amon, *Proc. of the 1995 ECS Symp. on Low Temperature Electronics and High Temperature Superconductivity* (ECS PV 95-9, The Electrochemical Society, Pennington), p. 199, Reno, Nevada (1995).

/26/ D. B. M. Klaassen, *Solid-State Electron.* **35**, 953 (1992); *Solid-State Electron.* **35**, 961 (1992).

/27/ S. Sokolić, and S. Amon, *J. Phys. IV* **6**, C3-131 (1996).

/28/ S. Sokolić, and S. Amon, to be published in *Proc. MIEL'96*, Nova Gorica, Slovenia (1996).

dr. Saša Sokolić, dipl. ing.
dr. Slavko Amon, dipl. ing.
Faculty of Electrical Engineering
University of Ljubljana
Tržaška 25, 1000 Ljubljana
SLOVENIA
tel.: (+386 61) 1768 303
fax.: (+386 61) 1264 630
e-mail:
sasa.sokolic@fer.uni-lj.si
slavko.amon@fer.uni-lj.si

Prispelo (Arrived):20.7.1996 *Sprejeto (Accepted): 20.8.1996*

UDK621.3:(53+54+621+66), ISSN0352-9045 Informacije MIDEM 26(1996)3, Ljubljana

HYDROTHERMAL SYNTHESIS OF MnZn FERRITE POWDERS AND THEIR SINTERING

Marko Rozman, Miha Drofenik,
Institut Jožef Stefan, Ljubljana, Slovenia

Keywords: ceramics, MnZn ferrites, nanocrystalline powders, nanosized powders, powder sintering, hydrothermal synthesis, wet chemical method

Abstract: Hydrothermal synthesis was used to produce nanosized MnZn ferrite powder. The results show that the pH value of the starting suspension has a decisive influence on the composition of the hydrothermally prepared MnZn ferrite powder. The grain size of the powder increases with the temperature and time of hydrothermal treatment and also with the concentration of cations in the mother solution. The nanosized ferrite grains are very prone to oxidation and disintegrate above 250°C in air.

Nanocrystalline ferrite powders are very reactive and can be sintered in inert atmosphere at very low temperatures to nearly theoretical density without sintering additives. In compacts prepared from superstoichiometric powders, the formation of intergranular porosity was observed when the sintering temperature exceeds 1000°C. The formation of porosity is a consequence of oxygen evolution from MnZn ferrites in the reaction incorporating excess α - Fe_2O_3 into the spinel lattice.

Hidrotermalna sinteza MnZn feritnega prahu in njegova sinterabilnost

Ključne besede: keramika, MnZn feriti, prahovi nanokristalinični, prahovi nanometerski, sintranje prahov, sinteza hidrotermalna,metode keramične mokre

Povzetek: S hidrotermalno sintezo smo pripravili nanokristalinični prah MnZn ferita. Rezultati so pokazali, da ima pH vrednost izhodne suspenzije hidroksidov precejšen vpliv na sestavo feritnega prahu pripravljenega s hidrotermalno sintezo. Velikost delcev narašča z višjo temperaturo sinteze in s koncentracijo kationov v izhodni suspenziji. Nanokristalinični prah je zelo reaktiven in se pri temperaturah nad 250°C oksidira. V inertni atmosferi se nanokristalinični prah sintra pri nizkih temperaturah do visoke gostote brez dodatkov za sintranje. V oblikovancih z nadstehiometrično sestavo se pri višjih temperaturah sintranja na mejah med zrni pojavi poroznost in gostota sintranim vzorcem se opazno zniža. Povečanje poroznosti pripišemo sproščanju kisika pri vgrajevanju α - Fe_2O_3 v spinelno rešetko ferita.

Introduction

Fine powder preparation has become an important part of modern ceramics research. There is a strong trend towards the application of chemical methods for powder preparation in electronic ceramics. In spite of their initially higher cost than ceramic powders prepared by conventional solid-state reaction of mechanically mixed and calcined starting materials, the improved performance and reproducibility achievable with chemically - derived powders ultimately saves money and adds value. There are various methods of fine powder preparation such as coprecipitation, spray drying, freeze drying, the sol-gel process and the hydrothermal process /1/. Among these processes the hydrothermal method is very promising. It is a typical build-up method where fine particles are made from much smaller particles, such as clusters, molecules, ions and atoms. With ever increasing energy costs, the hydrothermal method could possibly become very attractive for fine powder preparation because of the low temperatures involved and the good sinterability of the powder prepared. The advantages of this process, such as for example the improved control of powder homogeneity and particle uniformity, could make the use of this process dominant for electronic ceramics in the next few years /2,3/.

When we neutralize a nitrate solution of Fe^{3+}, Mn^{2+} and Zn^{2+} ions with ammonia and treat this suspension under controlled hydrothermal conditions a nanosized MnZn ferrite powder can be obtained. The hydrothermal synthesis of ferrites is associated with the chemical reaction (1) /4/;

$$xMn^{2+} + yZn^{2+} + (3\text{-}x\text{-}y)Fe^{3+} + 8OH^- \rightarrow \rightarrow Mn_xZn_yFe_{3-x-y}O_4 + 4H_2O \quad x+y=1 \qquad (1)$$

The aim of this work was to study the relationship between the yield and the composition of the ferrite powder, its homogeneity, morphology and the processing parameters, i.e. the starting composition, the pH value of the suspension, the temperature and the time of synthesis. Additionally, the thermal stability, grain growth and the sintering of nanosized ferrite powder was investigated.

Experimental

Stock solutions containing Fe^{3+}, Mn^{2+} and Zn^{2+} ions were prepared using $Fe(NO_3)_3.9H_2O$, $Mn(NO_3)_2.xH_2O$ and $Zn(NO_3).xH_2O$ (Johnson Matthey) as source materials. The solution of appropriorate ammount of nitrates in deionized water was then hydrolized with diluted aqueous ammonia in a teflon cup. The pH value was varied from 7 to 12 and the residue obtained after filtration was analyzed by atomic absorption spectros-

copy. The pH value was maintained around a value where the concentration of both ions, i.e. Zn^{2+} and Mn^{2+}, found in the residue after filtration was the lowest. When the desired pH value was obtained the teflon cup was mounted in a Parr autoclave (Model 4563M) and heated at a rate of about 3°C/min. The hydrothermal synthesis was carried out under equilibrium water pressure.

After hydrothermal treatment the pressure vessel was cooled and the product was washed free of ammonia salts with hot water and with ethanol to prevent the formation of hard agglomerates, which can cause inhomegeneities in green samples and consequently in the sintered ferrites /5/. The wet powder was granulated with 0,2 % of PEG in ethanol media. The residue obtained after filtration was analyzed by using flame atomic absorption spectroscopy, (Varian - AA5). Individual grains of ferrite were inspected and analized using a TEM (Joel 2000 FX) equipped with a Link EDX system. The particle size determination was performed by employing the XRD line broadening effect /6/. TEM and SEM (Leitz) were used to observe the morphology of the powder and the individual particle size. Thermogravimetric (TGA) and differential thermal analysis (DTA) studies were carried out in an inert atmosphere and air at a heating rate of 5°C/min. The measurements were performed using a Netzsch - STA 409 apparatus. Sintering behavior was checked by dilatometric measurements (BÄHR) and with density measurements.

Results and discussion

Synthesis of powder

In Fig. 1 the pH value of the starting suspension vs. the MnZn ferrite composition after the hydrothermal synthesis is shown. From the diagram we can see that the composition of the MnZn ferrite formed by hydrothermal synthesis strongly depends on the pH value of the starting suspension. $Zn(OH)_2$ is amphoteric and readily dissolved in excess ammonia, while $Mn(OH)_2$ is stable in the more alkali media. The excess of $Fe(OH)_3$ retained when the pH value is not close to 8,6 transforms into α - Fe_2O_3 during hydrothermal treatment. The composition of the powder formed during hydrothermal synthesis from the nominal composition $Mn_{0.5}Zn_{0.5}Fe_2O_4$ can be written as:

$$(0,5\text{-}x)MnO(0,5\text{-}y)ZnO(1\text{-}x\text{-}y)Fe_2O_3 + (x+y)Fe_2O_3.$$

When $x + y > 0$ the excess of α - Fe_2O_3 can be detected in the synthesized ferrite powder. The morphology of the synthesized powder depends on the temperature and time of synthesis as shown on Fig. 2. Fig. 3 shows the TEM image and corresponding diffraction pattern of MnZn ferrite powder prepared at 140°C.

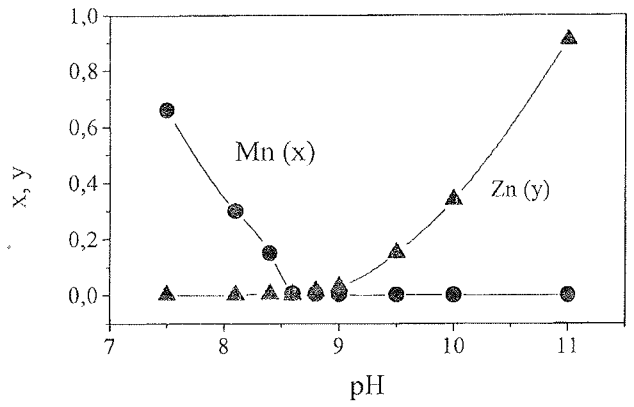

Fig. 1: Composition of the ferrite powder (1/2-x)MnO(1/2-y/)ZnO(1-x-y)Fe_2O_3 +(x+y)Fe_2O_3 formed during hydrothermal synthesis at 140°C vs. the pH value of the initial suspension.

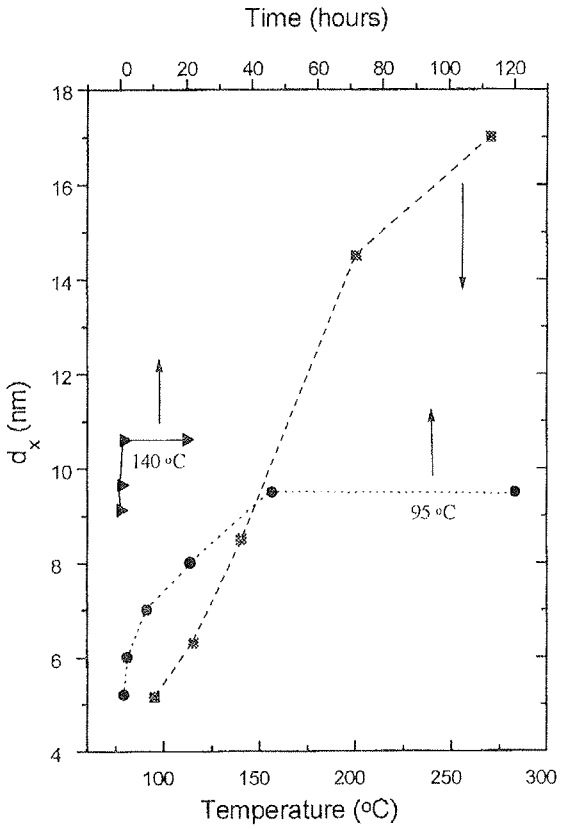

Fig. 2: Average grain size of MnZn ferrite hydrothermally treated for 2 hours at different temperatures and at 95°C and 140°C for various times.

Nanosized hydrothermally prepared powder is superparamagnetic /7/ and above 200°C disintegrates in an oxidizing atmosphere according to the reaction:

$$Mn_xZn_{1-x}Fe_2O_4 + \frac{x}{4}O_2 \rightarrow (1-x)ZnFe_2O_4 + \tag{2}$$

$$+\frac{x}{2}Mn_2O_3 + xFe_2O_3$$

Nanosized MnZn ferrite powder is reactive and can be sintered to high densities at low temperatures.

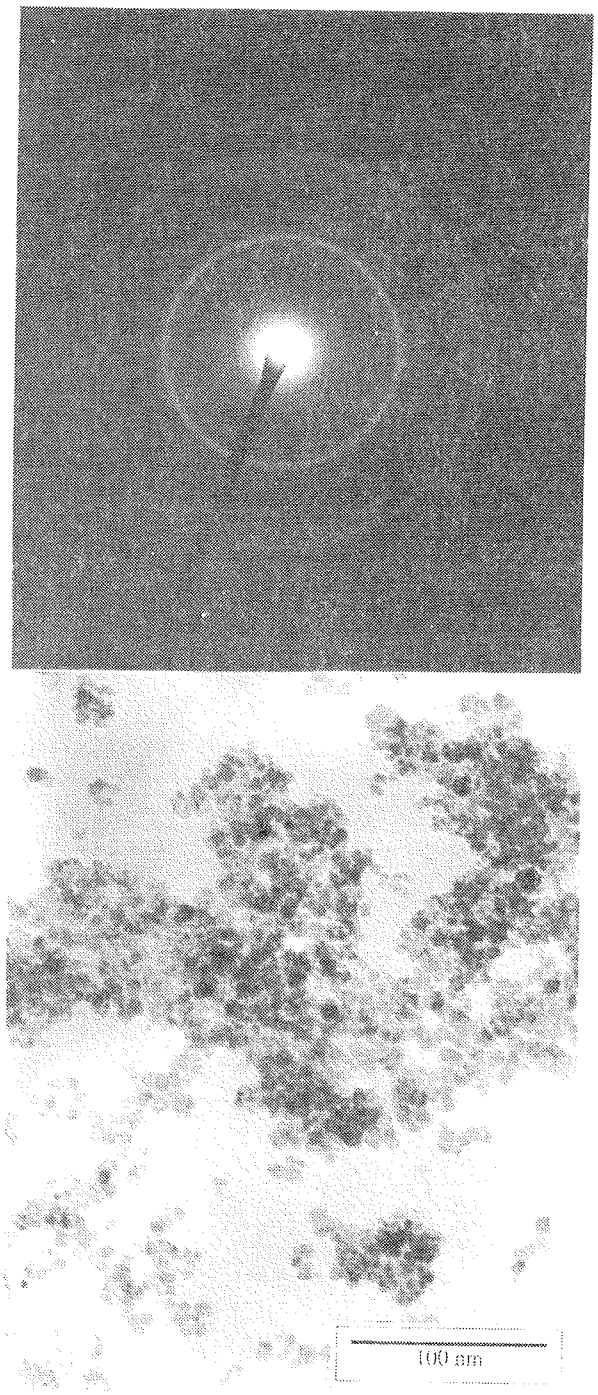

Fig. 3: *TEM image with corresponding diffraction patterns of hydrothermally synthesized* $Mn_{0.49}Zn_{0.48}Fe_{2.03}O_4$.

Sintering of powder

Fig. 4 shows the porous microstructure of nanocrystalline MnZn ferrite sintered in air atmosphere. During heating to the sintering temperature, nanocrystalline MnZn ferrites oxidize in according with reaction (2). In this case reaction sintering takes place resulting in a porous microstructure /8/. To prevent ferrite disintegration nanocrystalline MnZn ferrites must be sintered under equilibrium atmospheric conditions. This means

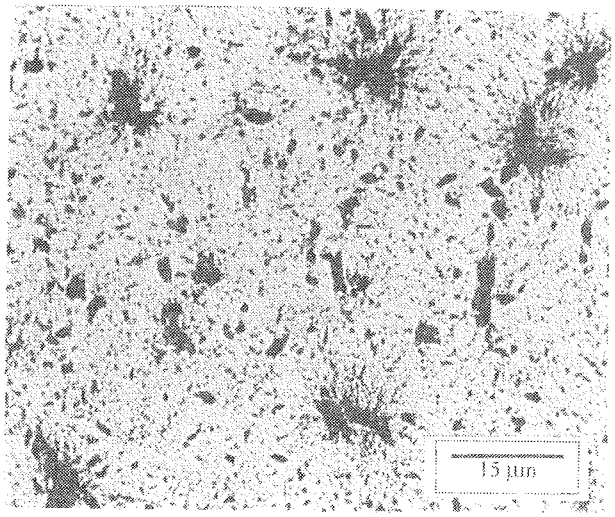

Fig. 4: *Microstructure of MnZn ferrite sintered in air at 1100°C.*

that under 900°C sintering should be performed in an atmosphere of pure nitrogen. In this case very reactive nanosized MnZn ferrites can be sintered to nearly theoretical density at temperatures around 700°C, Fig. 5. However this property can lead in superstoichiometric MnZn ferrites, i.e. a mol ratio of MnO + ZnO/Fe_2O_3< 1, to intergranular porosity when sintering temperature above 900°C is applied. Superstoichiometric MnZn ferrite powders contains excess α - Fe_2O_3 which at temperatures higher than 800°C dissolves in the spinel ferrite lattice, yielding an equivalent amount of Fe^{2+}. This is a desirable for optimization of the magnetic properties of MnZn ferrites. Dissolution of excess α - Fe_2O_3, reaction (3), is associated with oxygen release, as shown in Fig. 6.

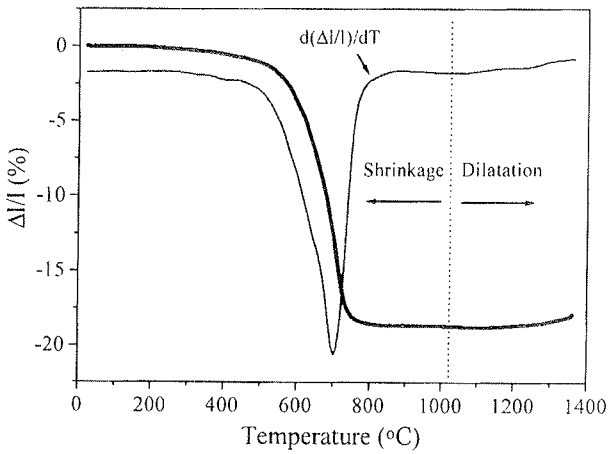

Fig. 5: *Dilatometric curve and its derivation for hydrothermally prepared* $Mn_{0.49}Zn_{0.48}Fe_{2.03}O_4$ *in nitrogen.*

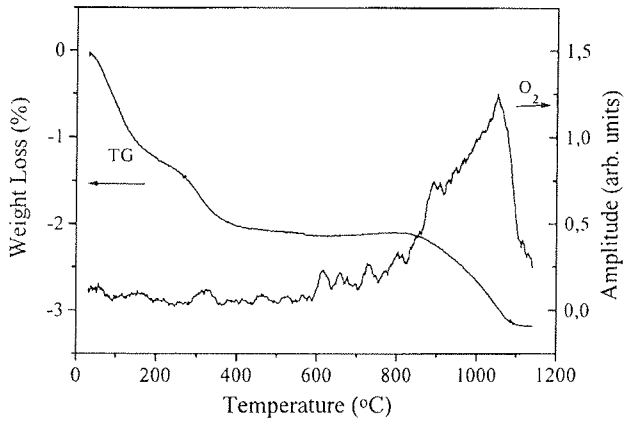

Fig. 6: TGA analysis and evolution of oxygen from superstoichiometric MnZn ferrite powder.

$$Fe^{3+} + \frac{3}{8}V_c + \frac{1}{2}O^{2-} \Leftrightarrow Fe^{2+} + \frac{1}{4}O_{2(g)} \,. \qquad (3)$$

Since the nanosized MnZn ferrites densify to almost theoretical density below the temperature where oxygen release occurs, porosity will be induced in the low permeable dense microstructure. This leads to lower densities of samples sintered at higher temperatures, Fig. 7. To ensure the optimal magnetic properties the grain size of MnZn ferrites should exceed the monodomain size, i.e. 2 μm. A two step sintering profile was applied in order to fulfill this demand. Samples were preheated at 850°C and then sintered at 1150°C. At 850°C a moderate dissolution of α - Fe_2O_3 into the spinel lattice associated with oxygen release can be expected. During further sintering at 1150°C additional grain growth takes place associated with dissolution of the residual α - Fe_2O_3. However in the case of stepwise sintering the accompanying oxygen release and porosity formation will not be so harmful for the microstructure

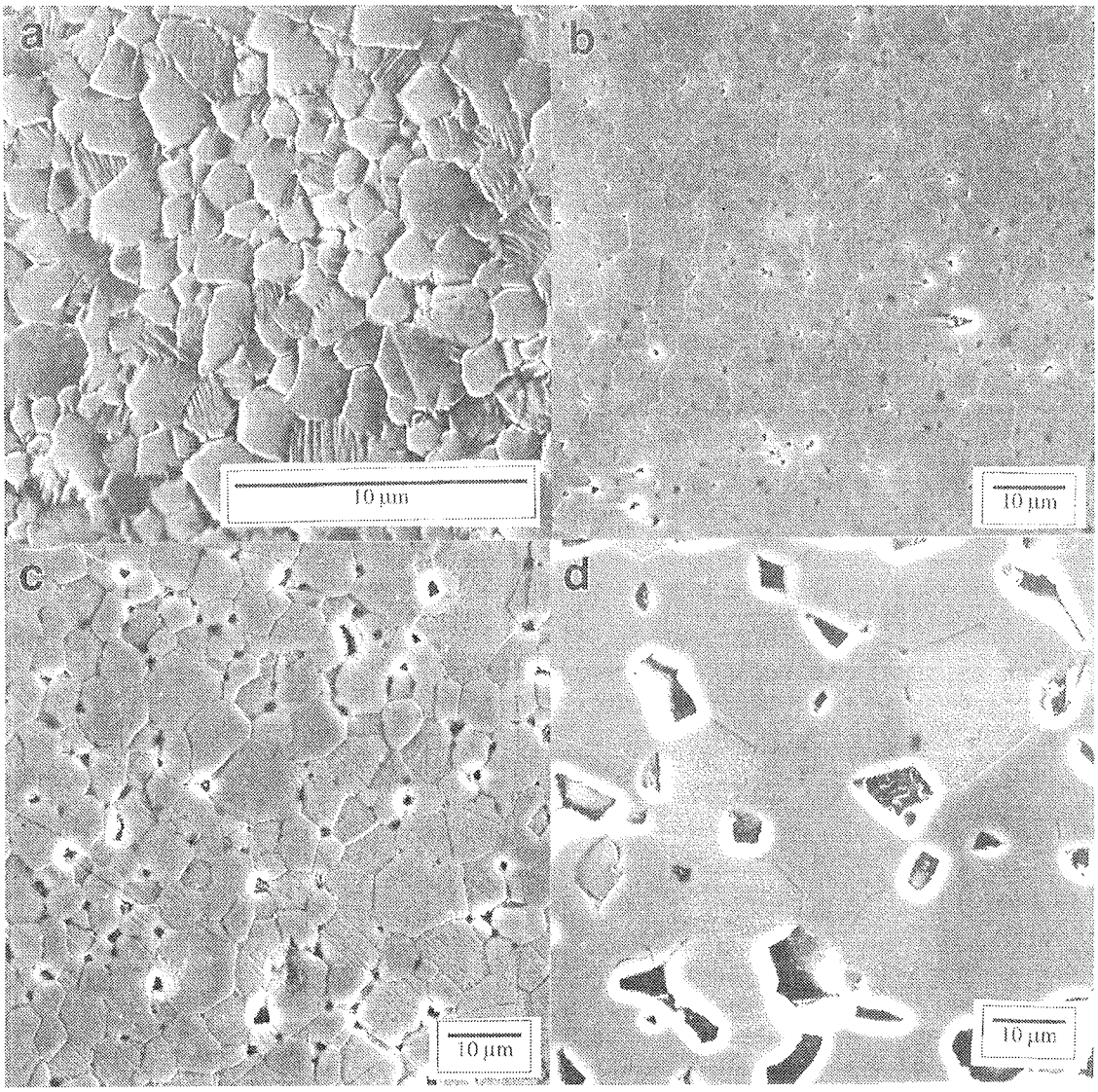

Fig. 7: Microstructures of nanocrystalline $Mn_{0.49}Zn_{0.48}Fe_{2.03}O_4$ sintered under equilibrium atmosphere at: a.) 1000°C , b.)1100°C , c.)1200°C , d.) 1300°C.

evolution. The result of the stepwise sintering is a microstructure with the grain size beyond the monodomain size and with high relative density, i.e. $\overline{D}$ = 4 μm, ρ = 98 % t.d., Fig. 8.

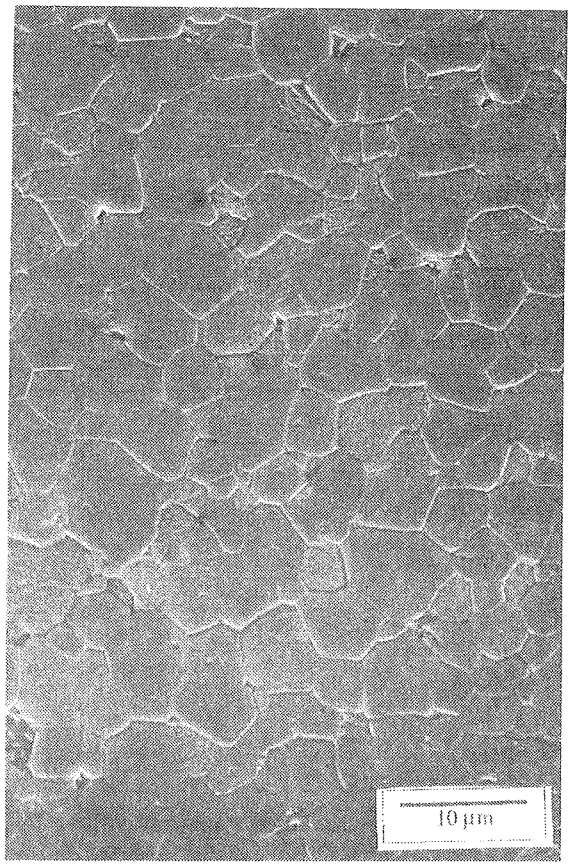

Fig. 8: Microstructure of $Mn_{0.49}Zn_{0.48}Fe_{2.03}O_4$ sintered at 850°C and 1150°C.

Conclusions

Hydrothermal synthesis of MnZn ferrite powder from nitrates neutralized with ammonia yields a nanosized crystalline powder. Control of the stoichiometry of the powder is strongly dependent on the pH value of starting suspension. The ideal pH value for synthesis of $Mn_{0.5}Zn_{0.5}Fe_2O_4$ is 8.6.

Nanocrystalline MnZn ferrites are extremely sensitive to oxidation and completely disintegrate at 600°C in air.

Sintering in air leads to a very porous microstructure due to reaction sintering of disintegration products.

To achieve nearly theoretically dense ferrites, sintering must be performed at low temperatures, between 700°C and 900°C. At higher temperatures (especially above 1200°C) the density of ferrite compacts was significantly lower due to evolution of oxygen.

Stepwise sintering at 850°C and 1150°C enables the preparation of MnZn ferrite samples with a high relative density and grain dimension above the monodomain size.

References

/1/ D. Segal, "Chemical Synthesis of Advanced Ceramic Materials", Cambridge University Press, Cambridge, (1989).

/2/ W.J. Dawson, "Hydrothermal Synthesis of Advanced Ceramics Powders", 67(19), 1673-78 (1988).

/3/ S. Komarneni, R. Roy, E. Brevel, M. Ollinen, Y. Suwa, "Hydrothermal Route to Ultrafine Powers Utilizing Single and Diphasic Gels", Advanced Ceramic Materials, 1(1), 87-92 (1986).

/4/ F. Hagesava, K. Watanabe and K. Nakasaka, "Size Control of MnZn Ferrite Particles Synthesised by the Hydrothermal Process", Ferrites: Proceedings of the ICF-6, T. Yamaguchi, M. Abe, (Ed.), Tokyo and Kyoto (1992), The Jap. Soc. of Powder and Powder Metalurgy, 112 -114.

/5/ M. S. Kaliszevski and A. H. Heuer, "Alcohol Interaction with Zirconia Powders", J. Am. Cer. Soc., 73 (6), (1990), 1504-1509.

/6/ H. Klug and L. Alexander, "X -Ray Diffraction Procedures", John Willey and Sons, New York, (1962), p. 491.

/7/ T. Pannaparayil, R. Marande, S. Komarneni, "Magnetic Properties of High density MnZn Ferrites", J. Appl. Phys. 69(8), 5349-51 (1991).

/8/ F.J.C.M. Toolenaar, M.T. Van Lierop-Verhees, "Reactive Sintering of Manganese Ferrite", J. Mat. Sci. 24, 402-408 (1989).

Mag. Marko Rozman, dipl.ing.,
prof.dr. Miha Drofenik, dipl.ing.
Institut Jožef Stefan
Jamova 39
1000 Ljubljana
Slovenija
tel. +386 61 1773784, +386 61 1773900
Fax +386 61 126 3 126

Prispelo (Arrived): 12.7.1996 *Sprejeto (Accepted): 20.8.1996*

ELECTROCHEMICAL DEPOSITS OF GOLD IN TRANSISTOR ASSEMBLING PROCESS

M. Gojo
Faculty of Graphic Arts, Zagreb, Croatia
N. Cikovic
Faculty of Food technology & Biotechnology, Zagreb, Croatia

Key words: transistor assembling, electrochemical deposits, gold deposition, gold coating, AES analysis, SEM, scanning electron microscope, SEM analysis, Au-Si eutectic alloy

Abstract: A montage of semiconductive components on metal basements in the electronic industry is of the great practical importance. For this purpose the process of electrochemical deposition of gold on the backside of silicium wafer consisting of Au-Si eutectic alloy has been developed.
The process of electrochemical deposition of gold from citrate solutions containing thalium ions is studied on rotating disc electrode using cyclic voltametry the method polarization.
Structure and morphology of gold coatings are determined by AES and SEM methods of analysis.
Gold deposits were observed to be of bright yellow-gold colour and of small-size grain. In the presence of Tl^+ ion was possible to achieve higher current density of gold deposition, but the current rise had no consequences on the grain size.
The chemical composition of Au-Si eutectic alloy had no greater influence on the electrochemical process thus the electrochemical deposition of gold was equal to that one on the pure gold background.

Elektrokemijske prevlake zlata u procesu montaže tranzistora

Ključne riječi: montaža transistorjev, nanosi elektrokemični, nanašanje zlata, prevleke zlate, AES analize, SEM mikroskopi elektronski skanirni, SEM analize, Au-Si zlitina eutektična

Sažetak: Za potrebe montaže poluvodičkih komponenti na metalna podnožja u elektroničkoj industriji razvijen je proces elektrokemijskog taloženja zlata na stražnju stranu silicijeve pločice koja se sastoji od eutektika zlato-silicij.
Metodom cikličke voltametrije, na rotirajućoj disk elektrodi, ispitivali su se elektrokemijski procesi taloženja zlata iz citratnog elektrolita bez i s dodatakom talij (I) nitrata različitih koncentracija.
Struktura i morfologija dobivenih prevlaka zlata određena je AES i SEM analizom.
Dobivene prevlake zlata su plošno centrirane sitnozrnate strukture sjajne zlatno-žute boje. Dodatak talija omogućuje povećanje gustoće struje, no to povećanje ne uzrokuje promjenu strukture taloga.
Kemijski sastav eutektika zlato-silicij nema značajnijeg utjecaja na elektrokemijski proces, odnosno elektrokemijsko taloženje odvija se kao taloženje zlata na zlatu.
Montirani uzorci pokazuju visoki postotak zalegiranosti bez obzira na kemijski sastav i strukturu eutektika zlato-silicij.

1. INTRODUCTION

20 μm gold preform (a thin band of gold with a 0.5 wt% silicon) is used in semiconductor industy for the purpose of assembling semiconductive components

In the process of assembling, the preform is cut into small wafers that are put between the heated basement and a semiconductive element. An electrochemical deposition of pure gold whose properties and thickness allow good assembling was performed on the back-side of a monocrystal wafer containing a layer of vacuum vapoured and alloyed gold; the aim was to reduce the waste as well as to increase productivity and save the precious material.

In order to be applied in semiconductive technology, a gold deposit, apart from the process of gold deposition itself, must fulfil some specific technological requirements such as mechanical properties, eutectic bonding and the purity of gold deposits.

2. EXPERIMENTAL

Samples used in the experiments of cyclic voltametry, AES and SEM analysis as well as in examining the quality of eutectic bonding were prepared from monocrystal silicon wafers of crystalographic orientation (111) and (100). On the frontside of silicon wafer there were active semiconductive components, while on the backside there was a thin layer of gold which has been previously deposited using vacuum vaporization method and then alloyed at 703 K. In all the experiments of cyclic voltametry and elecrochemical deposition of gold, the electrolyte used was a citrate solution containing:

di-basic amonium citrate: $C_6H_{14}N_2O_7$, 50 gdm^{-3} (0.22 $moldm^{-3}$)

potassium gold(I) cianide, $KAu(CN)_2$, 20 gdm^{-3} ($6.94x10^{-2}$ $moldm^{-3}$)

talium(I) nitrate, $TlNO_3$, $3.75x10^{-4}$ $moldm^{-3}$

pH of the elektrolyte was from 5.8 to 6.2.

All the chemicals used were of p.a. purity /1/.

In order to protect the prepared semiconductive components and aluminium contact from the influence of the electolyte, the frontside of the silicon wafer was protected. Satisfactory results of protection were obtained by SHIPLY's pozitive photoresist AZ 1350 J which was applied on the wafer /2/.

Experiments were done in the presence of nitrogen at 343 K. The polarization rate was 20 mVs^{-1} and the potential values were changed from the steady state potential value of +95 mV to -1000 mV. The electrode rotation speed was 500, 750, 1000, 1250, 1500, 1750 and 2000 min^{-1}. The purity of the gold deposits was determinated by AES analysis.

The deposit was etched by argon ions (Ar^+) until the Au-Si interface was reached. In profile analysis, the following parameters were used:

energy of the primary electrone beam 3 keV, electron current 0.5 μA, and the diameter of the electrone beam 40 μm. The ionic etching of the sample was performed by use of the argon ions stream. The applied energy was 1 keV, the ion current intensity 6.8 nA, the angle of incidence 47°. The surface area of the sample was 5 x 5 mm.

Chips with the electrochemically deposited gold were installed on the nickel- plated basements of the type TO 18 and TO 39. The assemling was performed on a semi-automatic machine under following working conditions:

- the temperature in the tunnel: zone A 793 K; zone B 793 K
- the gas flow N_2: zone A 2.5 dm^3min^{-1}; zone B 1.5 dm^3min^{-1}
- H_2: 0.70 bars
- forming: zone A 20 % H_2; zone B 15 % H_2
- the passage rate through the tunel: 2 basements per minute

The research of eutectic bonding was done by a destructive test of plucking the chips from the basement and the criterion of a good eutectic bonding was that minimum 75 % of silicon surface of the chip must remain on the basement.

3. RESULTS AND DISCUSSION

3.1.Polarization Measurements

The elecrochemical deposition of gold on a gold - silicon surface was studied using the cyclic voltametry polarization method.

Figure 1. shows the voltamograms of electrode polarization in citrate solution free from thalium. Starting from the steadystate up to the potential of -700 mV, a small increase of current density was observed while a dependence on the electrode rotation speed has not been noticed.

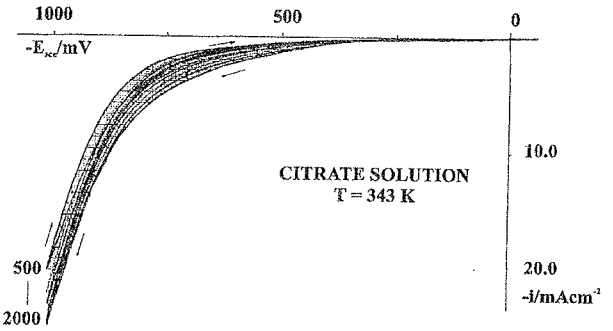

Fig. 1. Voltamograms of chatodic polarization free from thalium

After the potential of -800 mV, the current density was increasing more rapidly and a small dependence on the rotation speed occurs. The reverse branch of the polarization curves follows the starting branch, only the current density is smaller.

The addition of $TlNO_3$ in to the citrate solution considerably changes the electrochemical conditions of gold deposition (fig. 2).

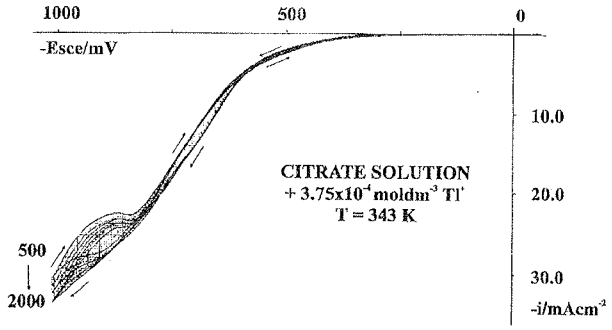

Fig. 2: Voltamograms of chatodic polarization in the presence of thalium

Voltamograms of chatodic polarization of Au-Si eutectic show a slow increase of current density on the starting branch of curves, beginning from the steadystate potential value of +100 mV up to the potential of -300 mV. After this potential, current density begins to increase significantly. At the potential value of -750 mV an inflection occurs after which the increase of current density is not so significant. On the revers branch of polarization curves, the decrease of current density is greater than on the starting branch, in the same area of potential. At -800 mV a stagnation of current density occurs. With the following decrease of the potential, the current density rapidly decreases until -500 mV, then the decrease is somewhat slower until the steadystate potential value is reached.

Voltamograms also show a slight dependence of current density on the electrode rotation speed on both starting and reverse branch of polarization curves as from the potential of -500 mV. The dependence is especially distinct in the area of current stagnation (- 800 mV to -1000 mV), which is due to the change of the reaction mechanism in the presence of thalium.

3.2. AES Analysis of Gold Deposits

By examining electrochemical deposits of gold obtained from citrate electrolyte at 343 K, with applied current density of 1.5 $mAcm^{-2}$, the profile diagram shows that the surface of the deposit consists of about 80 atomic per cent of gold and about 20 atomic per cent of carbon with small treaces of oxygen and nitrogen. The ionic etching removes these impurities and the pure gold remains (fig. 3).

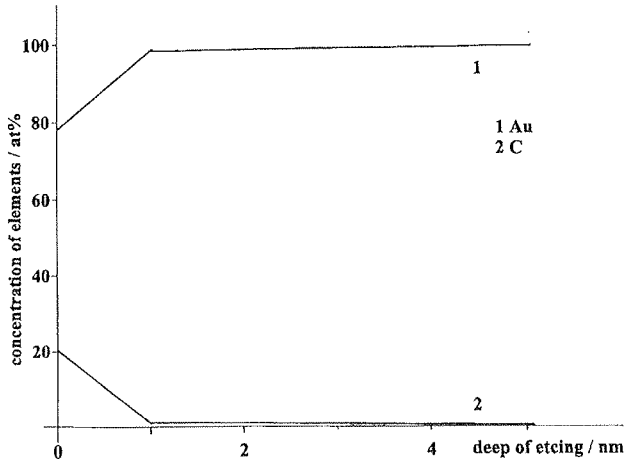

Fig. 3: AES analysis of gold deposit free from thalium

AES Analysis was also preformed on samples obtained from citrate solution containing 3.75 x 10^{-4} $moldm^{-3}$ of thalium, at the temperature of 343 K and the applied current density of 10 $mAcm^{-2}$.

The profile diagram in fig. 4. shows that the surface of the deposit consists of about 80 atomic per cent of gold, 16 atomic per cent of carbon and of impurites in the concentration up to 1 atomic per cent.

By the ionic etching into the inside of the gold deposit up to 1 nm, all the impurities are removed from the surface an the pure gold remains.

The profile diagram (fig. 5) shows clearly that the surface of the sample consists almost of pure gold (99 atomic per cent) and negligible impurities.

By the ionic etching into the inside of sample and through the entire gold deposit, we see that only a pure gold is present in the deposit. When the Au-Si intersurface is reached silicon is registered and its concentration continously increases. Traces of thalium have not been found.

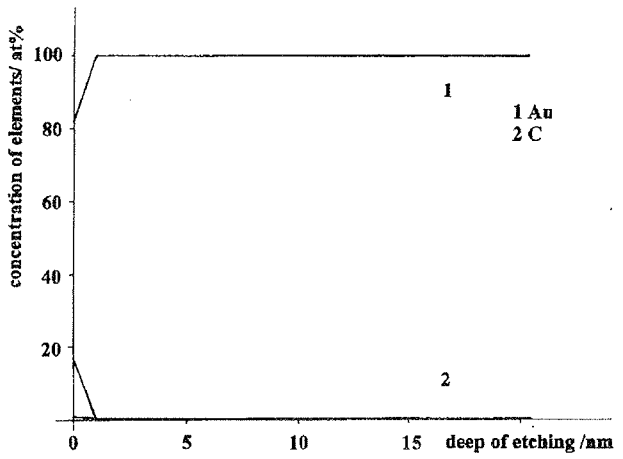

Fig. 4: AES analysis of gold deposit in the presence of thalium

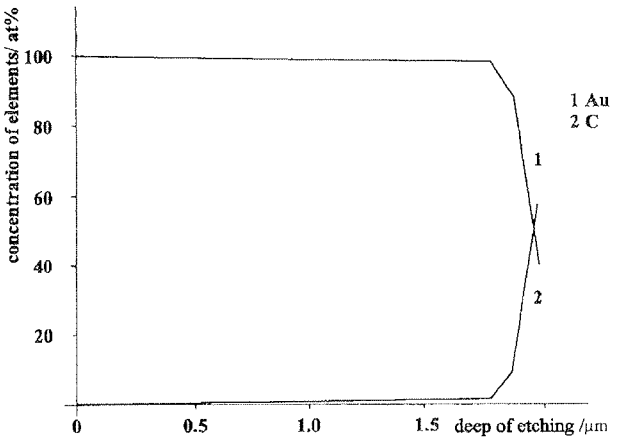

Fig. 5: Profil AES analysis of gold deposit in the presence of thalium

3.3. SEM Analysis of Gold Deposits

Depending on the treatment of the backside of the silicon wafer /3/, the morphology of the gold deposit surface is changed.

The morphology of the surface changes depending on the type of grinding,etching, alloying the vapourized gold and on the electrochemical conditions of the experiment.

After the treatment of the back side of the silicon wafer by etching solution of the composition HF : CH_3COOH : HNO_3 = 1 : 2.5 : 3 and the later vapourizing/alloying of gold a well defined tetrahedronic structure is obtained (Fig. 6).

When an electrochemical deposition of gold is performed on such a surface (experimental conditions: temperature 343 K, current density 1.5 $mAcm^{-2}$, citrate

solution free from thalium) tetrahedrons disappeare and the gold deposit of small size grains is evident (Fig. 7).

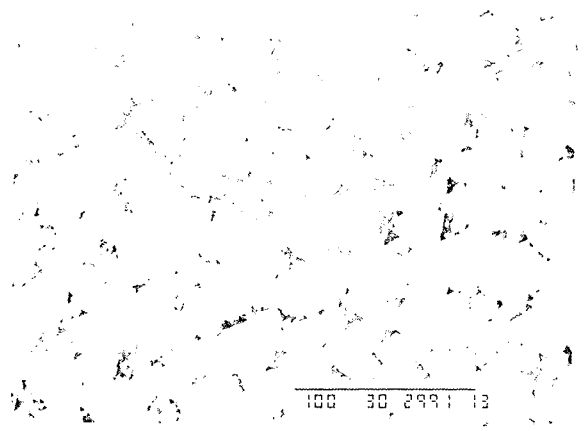

Fig. 6: SEM analysis of the surface silicon wafer with vapourizing and alloying gold deposit

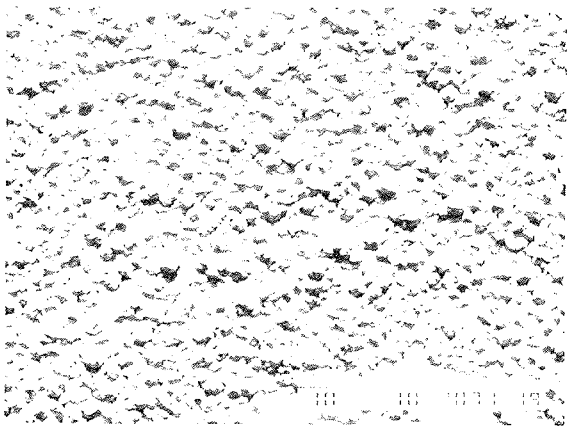

Fig. 7: SEM analysis of gold deposit free from thalium

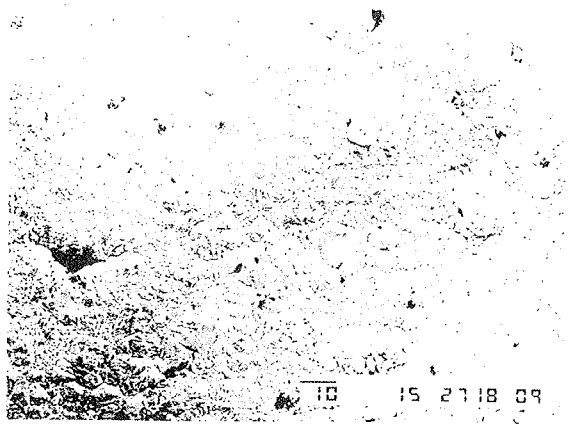

Fig. 8: SEM analysis of gold deposit in the presence of thalium

The addition of 3.75×10^{-4} moldm^{-3} of thaliium into the citrate solution at the same experimental conditions increases to some extend the grain size, but the deposit remains compact and unporous (Fig. 8).

The structure of gold deposit also changes varying the temperature: by the increased temperature the grain size is reduced. The value of the applied current density as well as the concentration of thalium have also a certain effect on the structure of gold deposit. In the presence of thalium and the current density value of 5.0 mAcm^{-2} the gold deposit is still compact and of a fine-grained structure.

Thus depending on the previous treatment of the silicon wafer, the conditions of alloying, the type of the eutectic alloy obtained as well as on the experimental conditions of gold deposition (temperature, current density, stirring) gold deposits of different morphology can be obtained.

3.4. Checking of Eutectic Bonding

A visual analysis of the transistor samples which are assembled on nickel-plated basements of the type TO 18 or TO 39, and which are covered with thin layer of electochemically deposited gold has shown that the eutectic is equally spread all over the surface, it covers well the lateral sides of the chip, the meniscus is of the equal height and it reaches a half of the lateral surface. The chip - basement connection seems to be solid with no indications of bad eutectic bonding, or chip separation from the basement. The eutectic has a regular structure on the chip - basement borderline, and in the part where the eutectic is spread all over the surface of the nickel - plated basement, it looks like fine molten metal. The results of the destructive test of plucking the chip from the basement are shown in table 1:

Table 1: Alloyed of chip without thalium in citrate solution

Sample No:	Eutectic bonding %	Sample No:	Eutectic bonding %
1	100%	14	100%
2	100%	15	100%
3	100%	16	100%
4	100%	17	100%
5	90%	18	100%
6	100%	19	100%
7	100%	20	100%
8	100%	21	100%
9	100%	22	90%
10	100%	23	100%
11	100%	24	100%
12	100%	25	100%
13	100%	26	80%

The addition of thalium into the citrate solution changes the structure of the eutectic, and a visual analysis indicates that it does not cover sufficiently the chip. Such Au-Si chip is an indicator of bad eutectic bonding, but the results show that such an eutectic structure has also high percentage of eutectic bonding (table 2).

Table 2: Alloyed of chip with thalium in citrate solution

Sample No:	Eutectic bonding %	Sample No:	Eutectic bonding %
1	100%	14	100%
2	100%	15	100%
3	100%	16	100%
4	100%	17	100%
5	100%	18	100%
6	100%	19	100%
7	100%	20	100%
8	100%	21	100%
9	100%	22	80%
10	100%	23	100%
11	100%	24	100%
12	100%	25	100%
13	100%	26	100%

4. CONCLUSIONS

References /6/ show that the addition of small amounts of foreign elements into the electrolyte for metal deposition considerably affects the electrochemical process, as well as the structure of the deposits obtained.

The addition of thalium into the citrate solution shifts the potential of the electrochemical deposition of gold towards more positive values, which indicates that a gold deposition is occuring earlier than in the case when thalium is not present in a solution.

At the same time, the addition of thalium makes possible an increasing of the current density, it changes the mechanism of electrochemical deposition of gold due to its catalytic action, it decreases also the activation energy and it has an important influence on electrocrystalization of gold.

The profile AES analysis also indicates the catalytic role of thalium because the presence of thalium is not observed in the gold deposit.

The structure of the deposit also depends on the temperature, current density and the constitution of the electrolyte, which is evident from the morphology of gold deposits.

References /7,8/ prove that different structures of deposits may be obtained from citrate electrolyte, depending on the applied current density and the electrode rotation speed. At smaller values of current density, the gold is configured in face-centered crystal lattice. By increasing current density, the structure of the deposit changes and becomes of the mixed character while at higher values an appearance of peacks is prevailing.

During the electrochemical deposition of gold from citrate solution free from thalium, the maximum current density is about 1.5 $mAcm^{-2}$ at 343 K. The deposit obtained is of small grained face-centered structure, it is of bright yellow colour and fulfil the necessary requirements for semiconductive components.

However, the addition of thalium into citrate electrolyte enables the increase of current density to 5.0 $mAcm^{-2}$ and deposits obtained retain their original colour and structure, and peacks do not appear as it was said in references. The results of eutectic bonding of chips on nickel - plated basements TO 18 and TO 39 indicate that the change in morphology which is caused by the addition of thalium has no effect on the strength of the chip - eutectic - basement link, even the strength is slighly increased. It is obvious that the adsorbtion of thalium on the electrode considerably effects the course of the electrocrystallizaton of gold.

5. REFERENCES:

/1/ M. Gojo, Ph.D. Thesis, University of Ljubljana, Slovenia, (1995).

/2/ M. Gojo, Proc. of Conf. SD '89., Maribor, (1989), 199.

/3/ M. Gojo, M. Petrinec, J. Vuković, M. Turčec, Proc.of Conf. SD '87., Topolšica -Velenje, (1987), 377.

/4/ B. Praček, M. Gojo, Proc. of VI. Yugoslav Vacuum Congress, Gozd Martuljak, (1990), 550.

/5/ M. Gojo, N. Ciković, Proc. of MEET '95, Rijeka, (1995), 2-1.

/6/ J.D.E. McIntyre, W.F. Peck Jr., J. Electrochem. Soc., 123, (1976), 1800.

/7/ H.Y. Cheh, R. Sard, J. Electrochem. Soc., 118, (1971), 1737-1747.

/8/ D.M. MacArthur, J. Electrochemical Soc., 119, (1972), 672.

Dr. Miroslav Gojo, dipl. ing.
Faculty of Graphic Arts,
Univesity of Zagreb
HR 10000 Zagreb, Getaldićeva 2
tel: + 385 1 21 64 44
fax: + 385 1 233 53 97
E-mail: gojo @ magrf.grf.hr.
Prof. dr. Nada Ciković, dipl. ing.
Faculty of Food technology & Biotechnology,
University of Zagreb
HR 10000 Zagreb, Pierottijeva 6
tel. + 385 1 44 00 05, 44 04 22/385
fax: + 385 1 41 82 30
E-mail: ncikov @mapbf.pbfrng.hr

Prispelo (Arrived): 27.5.1996 *Sprejeto (Accepted): 18.6.1996*

UPORABA PLAZME V ELEKTRONIKI
APPLICATION OF PLASMA IN ELECTRONICS

PLASMA PROCESSES

PART III: SURFACE ACTIVATION AND ASHING

I. Šorli*, W. Petasch, B. Kegel, H. Schmid, G. Liebel, W. Ries
*MIKROIKS d.o.o., Ljubljana, Slovenia
Technics Plasma GmbH, Kirchheim, Germany

Applications of plasma processes are becoming increasingly popular in many industrial and research communities. Electronics, microelectronics, automotive, aircraft, and food industry are among the most frequent plasma users. This is not surprising if we consider e.g. the field of cleaning applications. There, plasma cleaning or plasma combined with some suitable wet precleaning technique can totally replace CFC and some other toxic cleaning agents.

The first article described basic plasma physics and plasma generation, the second application of plasma in electronics, while the third one gives an overview of plasma application in the field of surface activation and ashing for trace analysis.

Technics Plasma GmbH in Kirchheim, Germany is among the pioneers and leaders in plasma technology and its application in academic and industrial environments. At the end of this article we will give an overview of their most popular plasma systems.

1.0 INTRODUCTION

Plasma is obtained by producing a discharge in gases or gas mixtures under vacuum through the application of high frequency alternating voltage. The gas in the chamber is brought to an excited (ionized) state. As well, active radicals and UV radiation are released. Electrons and UV light, resulting from the recombination processes are essential for maintaining the plasma. These components are the actual energy carriers, which are ultimately responsible for the production of chemically active radicals. This highly active process gas is capable of reacting with the surface of the material to be treated even at low temperatures. During the process fresh gas is continuously fed into the chamber. The reaction products are evacuated by the vacuum pump.

Plasma excitation via microwaves (2.45 GHz) has proved especially effective, since the efficiency of the gas discharge increases considerably with increasing frequency but still requiring very low electrical power. This results in strong, intensive ionization and production of radicals and thus a more cost effective process. Today's microwave excitation technology makes it possible to use the low pressure plasma processes economically in industrial mass production in either continuous or batch systems using large process chambers. Small bulk parts, as well as large components can be effectively cleaned and activated.

Very important issue of low pressure plasma is its penetrability. The gas enters the smallest crevices, making it possible to process three - dimensional parts with complex geometries. Another very important fact is that plasma processes are environmentally friendly and as such are alternatives to CFC cleaning processes. Thus, main advantages of low-pressure plasma technology are:

- dry process
- energy saving through low power consumption
- inexpensive supplies, cost - effective gases
- switch - off chemistry: the process stops immediately when the power is turned off, no disposal of waste
- cleaner, safer workplace, simple operation
- high penetration power into narrow spaces - an advantage in degreasing or activating parts with complex shapes
- constant process conditions, good reproducibility
- meets or exceeds air emission standards
- parts are absolutely dry after treatment

2.0 SURFACE ACTIVATION

In order to increase adhesion properties of nonpolar plastic surfaces, the treatment in a low pressure, microwave generated oxygen plasma is the key to further processing. Surface energies are raised to levels which ensure excellent adhesion before lacquering, glueing, printing, painting, foaming, coating and laminating.

In table 1 we show surface tension of most commonly used plastic materials. If for example, the paint used for painting the surface of the polymer has higher surface tension than the polymer itself, insufficient adhesion occurs.

The toughest adhesion test to the polymer surface is done with the measurement of wettability, i.e., contact

angle between water drop (water has surface tension of 72 mN/m) and the treated surface, figure 1.

Three phenomena are responsible for changes in the surface characteristics after plasma treatment:

Removal of weak boundary layers

A residue free ashing process removes the surface layers with the lowest molecular weight (i.e., organic separation agents). At the same time, the chemical reaction of the oxygen radicals is responsible for the oxidation of the uppermost atomic layer of the polymer

Cross-linking of surface molecules

Oxygen radicals and UV radiation help break up bonds and promote the three dimensional cross-linking of molecules

Generation of polar groups

Oxidation of the polymer is responsible for the increase in polar groups which is directly related to the adhesion properties of the polymer surface.

Table 1: Surface tension of polymers

Polymer	Surface tension (mN/m)	Comment
Paraffin	19	problematic adhesion
PTFE	18.5	
Silicon (PMDS)	24	
PP	29	
PE	31	
PMMA	33 ... 44	good adhesion
PS	33 ... 35	
PC	34 ... 37	
PVC	40	
PET	43	
PA 6,6	46	
Epoxidharz	47	

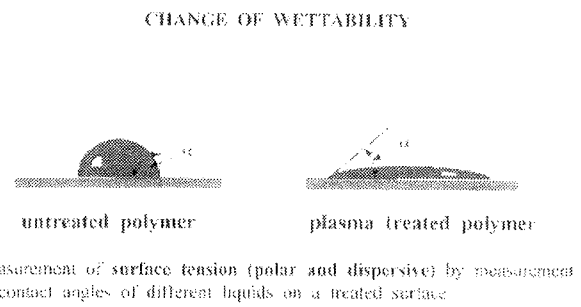

Fig. 1: Measurements of the treated surface wettability

Table 2:

result in %	UNTREATED PP	O_2 TREATED after 8 days	O_2 TREATED after 25 days
Atom C	96	81	85
Atom O	3.5	18	14.5
Bonds C-C	93	75	79
Bonds C-OH	5.5	16	14.5
Bonds C=O	1.5	6	5
Bonds COOH	/	3	1.5

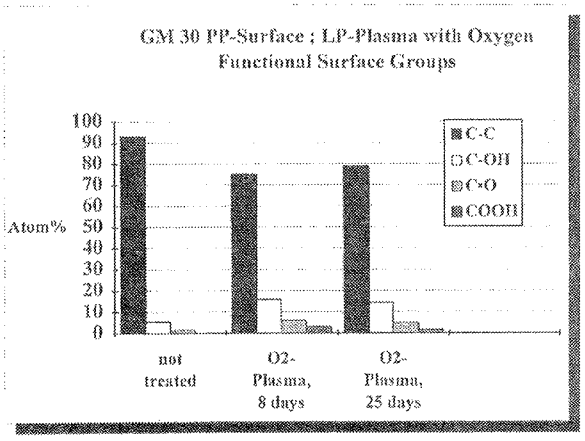

Fig. 2: Functional groups on PP surface before and after oxygen plasma treatment

As a demonstration of the above described phenomena in table 2 and figure 2 we show the results of ESCA (Electron Spectroscopy for Chemical Analysis) measurements of the untreated and treated polypropylene surfaces. The percent change in polar functional groups on the surface is obvious.

The same results are also confirmed by measurements of plasma treated polymer surface wettability. The results in table 3 demonstrate contact angles of plasma treated polymers measured with water (Treated in oxygen plasma for 2 minutes, pressure: 1.65 mbar, power: 200 W).

Table 3: Contact angles of plasma treated polymers

Polymer	Untreated, α in °	Treated, α in °
PVC (polyvinylchloride)	90	35
HDPE (High density Polyethylene)	87	22
PP (Polypropylene)	87	22
PC (Polycarbonate)	75	17
PET	71	18

Another very important and beneficial effect of plasma treatment is that the surface activation stays in effect for long period of time. However, the activated parts loose their activation if they

- are heated to high temperatures, depending on the plastic material
- are thoroughly mechanically scrubbed with a towel or paper
- become contaminated by handling

In table 4 we show the comparison of different methods used for adhesion improvement. Besides some obvious pros compared to competitive processes, plasma has one drawback. Equipment where industrial plasma processes are performed tend to be large and expensive. However, operational costs for plasma process are incredibly low (two process gases and electricity).

Industrial examples of surface activation

- Automobile rear-view mirror housings, as well as automobile bumpers are plasma treated to meet the strict requirements for paint adhesion, figure 3.
- Polypropylene car instrument consoles are activated prior to foaming with polyurethane.
- Polystyrene containers used in biomedical research are hydrophilized in low pressure plasma to facilitate wettability by liquids. These activated surfaces preserve their characteristics for several months. The material itself is not modified by plasma.
- Plastic parts of disposable syringes are pretreated prior to glueing the barrel to the cannula (needle).
- Polypropylene pen casings are plasma treated prior to printing, figure 4.

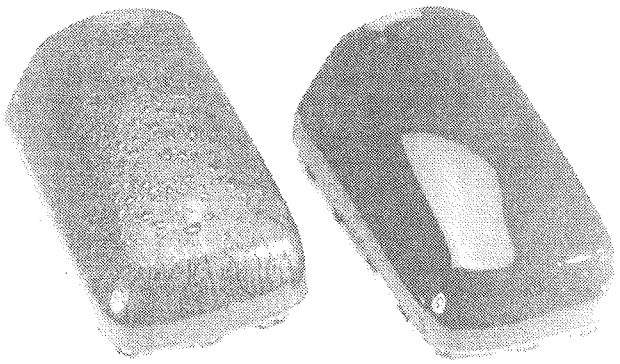

Fig. 3: Comparison of untreated and plasma treated rear - view mirror housings

Table 4: Comparison of different methods used for adhesion improvement

	FLAMING	UV TREATMENT	CORONA	NO-TREAT MATERIAL	GHz PLASMA
ACTIVATION EFFECT	1-2 days	?	6 - 7 hours	activation not needed	5 -7 days
TREATMENT OF 3D OBJECTS	difficult	limited	difficult	/	very suitable
MAX. STRESS DEVIATIONS	large 1- 2 cm	small	up to 1 cm	none	none
SURFACE CLEANING OF PLASTICS	unsuitable	partial	unsuitable	none	very suitable
PLASMA DENSITY	low	medium	medium	/	high
ADHESION PROMOTERS	needed (contain Cl)	needed (contain Cl)	needed	none	none
OPERATIONAL COSTS	high	low	medium	expensive material	low
SAFETY HAZARD	fire risk	low chemical waste	low ozone emission	none	low enviro - friendly
INVESTMENT	low	medium	high	/	medium

- PP and PA capacitor cups and ignition coils housings are activated in plasma in a bulk process prior to mounting and filling with epoxy. This pretreatment was previously performed with chrome-sulfuric acid.
- The PC - Polycarbonate helmet visors are coated with a special lacquer: the surface must be clean and activated in plasma for this purpose.
- POM covers for ski bindings are plasma activated prior to printing
- PP loudspeaker diaphragms are plasma treated prior to glueing

Fig. 4: Treatment of polypropylene pen casings in plasma processor 3000-5D

3.0 APPLICATION OF PLASMA TECHNOLOGY IN TRACE ANALYSIS

Huge advances in the development of analytical methods, such as AAS (atomic adsorption spectro-scopy) and ICP (inductively coupled plasma) open up new frontiers of detection today, which would have been unthinkable a few years ago, As a result of this high sensitivity, the requirements for the organic matrices ashing techniques, which are decisive for the success of an analysis, have also increased considerably.

The earlier small single - or multiple - plasma chamber machines were replaced by large quartz chambers, allowing much larger amounts of substances to be processed. The improved gas flow reliably prevents the mixing of ashes when more than one sample is processed. Smooth shamber walls quarantee clean working conditions.

Plasma ashing as an alternative to wet ashing is:
- gentle
- simple
- clean
- safe
- environment - friendly

The process chamber is hermetically closed, preventing any atmospheric contamination from getting into the chamber. Only gaseous oxygen is used as an oxidant, which makes handling acids unnecessary and trace elements cannot be entrained by the acid.

Here we briefly describe some of the most typical applications:
- ashing of filters for alpha particles determination
- ashing of foodstuff for spectroscopic analysis of anorganic residues
- even materials difficult to ash by conventional methods, are easily prepared in plasma (PVC, PE, PS)
- removal of organic matrices for structural analysis
- preparation of specimen for electron microscopy

Table 5: Typical ashing times for different materials

Specimen	time needed	
Animal feed	appr. 10	hours
Blood samples	2-4	hours
Cane sugar	appr. 4	hours
Cocoa	10-12	hours
Filter	1-2	hours
Hay, grass	10-12	hours
Leaves	4-8	hours
Linseed	5-15	hours
Liver	appr.12	hours
Pumpkin seed	8	hours
Salad oil	appr. 20	hours
Wheat flour	2-3	hours
Cigarettes	appr. 1	hour
Detergent powder	appr. 15	hours
Graphite	3-4	hours
Nylon fabric	3-5	hours
Paper	1-2	hours
Polyamide fibers	2-3	hours
Polyamide granule	6-8	hours
Polyester	appr. 3	hours
Polyethylene	appr. 25	hours
PVC	appr. 20	hours
Soil samples	5-15	hours

Table 6: Overview of Technics Plasma Systems

SYSTEM	GE100	200G	300	Autoload 300 PC	440 -T2000	3000 - 5D	4000 - 7
Generator power, max W	300	400	600	1000	600	4x600	8x600
Process chamber material	Quartz	Quartz	Quartz	Quartz	Aluminum	Aluminum	Aluminum
Chamber volume, l	2	11	19.6	18	43	160	2800
Loading capacity, wafers/run	single	10 - 20	40 - 50	50	depending on substrate	/	/
System control E=single process automatic M=multistep recipe oper.	manual/ timer	E	E or M	E or M	E or M	E or M	E or M
Gas channels	2	2	2 MFC	2 MFC	2 MFC	2 MFC	2 MFC
IR temperature monitor		option	YES	YES			
Optical end point			YES	YES			
Typical applications							
Photoresist stripping	YES	YES	YES	YES+YES			
Substrate cleaning	YES	YES	YES	YES	YES	YES	
Hybrid cleaning	YES	YES	YES	YES	YES+YES		
Etching of passivation layers	YES	YES	YES	YES			
Etching of contact holes	YES	YES	YES	YES			
Polyimide etching	YES	YES	YES	YES	YES		
Depotting of electronic devices	YES+ YES						
Low temperature ashing	YES	YES+YES	YES				
Metal degreasing	YES	YES			YES+YES	YES	
Surface activation	YES	YES			YES+YES	YES+YES	
Surface activation in automotive industry						YES	YES+YES

Normally, specimen are ashed on Petri dishes or ashing plates made of Duran glass or quartz. After initial pump down cycle, oxygen is introduced at a rate of 100 ml/min, and after short stabilization time, plasma is initiated via MW 2.45 GHz magnetron source. The plasma is formed and distributed throughout the chamber, so that the entire volume can be used for specimen treatment. Typical working pressure is about 1 mbar. Reaction products are volatile and are pumped away by means of a vacuum pump.

The ashing time of a sample depends on the type of substance, its weight, ash contents, and the surface exposed to oxygen attack.
Up to 60 g specimens can be loaded in plasma processor 200 G (specially designed for ashing applications). Some typical ashing times on Petri dishes with 0.5 g - 2.0 g sample weight are given in table 5.

4.0 TECHNICS PLASMA LINE OF PLASMA SYSTEMS

With over 15 years of manufacturing experience, Technics Plasma produces plasma systems which guarantee high performance in numerous industrial and R&D applications and communities.

In the last part of the article we present in tabular form the most popular and mostly used plasma systems made by Technics Plasma. As well, their photographs are added.

5.0 LITERATURE

Technics Plasma GmbH, Application Reports

Nowadays, plasma systems are widely used in microelectronics and micromachining technology for resist stripping, thin film etching and bulk silicon etching. Technics Plasma also offers plasma systems specially designed to perform such tasks. However, we did not describe in detail these applications since they will be covered in several articles to be published in near future.

COMMENT: For more information about Technics Plasma systems and their applications, please call:

MIKROIKS d.o.o., Mr. Iztok Šorli
Dunajska 5,1000 Ljubljana, Slovenia
tel. +386 (0)61 312 898,
fax.+386 (0)61 319 170

Plasmasystem GIGA-ETCH 100

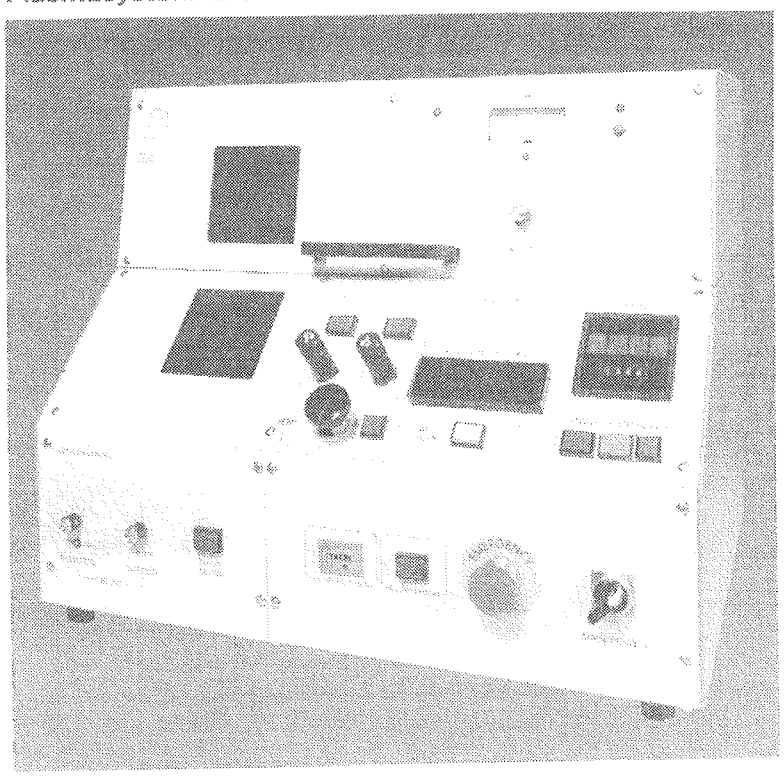

Compact low-pressure plasma system for the laboratory for

- Photoresist Stripping
- Depositing of devices
- Etching of Si_3N_4, Poly-Si and polyimide
- Low temperature ashing

Plasma-Processor 200-G

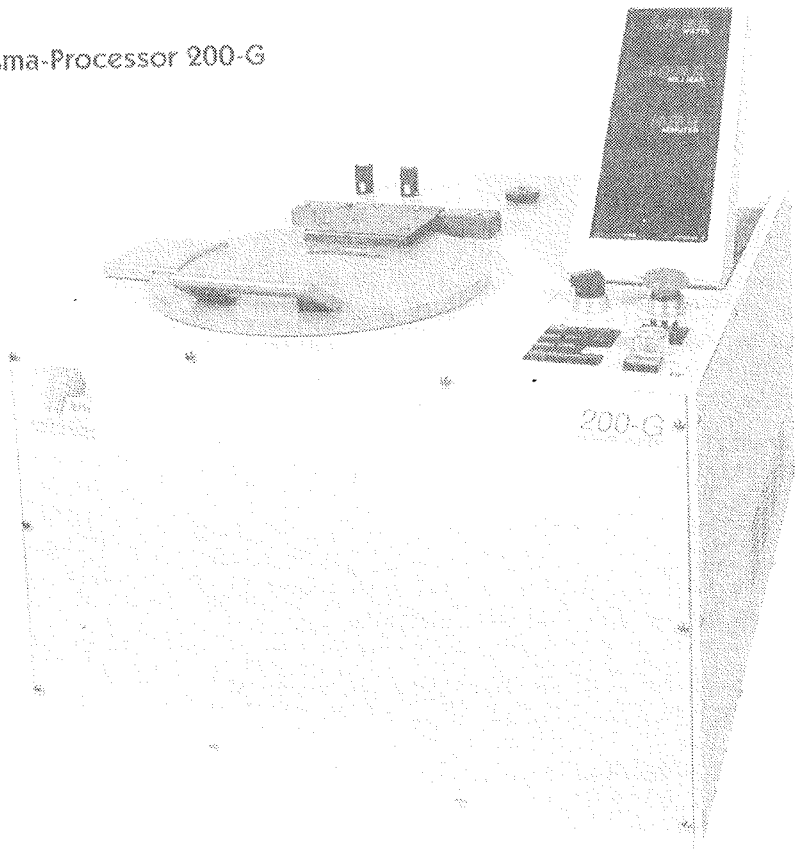

Sample carrier (Pyrex)

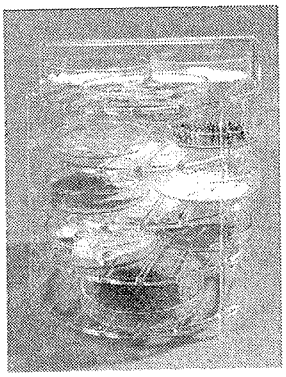

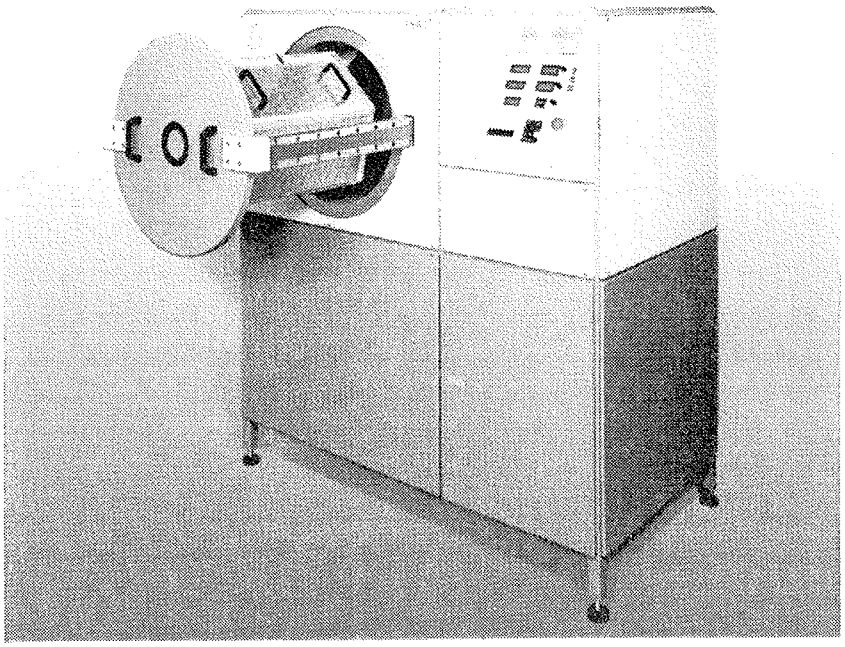

Mod. 3000-5 D Plasma System with bulk treatment drum

PLASMA SYSTEM 4000-7
for surface activation of plastics using microwave excitation

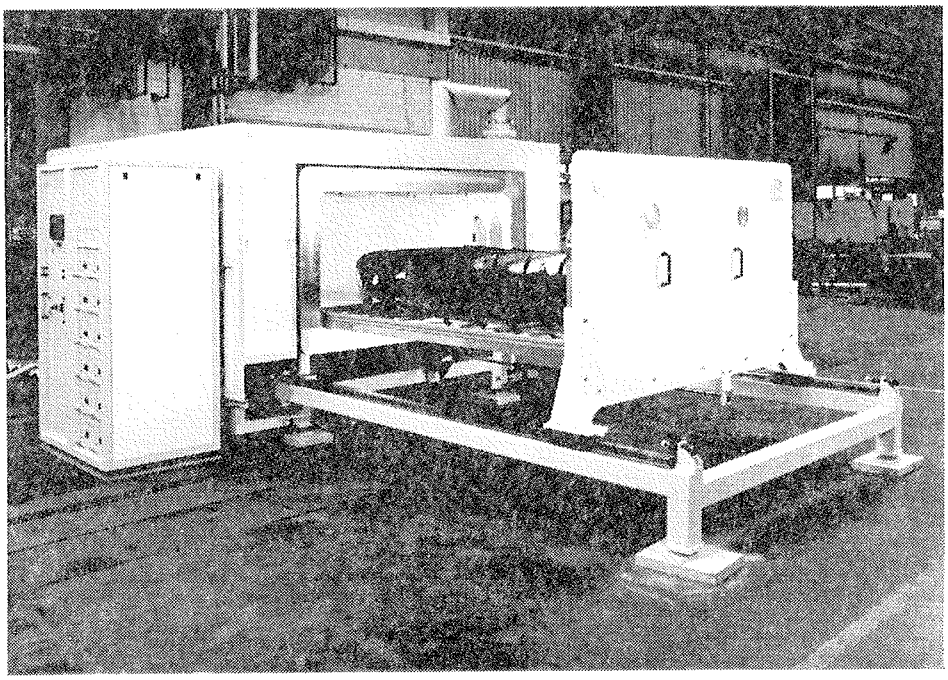

Industrial applications:	*Environmental advantages*
The plasma system 4000-7 is designed for treating plastic parts such as spoilers, instrument panels, wheel covers Surfaces are modified by a low pressure plasma, improving the adhesion of foam padding or paint.	In contrast to conventional treatment methods, plasma technology is environmentally clean. Only small quantities of the process gas such as oxygen are required. Additional safety precautions are not necessary

PREDSTAVLJAMO PODJETJE Z NASLOVNICE
REPRESENT OF COMPANY FROM FRONT PAGE

Novelties in Production Progamme of KEKO VARICON

KEKO VARICON continues 36 year long tradition in the field of electronic ceramic component production in Žužemberk. KEKO VARICON was established in October 1995 by KEKO, d.d. and Technological and Development Fund in order to maintain the production of the products with high marketing potential. So, KEKO VARICON continued the production of the KEKO's oldest and KEKO's youngest products: ceramic disc capacitors and ZnO varistors.

The spectrum of disc capacitors consists of low and high voltage general purpose ceramic disc capacitors, safety capacitors and radio frequency interference (RFI) suppression capacitors. The spectrum of ZnO varistors consists of disc varistors, high energy varistors, automotive varistors and varicons - our version of SMD varistors. So, major part of our production programme is composed of protective devices. It is our goal to widen that part and become the manufacturer of electronic protective devices including the fields of protection against transients, RFI, EMI and over-current and over-temperature protection. New regulations regarding protection against transients, RFI and EMI that came into power in January 1996 in Europe demand and stimulate the consumption of such kind of protective devices.

Approvals by internationally recognized institutions such as UL, CSA, VDE, etc. are an important aspect of sales of protective devices. We have the following approvals for varistors and capacitors:

1. UL, CSA and VDE approval for CV Series of disc varistors
2. CSA, VDE, S, N, D and FI approvals for safety and RFI suppression capacitors

Certain major changes have occurred in the field of disc varistors recently. Disc varistors are relatively old product with standard widely accepted performances. However, their performances are presently a matter of great improvements. We closely follow these trends, and we will be able to offer VDE approved varistors of size 10 mm, 14 mm, 20 mm and 23 mm with improved current and energy handling capabilities in near future. Our new CV^+ Series that covers AC operating voltage range from 60 V to 550 V, consists of 10 mm, 14 mm, 20 mm and 23 mm disc varistors with the following current handling capabilities:

Imax (8/20 μs) for ϕ 10 mm = 3,000 A
Imax (8/20 μs) for ϕ 14 mm = 6,000 A
Imax (8/20 μs) for ϕ 20 mm = 8,000 A
Imax (8/20 μs) for ϕ 23 mm = 2 x 8,000 A

We introduced similar improvements into our SV Special Varistor Series, where the spectrum of maximum surge currents is wider: ϕ 10 mm - 3,000 A, ϕ 14 mm = 6,000 A, ϕ 18 mm = 8,000 A, ϕ 20 mm = 10,000 A and ϕ 23 mm = 2 x 10,000 A. UL and CSA approval for this series is pending.

ZOV Series of high energy varistors also went through certain improvements. AC operating voltage now ranges from 60 V to 680 V and our varistors can now withstand higher maximum surge currents:

ZOV 23 mm -13,000 A
ZOV 25 mm -15,000 A
ZOV 32 mm - 30,000 A
ZOV 40 mm - 45,000 A
ZOV 60 mm - 80,000 A

Constant trend toward miniaturisation in electronics increases the demand for SMD varistors. Our VARICON ZV, AV and DV Series are especially competitive in that field both in automotive and low voltage electronics. When compared to electrically equivalent disc varistors they:

1. Require much smaller space on the PCB,
2. Guarantee much faster speed of response to transient surges
3. Have lower clamping voltage providing better protection level
4. Guarantee better flammability rating as they have no plastic coating
5. Provide continuous operating temperature up to +125 °C

There is one field of voltage surge protection where it is not at all possible to apply disc varistors due to their slow response, high capacitance and inductance and big size. This is the field of protection against electrostatic discharge (ESD). This kind of surges presents major cause of failures in CMOS and BiCMOS ICs with supply voltages in the range of 3 V to 20 V. Within ZV Series we offer special kind of SMD varicons that can satisfy all the requirements for efficient protection against ESD.

KEKO VARICON, d.o.o.
Grajski trg 15, 8360 Žužemberk
Phone (+386 68) 87-671
Fax (386-68) 87-634

Proizvodni program

KEKO VARICON

Keramični kondenzatorji

SLC	K Serija - Disk	KV Serija - Visokonapetostni	KZ Serija - Zaščitni	KM Serija - Proti motnjam
Kapacitivni obseg	**0.56 pF do 18 nF**	**2.2 pF do 10 nF**	**33 pF do 4.7 nF**	**1 nF do 10 nF**
Nazivna napetost	100 V, 500 V	1 - 10 kV	400 V/50 Hz	250 V/50 Hz
Temperaturna karakteristika	Tip 1, Tip 2	Tip 1, Tip 2	Tip 2	Tip 2 (X1, Y)
Velikost	4 mm do 13 mm	6 mm do 22 mm	9 mm to 22 mm	6 mm do 19 mm
Zaščita	Durez	Durez	Durez/epoksi	Durez/epoksi
Pakiranje	Razsuti ali trakani	Razsuti ali trakani	Razsuti ali trakani	Razsuti ali trakani
Atesti			VDE	VDE, CSA, S, N, D, FI

Varistorji

SLV	CV serija - Disk	CV+ serija - Disk	SV serija - Standardni	SV serija - Po naročilu
Napetost praga	**18 V do 1000 V**	**100 V do 1000 V**	**100 V do 1000 V**	**100 V do 1000 V**
Najvišji tokovni impulz	**100 A do 6500 A**	**3000 A do 10000 A**	**400 A do 12000 A**	**> 5500 A/cm²**
Najvišji energijski impulz	0.3 J do 280 J	17 J do 390 J	2.5 J do 390 J	> 400 J/cm3
Velikost	5 mm do 20 mm	10 mm do 23 mm	5 mm do 23 mm	poljubno
Zaščita	Epoksi	Epoksi	Epoksi	Epoksi
Pakiranje	Razsuti ali trakani	Razsuti ali trakani	Razsuti ali trakani	Razsuti ali trakani
Atesti	C-UL, VDE	C-UL, VDE v testiranju	C-UL v testiranju	

Močnostni	ZOV serija Standardni	ZOV serija - po naročilu
Napetost praga	**100 V do 1000 V**	**100 V do 1000 V**
Najvišji tokovni impulz	**13000 A do 80000 A**	**> 5500 A/cm²**
Najvišji energijski impulz	60 J do 2400 J	> 400 J/cm3
Izvedba	Metalizirana ploščica ali zalit	Metalizirana ploščica ali zalit
Velikost	23 mm do 60 mm	poljubno
Zaščita	Epoksi	Epoksi
Pakiranje	Razsuti	Razsuti

VARICON	ZV serija - Nizkonapetostni	AV serija - Avtomobilski	DV serija Srednjenapetostni
Napetost praga	**4 V do 68 V**	**18 V, 22 V, 27 V, 33 V, 47 V**	**18 V do 470 V**
Najvišji tokovni impulz	**40 A do 1000 A**	**100 A do 4000 A**	**40 A do 1000 A**
Najvišji energijski impulz	0.1 J do 12.0 J	1 J do 45 J	1 J do 23 J
Izvedba	Radialno ožičeni ali čipi	Radialno ožičeni ali čipi	Čipi
Velikost	0805, 1210, 2220	1210, 2220, 3225	3225, 4032
Zaščita	brez/Epoksi	brez/Epoksi	brez
Pakiranje	Razsuti ali trakani	Razsuti ali trakani	Razsuti ali trakani

VARICON	MV Serija - Nizkonapetostni	OV Serija - Avtomobilski
Napetost praga	**4 V do 33 V**	**18 V, 22 V, 27 V, 33 V, 47 V**
Najvišji tokovni impulz	**40 A do 250 A**	**1000 A**
Najvišji energijski impulz	0.05 J do 1.3 J	3.2 J do 6.0 J
Kapacitivni obseg	**10 do 100 nF**	**0.47 do 1.5 µF**
Velikost	1210	2220
Zaščita	Epoksi	Epoksi
Pakiranje	Razsuti ali trakani	Razsuti ali trakani

KEKO VARICON, d.o.o., Grajski Trg 15, 8360 Žuzemberk, SLO, Tel. (+386 68) 87-230, 87-671, Fax (+386 68) 87-634

MIDEM IN NJEGOVI ČLANI, ZANIMIVA POROČILA IN KOMENTARJI
MIDEM SOCIETY AND MEMBERS, INTERESTING REPORTS AND COMMENTS

Ministrov pogled na Eureko

Slovenski tehnološki razvoj potrebuje evropsko oporo

Ministrske konference Eureke v Bruslju se je udeležil tudi naš resorni minister *prof.* dr. *Andrej Umek*. Seveda v razpravah bruseljske konference Slovenija ni bila tako v ospredju kot lani v Švici in predlani na Norveškem - leta 1994 zaradi sprejema v Eureko in lani s svojo uradno predstavitvijo. Tako je imel naš minister na letošnji konferenci na voljo samo nekaj minut za predstavitev slovenskih stališč v zvezi z Eureko. To, kar je tam povedal, pa je bilo povod za naš pogovor z ministrom.

- *V svojem nagovoru na ministrski konferenci Eureke ste napovedali, da bo vaše ministrstvo še naprej spodbujalo in stimuliralo sodelovanje v Eureki. Kako naj bi to potekalo? Kakšne vsote oziroma deleže državnega denarja naj bi v prihodnje dobili tisti, ki bodo sodelovali v Eureki? Bo tega denarja toliko kot doslej ali bo vsak projekt dobil manj, če bo šlo za enako veliko skupno vsoto stimulacij in pričakovano večje število projektov?*

Sodelovanje v mednarodnih projektih, kamor prištevam tudi Eureko, je področje, ki ima že sedaj prednost pri financiranju s strani našega ministrstva in jo bo imelo tudi v bodoče. V proračunu za prihodnje leto bomo ponovno predvideli posebno postavko, ki bo pokrivala naše sodelovanje v Eurekinih projektih. Količino denarja bomo seveda prilagodili njihovemu številu, tako da bomo tudi vnaprej zagotavljali sofinanciranje v skladu z veljavnimi pravili.

- *V omenjeni izjavi na konferenci ste poudarili tudi skladnost veljavne slovenske znanstvene in tehnološke politike s principi Eureke, oz. s pravkar sprejetim srednjeročnim programom Eureke. Toda ali ni to vaše mnenje v nasprotju z dejstvom, da trenutno še ni jasno, kakšna bo usoda novega raziskovalnega zakona, ki bi šele lahko v celoti uresničil omenjeno, z Eureko usklajeno, državno politiko?*

Trdno računam, da bo novi zakon o raziskovalni dejavnosti sprejet, zato ker si evropske usmerjenosti Slovenije na področju raziskovalne dejavnosti brez sprejetja tega zakona ne morem predstavljati. Gre predvsem za evropsko primerljivo univerzo, na kateri po definiciji raziskovalno delo ni financirano samo projektno in za večji poudarek prenosu znanja v gospodarstvo, ter javne službe, skladno z načeli tržne ekonomije.

- *Eureka naj bi se v prihodnje bolj usmerila k srednjim in malim industrijskim podjetjem. V Bruslju ste dejali, da je takšna usmeritev za našo državo zelo ugodna. Bi lahko o tem povedali kaj več?*

V Sloveniji glede na evropska merila prevladujejo mala in srednja podjetja, zato menim, da bo poudarek na razvoju malih in srednjih podjetij omogočil vključevanje v evropske tokove najvitalnejšemu delu slovenske industrije. Ta si bo tako zagotovil tehnološki napredek in s tem konkurenčnost na svetovnem trgu. To je za Slovenijo zelo pomembno - ponuja nam razvojno možnost, ki jo moramo na vsak način izkoristiti.

- *Takoj po ministrski konferenci ste tudi izjavili, da si mora naša država zagotoviti sodelovanje v največjem novem Eurekinem projektu Medei, ki naj bi spodbudil razvoj evropske mikroelektronske industrije. Koga v Sloveniji naj bi vključili v ta projekt? So strokovnjaki že ocenili, da imamo za to realne možnosti, saj naj bi MEDEA po eni strani vključevala predvsem tiste, ki so bili doslej vključeni v JESSi, po drugi strani pa dosežki naše mikroelektronike, razen na posameznih delih tega izredno interdiciplinarnega področja, niso videti posebno bleščeči?*

Mikroelektronika je ena najbolj propulzivnih industrijskih panog v svetu, zato je sodelovanje v Eurekinem projektu MEDEA za Slovenijo izredno pomembno. Vključevanje vsakega podjetja ali raziskovalne institucije v Eureko je seveda njena podjetniška odločitev. Udeležbo Slovencev v Medei lahko zato spodbujamo predvsem z informacijami in tudi z ostalimi spodbudami, ki so že tradicionalno na razpolago ministrstvu za znanost in tehnologijo. Prepričan sem, da se bodo v ta projekt vključile najkvalitetnejše organizacije s področja mikroelektronike in da bodo sestavljale kondenzacijsko jedro, ki bo zagotavljalo tudi širši znanstveni in gospodarski razvoj.

- *Slovenija se je v kratkem času vključila v več kot 20 Eurekinih projektov in s to rastjo prehitela celo veliko bolj razvite države. Kdo ima po vaši oceni največ zaslug za tolikšno uspešnost? Kakšne so možnosti, da bo Slovenija vsaj približno tako uspešna tudi v prihodnje?*

Za sorazmerno veliko udeležbo Slovenije v projektih Eureke ima po moji oceni največ zaslug dejstvo, da Slovenija ne dosega kritične mase za samostojen razvoj. Veliko slovenskih podjetij je očitno pravilno spoznalo, da si lahko Slovenija zagotovi tehnološki razvoj in s tem ekonomsko uspešnost samo s povezovanjem v evropskem prostoru. Zato trdno verjamem v nadaljno uspešno sodelovanje Slovenije v projektih Eureke.

- *Kakšna je vaša osebna ocena pomena Eureke za slovenski razvoj?*

Sodim, da ima Eureka izreden pomen za slovenski razvoj. Omogoča nam, da svoje razvojne projekte uresničimo v povezavi s celotno Evropo in s tem presežemo oviro, ki jo zaradi svoje majhnosti predstavlja nacionalni prostor. Eureka nam tudi omogoča natančnejšo oceno razvojnih projektov in kvalitete predlaganih rešitev. S tem, ko se Slovenija polnopravno vključuje v evropski intelektualni razvojni prostor, si odpira enake možnosti kot druge veliko večje evropske države. To je tudi eden od osnovnih vzrokov za naš vstop v združeno Evropo.

Slovenija ima v Eureki kaj pokazati

Naša državaje doslej v Eureki sodelovala v 24. projektih - v tem številu so že upoštevani 3 projekti, ki so jih pravkar sprejeli na konferenci v Bruslju in že zaključeni projekti s slovensko udeležbo (EU 8 "COSINE" in EU 7 "EUROTRAC").

Nova trojica projektov: EU 1440 "FACTORY", krovni program (takoimenovani umbrella program) s področja robotike, kjer bosta sodelovala ministrstvo za znanost in tehnologijo ter Fakulteta za strojništvo v Mariboru; EU 1589 "EUROCARE ARCH IN-SITU" s področja okolja, kjer bodo sodelovali Restavratorski center RS Slovenija, Zavod za varstvo naravne in kulturne dediščine Novo mesto, Gradbeni inštitut - ZRMK Ljubljana in Milan Kovač Arhitekt d.o.o. Ljubljana kot prijavitelj in koordinator projekta, ter EU "MAINE ISRTDMS" s področja informacijske tehnologije, kjer bodo sodelovali GORENJE INOVA d.o.o. Velenje kot prijavitelj in koordinator projekta, Termoelektrarna Šoštanj in Institut "Jožef Stefan", Ljubljana.

Do letos je imela Slovenija največ projektov s področja varstva okolja, temu je sledilo področje informacijskih tehnologij tehnologija materialov, robotika in komunikacije. Nismo pa bili udeleženi v projektih na področjih medicine in biotehnologije, energije, laserja in transportne tehnologije.

Če primerjamo to s projektnimi deleži v celotni Eureki, vidimo, da ima tudi tam okolje prevladujoč delež po številu projektov, vendar tej sledi medicinska in biotehnologija, na tretjem mestu je informacijska tehnologija, na četrtem robotika in na petem tehnologija materialov. Najmanj projektov je s področja laserja in komunikacij.

Ob izteku prvega desetletja Eureke

To je bil evropski odgovor na ameriško "vojno zvezd"

Minuli teden je bil Bruselj prizorišče sklepnega dela "belgijskega" leta Eureke in to, da je bilo praznovanje desetletnice tega evropskega programa prav v evropski prestolnici, je bila gotovo pomenljiva naključnost. Belgija je namreč do vodilne vloge, ki jo je medtem že dobila Velika Britanija, prišla po vnaprej določenem vrstnem redu, kjer se zvrstijo vse članice Eureke. To zaporedje so v Bruslju določili še za nekaj prihodnjih let: Veliki Britaniji bo sledila Portugalska, tej Turčija, nato bo v letu 2000 prišla na vrsto Nemčija, za njo Španija in Grčija. In kdaj bo v Eureki "glavna" Slovenija? Gotovo bo - Eureki se, tako kaže, obeta dolgo življenje - tudi naša država prišla na vrsto. Kdaj, se še ne ve, vsekakor pa težko pred iztekom prihodnjega desetletja. Ne smemo pozabiti, da se je Slovenija v Eureko vključila takorekoč šele "včeraj", to je leta 1994 - za Madžarsko in Rusijo, vendar pred Poljsko in Češko, ki sta Eurekini članici postali lani. Letos pa se Eurekino članstvo ni povečalo.

Čez kakšnih 15 ali več let, ko bo torej slovensko leto Eureke in bo Ljubljana gostila tedanjih kdo ve koliko članic te skupnosti (zdaj jih je vključno z Evropsko komisijo že 25), bodo nove tehnologije, ki zdaj tudi s pomočjo Eurekinih projektov pospešeno prihajajo v naše življenje, že zdavnaj del vsakdanjosti in človeštvo bo soočeno s tehnološkimi izzivi, ki si jih zdaj težko predstavljamo. Toda naslednje generacije jih bodo morale sprejeti, saj razvojna naglica neusmiljeno kaznuje vsakogar, ki mu v tem drncu zmanjka sape... Posameznike, institucije, industrije, države in tudi celotne kontinente.

Eureka se je rodila prav po zaslugi takšne razvojne grožnje. Ob njenem spočetju sredi osemdesetih let - pri tem je odigrala glavno vlogo Francija, ki pa seveda ideje ne bi mogla speljati brez velike zavzetosti drugih visoko razvitih držav Evropske unije - se je namreč že z vso jasnostjo pokazalo, da bodo nove tehnologije - kompjuterizacija, telekomunikacije, biotehnologije, laserji itd. - dramatično vplivale ne obstoječo industrijsko podobo sveta.

Za Evropo je bilo najbolj dramatično opozorilo to, kar se je tedaj dogajalo v Združenih državah Amerike: Reaganova administracija je lansirala znamenit program "Vojna zvezd", ki je obetal velike spodbude tehnološkemu razvoju ameriške industrije. Najbolje je to razumel tedanji francoski predsednik Franqois Mitterand, ki je s svojimi evropskimi kolegi zasnoval evropski odgovor, imenovan EUREKA.

V desetih letih od 10 do 1000 Eurekinih projektov

Seveda obstajajo še mnogi drugi skupni evropski razvojni programi. Toda Eureka ima med njimi posebno vlogo in tudi veliko prednost v tem, da edina neposredno povezuje raziskovalno sfero in industrijo (zadnja ima pri tem povezovanju tudi ključno vlogo), zaradi takšne naravnanosti pa je Eureka tudi najmanj obremenjena z administriranjem in tudi najbolj prilagodljiva oziroma odzivna za nove potrebe. Primer za to niso samo novonastajajoči programi, temveč tudi denimo to, da so sprva v Eureki sodelovale zlasti velike industrije, zdaj pa vse bolj srednja in mala podjetja.

Leta 1985 je Eureko osnovalo 19 evropskih držav in Evropska komisija. Te so tedaj sprejele takoimenovano Hannovrsko deklaracijo (v njej so opredelili najvažnejše in še vedno veljavne principe delovanja Eureke). Tisto prvo leto so osnovali tudi prvih 10 Eurekinih projektov.

Že leta 1986 jih je bilo več kot 100, tri leta po nastanku Eureke se je število projektov povzpelo na 212, leta 1990 jih je bilo že 369, ki pa bi jim morali prišteti še 26 projektov, kolikor se jih je do tedaj že izteklo. Do leta 1993 se je kljub vse večjemu številu končanih projektov število tekočih projektov še domala podvojilo (omenjenega leta jih je bilo 675), lani pa so izvajali že 720 projektov Eureke, 290 pa se jih je že izteklo. Skupaj torej do letos čez tisoč Eurekinih projektov, ki se jim je na konferenci v Bruslju pridružilo še novih 150.

Projekti Eureke so v veliki meri interdisciplinarni, po prevladujoči usmeritvi pa se delijo na področja materialov, robotike in proizvodne avtomatizacije, medicine in biotehnologije, informacijske tehnologije, komunikacij, energetike, laserske tehnologije, tehnologije transporta in okolja. Za odobritev novega projekta velja nekaj osnovnih pravil: v njem morajo sodelovati partnerji iz vsaj dveh članic Eureke, projekt služi razvoju naprednih tehnologij, ne sme biti namenjen vojaškim namenom in mora imeti zagotovljeno financiranje.

Jasna Kontler - Salamon
DELO, 3.7.1996

MEDEA - evropski odgovor na razvoj mikroelektronike v ZDA in na Japonskem

Slovenija bi si morala prizadevati za pridružitev obetavnemu programu

Na letošnji ministrski konferenci Eureke (bila je junija v Bruslju) so sprejeli okrog 160 novih projektov, a samo enega med njimi - program MEDEA (Micro-Electronics Development for European Applications - razvoj mikroelektronike za evropsko uporabo) so počastili s predstavitvijo na posebni tiskovni konferenci. Toda temu se ni čuditi, saj predstavlja MEDEA v vsakem pogledu daleč najpomembnejši skupni razvojni vložek evropske industrije - v tem primeru industrije s področja mikroelektronike.

Projekt je načrtovan za prihodnja štiri leta (do vključno decembra 2000), stal naj bi okrog 2 milijardi ekujev in obsegal približno 12.000 delovnih let (angleško besedo "manyears" je tako težko pomensko prevesti, da v strokovnem žargonu navadno uporabljajo kar oznako "človek-leto", v tem primeru pa pomeni v povprečju 3000 polno zaposlenih raziskovalcev na leto - kako naj bi te dejansko razporedili v omenjenem obdobju, je razvidno iz tabele ob članku). Največje deleže razvojnega dela v okviru izvedbe projekta MEDEA naj bi prevzeli Nemčija (32 odstotkov) in Francija (29 odstotkov) z 10 odstotki jim sledi Italija.

Spisek industrij, ki so se odločile za vstop v Medeo, vzbuja spoštovanje - najvidnejšo vlogo bodo imele firme Alcatel, ASMI, Bosch Bull, Philips, SGS-Thomson in Siemens. Že iz tega je razvidno, da bo razvojno sodelovanje namenjeno predvsem področjem multimedijev, komunikacij in drugih informacijskih tehnologij, kjer ima mikroelektronika ključno vlogo.

MEDEA je posredno nastala zaradi krize, v kateri se je znašla celotna evropska ekonomija, mikroelektronika pa še posebno, v 80. letih, ko je postalo jasno, da sta ZDA in Japonska (tem pa bi lahko dodali še nekaj držav) neprimerno bolje pripravljeni na nove izzive prihajajoče, globalne informacijske družbe. Omenjeni pretresi so sprožili pobudo Francije, da se najbolj razviti del Evrope razvojno združi preko Eureke, kar je medtem preraslo v množično evropsko sodelovanje (v Eureko je vključenih že 24 držav in Evropska komisija). Življenjski interesi omenjenega dela evropske industrije pa so razlog, da je bil v minulem obdobju najdražji Eurekin program prav JESSI (The Joint European Submicron Silicon Program) in zdaj MEDEA kot njegovo nadaljevanje.

Program Jessi se je začel leta 1989 in v 8. letih je bilo zanj porabljeno 2,5 milijarde ekujev. Polovico tega denarja so prispevale industrije, polovico vlade in Evropska komisija.

Skupno je v njem sodelovalo okrog 210 partnerjev iz 16. evropskih držav (firme, raziskovalni inštituti, univerze in drugi). Skupno je bilo v tem času v ta program vloženih 17.000 razvojnih delovnih ur ("manyears"), od katerih jih je največ prispevala Nemčija (34 odstotkov), Francija (27 odstotkov), Nizozemska (14 odstotkov), Italija (10 odstotkov), Belgija (6 odstotkov) in Velika Britanija (5 odstotkov). V posamezne projekte v okviru JESSI so se vključile tudi Avstrija, Danska, Finska, Grčija, Irska, Norveška, Portugalska, Španija, Švica in Švedska - te so skupno prispevale 4 odstotke razvojnega deleža.

In kakšen je bil učinek tolikšnih vlaganj? Tudi to, kot vse ostalo v tem zapisu, povzemamo iz gradiva omenjene tiskovne konference na letošnji konferenci Eureke. Mednarodna skupina neodvisnih ocenjevalcev je ocenila, da je "JESSI demonstriral prilagodljivost in dinamičnost, temelječo na veliki učinkovitosti in storilnosti". Omenjeni izvedenci so tudi izjavili, da bodo podobni programi v prihodnosti uspešni, če se bodo zgledovali po programu JESSI.

Zgovorno mnenje je dal tudi francoski parlamentarni urad: "Vse države na tak ali drugačen način podpirajo svojo prednostno, a ne dovolj razvito industrijo in pri tem ne sme biti vprašanje to, ali naj Francija ali Evropa promovirata tak program, kot je JESSI, temveč je bolj primerno vprašanje, kako naj države pri tem sodelujejo."

Takšne sodbe resnično zvenijo kot propaganda. Toda v prid programa JESSI in njegovega nadaljevanja, pro-

grama MEDEA, govorijo rezultati, doseženi v minulih letih. Posebno prepričljiv je gotovo izjemen porast tržnega deleža firm, vključenih v JESSI, nekateri izdelki in tehnologije, razvite v okviru JESSI so se uspeli prebiti in uveljaviti tudi na trgu ZDA in Japonske. Razumljivo je torej, da so bili udeleženci v programu silno motivirani za nadaljevanje skupnega dela v Medei.

Po načrtu naj bi bila MEDEA izrazito tržno usmerjena, pri tem pa bi vendar tudi nadaljevala nekatere najbolj obetavne bazične raziskave. Strateški pomen za evropsko gospodarstvo naj bi imela predvsem zaradi razvoja tehnologij in sistemov za informacijsko družbo, oziroma zaradi svojega izjemnega deleža pri razvoju področij, brez katerih sije nemogoče zamisliti predvidene evropske povezave.

Se bo temu programu z velikim poslanstvom priključila tudi naša država? Naš predstavnik na letošnji ministrski konferenci Eureke, minister za znanost in tehnologijo prof. dr. Andrej Umek, je že v Bruslju napovedal, da bo v okviru svojih pooblastil spodbujal takšno odločitev. Zdaj je seveda še prezgodaj za ugotovitev, ali se je slovenska mikroelektronska industrija že odzvala na možnost, da vstopi v uspešno evropsko družbo.

Domnevamo lahko, da to sicer ne bo prav enostavno, saj je krog zaenkrat predvidenih udeležencev v Medei približno tak, kot je bil v programu JESSI. Toda čas za vstop je vendar še ugoden, saj se je pred enim mesecem pričela prva faza Medee, v kateri bo potekalo zbiranje, ocenjevanje in selekcija predlogov. Prvo sejanje osnutkov projektov se bo začelo v začetku septembra, po njihovi strokovni obravnavi pa bo konec leta ocenjevanje projektov. Toda tudi za tiste, ki se ob startu ne bodo vključili, ne bo nič zamujenega - januarja prihodnje leto bodo začeli zbirati pobude za nove projekte.

Kdo je prvi mož Medee?

V Medeo je vloženega veliko denarja in veliko upov. Da se bodo ti izpolnili, je v naslednjih letih potrebno vzorno sodelovanje evropske industrije in raziskovalcev, ki bodo vključeni v ta projekt. To pa je gotovo v precejšnji meri odvisno od pravih odločitev moža, ki je na čelu tega velikanskega projekta - dr. Horsta Naska.

Dr. Nasko je 62-letni Avstrijec, ki je svoj študij elektrotehnike vključno z doktoratom opravil na Tehniški univerzi v Gradcu. Nato je opravljal pomembne funkcije v razvoju in vodenju velikih frm s področja mikroelektronike oziroma informatike.

Začel je leta 1958 v AEG/Telefunken, kjer je do leta 1973 postal eden izvršnih direktorjev, zadolžen za raziskave in razvoj, leta 1977 pa je prevzel še celotni inženiring.1983. leta se je dr. Nasko preselil v firmo Nixdorf Computer AG. Od leta 1990 je podpredsednik upravnega odbora Siemens Nixdorf Informationssysteme AG, med drugim zadolžen za sistemsko strategijo. Ob takih izkušnjah je razumljivo, da je bil dr. Horst Nasko že dolga leta zainteresiran za skupne evropske razvojne programe v okviru Eureke in je tudi aktivno sodeloval pri njihovem nastajanju. Bil je vodja projekta ESPRIT in zelo zgodaj se je vključil tudi v delo JESSI.

Februarja lani je bil izbran za pomočnika vodje projekta JESSI, predhodnika Medee, od lanskega oktobra ga je vodil sam. Novo delo je prevzel ta mesec - čeprav se bo MEDEA, kot je bilo omenjeno, uradno pričela šele prihodnje leto, bo pred tem z njo že veliko opravkov in za Naska bo to gotovo najbolj naporno obdobje.

Jasna Kontler-Salamon
DELO, 7.8.1996

VESTI - NEWS

RAZŠIRITEV TOVARNE SIEMENS V BELJAKU

Po pristopu Avstrije k EU so se povečala konjukturna pričakovanja, zato se je zelo razmahnila investicijska dejavnost. V teku so številna manjša in srednja investicijska vlaganja ter deset zelo velikih projektov v skupni vrednosti 30 mrd šilingov. Med slednje sodi tudi razširitev tovarne polprevodikov v Beljaku. Vrednost tega projekta je 5 mrd šilingov.

Na odločitev koncerna Siemens, da razširi in poveča proizvodnjo polprevodnikov, je vplivalo več faktorjev. Pomembna je stalna 15-20 procentna letna rast v zadnjih 35 letih in predvidevanje, da se bo tak trend rasti nadaljeval še 5-8 let. Za odločitev, da Siemens AG zgradi nov center za proizvodnjo močnostnih polprevodnikov prav v Beljaku pa je bila pomembna dosedanja strokovna in poslovna uspešnost tovarne, njeni kadri in ne nazadnje osvojitev proizvodnje 6" silicijevih rezin, kar je osnova za nadaljno racionalno in cenovno konkurenčno proizvodnjo, poleg tega pa pripravljenost mesta Beljaka, Koroške deželne in Zvezne avstrijske vlade za sovlaganje ter Visoka šola v Beljaku, ki zagotavlja kadre.

Z razširitvijo tovarne se bo Siemens OHG razvil v mednarodni center za raziskave, razvoj in proizvodnjo močnostnih polprevodnikov. Zgradili bodo nov brezprašen (čist) v prostoru, ki bo ustrezal zadnjemu stanju tehnike in najostrejšim zahtevam. Izgradnja bo potekala predvidoma med junijem 1996 in februarjem 1997, ko bo nova hala, opremljena z ustrezno infrastrukturo, sprejela prve nove sodelavce. Postopoma se bo število vseh zaposlenih povečalo od 1600 na 1900. Na novo bodo zaposlili približno 100 strokovnjakov z visokošolsko in

100 s srednješolsko izobrazbo ter 100 strokovno kvalificiranih delavcev. Brez omenjenega dodatnega investiranja pa bi moral Siemens OHG število zaposlenih postopoma zmanjšati na 1200.

V letošnjem letu Siemens OHG načrtuje prodajo v vrednosti 2,9 mrd šilingov, že v naslednjem letu pa bo narastla na 3,2 mrd šilingov.

Uporabnost MOS močnostnih polprevodnikov v obliki diskretnih in integriranih komponent je zelo raznolika. Glavne veje uporabe močnostnih polprevodnikov so v avtomobilski industriji, industrijski elektroniki in v komunikacijski tehniki. Pri proizvodnji avtomobilov pričakujemo, da bo vse več avtomobilov srednjega razreda in ne več samo višjega, opremljenih z elektroniko, ki skrbi za varnost in udobje potnikov. Uporaba novih "inovativnih" polprevodnikov bo omogočila tudi krmiljenje porabe energije in s tem varčevanje z gorivom.

Nova linija za proizvodnjo 6" silicijevih rezin je odprla možnosti za gospodarnejšo proizvodnjo močnostnih integriranih komponent. Ekonomske učinke bo izboljšala tudi uporaba novorazvitih tehnologij S - Smart in SPT - 4 na 6" rezinah. Obe tehnologiji omogočata načrtovanje čipov s 30-45% manjšo površino pri nespremenjenih lastnostih.

Siemens predvideva, da bo obe tehnologiji na 6" rezinah osvojil že v letu 1997, prodajo komponent pa v poslovnem letu 1997/98. Hiter razvoj in natančno načrtovanje omogoča novo razvita CAD tehnika četrte generacije, razvita v sodelovanju med EZM (Razvojni center za mikroelektroniko) in proizvodnjo. S tem bo postala tovarna Siemens OHG v Beljaku konkurenčna največjim svetovnim proizvajalcem.

Pripravila Meta Limpel

SODELOVANJE S TO NA USM

V okviru Ministrstva za znanost in tehnologijo MZT je kot poznano Urad za standardizacijo in meroslovje USM, ki je med drugim tudi pristojen, da v tehničnih odborih TO, ki obdelujejo problematiko elektrotehnike v 53 odborih TO, pripravlja tekste za IZDAJO SLOVENSKIH STANDARDOV. Zaradi pomanjkanja strokovnjakov pa na žalost to ni usklajeno s potrebami gospodarstva.

Za pospešitev tega vas pozivamo, da v okviru vašega društva vzpodbujate vaše člane, ki poznajo problematiko in ki bi bili zainteresirani za sodelovanje s TO, da se prijavijo ali naravnost na USM ali preko Komisije za tehniško regulativo KTR pri EZS. Razpise za sodelovanje v TO-jih objavlja USM v svoji publikaciji SPOROČILA, ki so na razpolago tudi v pisarni EZS, Dunajska 10, telefon 061-316-880.

Elektrotehniška zveza Slovenije,
predsednik,
prof.dr. Plaper Marjan

News from AMS

First 0.8 micron AMS Group Process

The AMS Group announces the introduction of its first new joint process development: A high performance, mixed signal 0.8 micron CMOS process, designated as "CXQ" for 5 Volt applications in double-poly and high resistive poly analogue options.

The new AMS Group process is the result of the harmonized merging of the proven process "CYE" at Austria Mikro Systeme with the Thesys process "CN08" combining and utilizing the superior advantages of both: Coupling the exceptional analogue capabilities of the Austria Mikro Systeme process with the high density digital features of the Thesys process. The harmonized process is supplemented by an RC module consisting of a high resistive poly resistor with a highly linear poly-poly capacitor.

The main advantages of this new process for applications are:

- existing designs can be alternatively manufactured either at Thesys or Austria Mikro Systeme;
- easy migration from the preceding Austria Mikro Systeme or Thesys processes to the new CXQ process with a minimum of design efforts involved;
- added high performance functionality that can be immediately implemented making the final circuit more cost effective, with additional functions at higher densities.

Full compatibility of this process to the previous two original ones is guaranteed: The design rules for the new CXQ process were laid out in such a way as to incorporate all of the analogue cells from the Austria Mikro Systeme process and the complete Thesys digital cell library, hence nearly doubling the number of cells available to choose from.

The AMS Group is currently developing the 0.6 micron version of this process planned to be available in the fourth quarter of this year.

For a free data sheet and further information please contact your local: Austria Mikro Systeme Sales Office or Corporate Communications, Schloß Premstätten, A-8141 Unterpremstätten, Austria.

REPORT TO SHAREHOLDERS FOR THE FIRST HALF OF 1996

Dear Shareholder

We have pleasure in enclosing our shareholder's report (unaudited) for the first half of 1996. In this report we comment on the market situation for microchips, the continuing integration of SAMES and Thesys, the financial results for the period ending 30th June 1996 and the prospects of the AMS Group for the rest of the year.

The AMS Group consists of the parent company Austria Mikro Systeme in Austria, SAMES in South Africa (51 % owned) and Thesys in Germany (51.25% owned).

The Market

During the first half of 1996, the US$150 billion semiconductor industry has encountered an unpredicted worldwide slowdown which has resulted in losses, production cutbacks, plant closures and layoffs. The book-to-bill ratio of the US semiconductor market fell to its lowest for nine years in January at less than 0.8, and still remains at 0.85 in July (Semiconductor Industry Association).

During 1995, 50 new semiconductor factories began production and by the end of the year were running at full capacity, producing chips for a PC boom which failed to materialize. The prices of DRAMS and Megas were slashed and inventories built up.

This collapse affected fully both SAMES and Thesys as foundry suppliers. However, WSTS (World Semiconductor Trade Statistics) indicated at the Vienna Conference in April that the ASICs market, which represents the core business of Austria Mikro Systeme, is not eroding.

The Transition Strategy at SAMES and Thesys

The strategy implemented at both SAMES and Thesys is designed to repeat the ASICs concept which has been successfully developed by Austria Mikro Systeme during the past ten years. As SAMES and Thesys are being transformed into becoming mainly suppliers of ASICs, they are expected to return to profitability. Measures taken to achieve a closer integration of SAMES and Thesys within the Group include:

- Installation of a unified sales and marketing organization;
- Standardization of ASICs designs including common engineering platforms, design tools and resources;
- Merging the advantages of Thesys and AMS processes;
- Adaption of headcount.

It is anticipated that, by the end of 1996, ASICs production will represent approximately 50% of the revenues of SAMES and Thesys. Provided the problems in the microchip market do not get any worse, the remedial measures described above should enable SAMES to break even by the end of 1996 and Thesys by mid 1997.

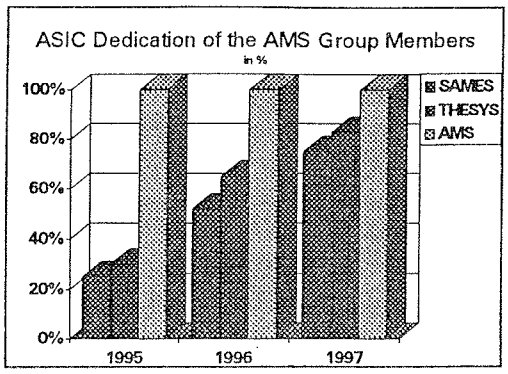

The significant increase in design expertise, product portfolio and production capacity which Thesys and SAMES contribute to the AMS Group, has confirmed the AMS Group as a serious player in the design and production of ASICs. The AMS Group's threefold manufacturing base and its leadership in providing customer oriented solutions enable to compete at the highest level.

Austria Mikro Systeme

The success in providing customer oriented solutions is reflected in the increased level of design work for customers. During the first six months of 1996, Austria Mikro Systeme has seen a significant increase in design projects won.

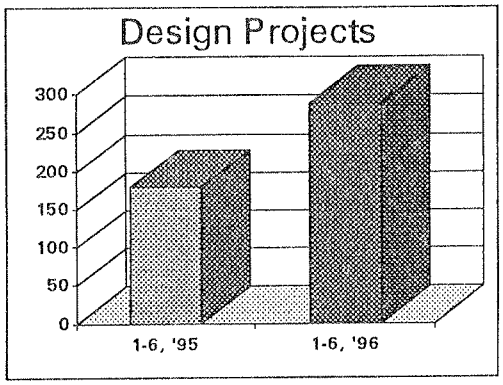

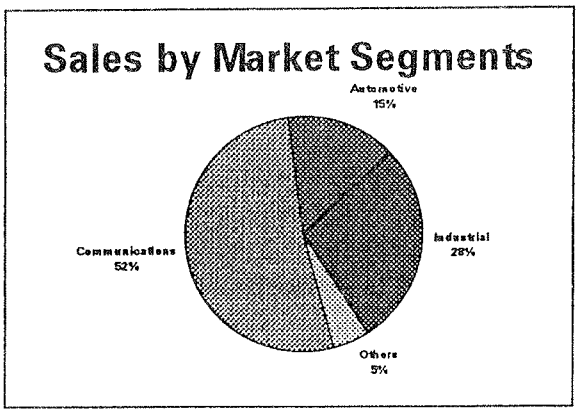

Business has not been affected by price pressure, however, a main customer in the communications sector reduced its demand drastically, resulting in a significant change of the market segments.

New 0.6 micron technology

Austria Mikro Systeme is currently developing a new 0.6 micron process expected to be available in the fourth quarter of this year.

A new high performance mixed signal 0.8 micron CMOS process was introduced by the Group. This offers new potentials for the communications, automotive and industrial markets. The process has been developed as a consequence harmonizing a proven Austria Mikro Systeme process with an advanced Thesys process, combining and utilizing exceptional features of both.

Plans for Unterpremstätten

In response to the challenge of many new design projects, the master plan for a pilot line with submicron manufacturing capabilities of structures of 0.25 microns, adaptable to 0.18 microns and smaller, has been completed. This technology should enable the AMS Group to maintain its lead at the forefront of microelectronics technology beyond the turn of the century. This investment (around 1 billion ATS) was announced last year, however, the pace at which the new technology is introduced will reflect any changes in market conditions.

Law Suit from Lucent Technologies, Inc.

On June 13th, Lucent Technologies, announced that it had filed a patent infringement law suit at the San Jose District Court against Austria Mikro Systeme International AG and its Californian subsidiary relating to areas of wafer etching, chip layout, electrostatic discharge protection and operational amplifier design for products sold into the US.

Lucent Technologies has made similar allegations against other leading US and European semiconductor and equipment manufacturers. The AMS Group has taken appropriate legal advice and has no reason to believe at this stage that these allegations are justifiable and it firmly believes to have valid defenses to oppose Lucent's claims.

SAMES - World Leader in Energy Measurement Solutions

SAMES has developed a new range of ASIC products for the electronic current metering and security and identification markets. SAMES is currently the world leader in energy measurement solutions with ASICs versions ranging from single phase to three phase products.

SAMES aims to become a leader in the security and identification markets. The company is designing a new Universal Security Chip for keyless entry control, garage door initiators, gate controls, alarms and immobilizers.

Thesys - New Universal Serial Bus Standard

Currently each type of PC connector for keyboards and mice, for printers on parallel ports, for modems on serial ports, LAN interfaces and scanners on separate cards, for speakers, microphones, joysticks etc. are not completely interchangeable. The Universal Serial Bus (USB) standard is the solution. By 1997, new PCs will have USB ports built in.

Thesys offers the first generation USB products. There was widespread interest from potential customers at the CeBIT Show in Hannover.

FINANCIALS

The Business Development of the AMS Group

During the first six months of 1996 the three companies within the AMS Group have experienced markedly different conditions.

Austria Mikro Systeme International AG saw turnover fall by 13% compared with the first six months of 1995 but with a satisfactory 26% increase in profit on ordinary activities (see position 12 of the Income Statement). This reflects the strength of the ASICs market where stable prices were maintained in difficult market conditions.

By contrast, SAMES and Thesys, which are still active in foundry business (for other companies), were badly affected by the poor market conditions which have prevailed since the beginning of the year, and saw a very sharp fall in orders and experienced losses as a result.

As stated above, both SAMES and Thesys are being transformed into becoming ASIC specialists. This should protect them from further deterioration in the

	AMS AG			
	1st Half 1996 in MATS	1st Half 1995 in MATS	Change in %	**AMS Group consolidated 1st Half 1996 in MATS**
Sales	**710.4**	814.0	- 12.7 %	**1.056.9**
Order Entry	**565.3**	1,063.3	- 46.8 %	**762.4**
Backlog (30.6.)	**402.4**	998.0	- 59.7 %	**737.0**
Employees (30.6.)	**698**	708	- 1.4 %	**1.448**
Capital Expenditure	**82.6**	138.2	- 40.2 %	**240.0**
Net Income	**102.3**	102.2	+ 0.1 %	**50.2** [1]
Return on Sales (in %)	**14.4**	12.6	-	**4.8**
Cash Earnings	**186.1**	183.6	+ 1.4 %	**142.0**

[1] Excluding Minority Interests

The Income Statement for the First 6 Months of 1996

	AMS-AG 1st 6 Months of 96 (1000 ATS)	1st 6 Months of 95 (1000 ATS)	AMS-Group Consolidated 1st 6 Months of 96 (1000 ATS)
1. Sales	710,422	813,960	1,056,884
2. Movement in partly-finished and finished products inventory and work in progress	-44,386	59,508	-45,246
3. Other operating income	21,702	2,631	98,760
4. Costs of materials and services received	157,193	385,080	308,260
5. Personell expenses	213,146	194,719	386,100
6. Depreciation on intangible and tangible fixed assets	80,375	79,978	190,600
7. Other operating costs	107,755	105,961	199,363
8. OPERATING RESULT	**129,269**	**110,361**	**26,075**
9. Interest income, income from securities and similar income	8,142	4,148	13,068
10. Interest and similar expenses	9,059	12,357	42,227
11. FINANCIAL RESULT	**-917**	**-8,209**	**-29,159**
12. PROFIT ON ORDINARY ACTIVITIES	**128,352**	**102,152**	**-3,084**
13. Extraordinary expenses	-518	0	-518
14. Taxes on income	-25,500	0	-18,921
15. NET INCOME INCLUDING MINORITY INTERESTS	**102,334**	**102,152**	**-22,523**
16. Minority interests	0	0	72,699
17. NET INCOME EXCLUDING MINORITY INTERESTS	**102,334**	**102,152**	**50,176**

[1] The taxes on income for the first 6 months of 1996 were calculated with the expected effective tax rate for the year 1996.

microchip market, giving confidence that they will be able to follow the success achieved by Austria Mikro Systeme.

The following interim financial statements present the results of Austria Mikro Systeme International AG and the consolidated results of Austria Mikro Systeme International AG. The consolidated financial statements are comprised of the financial statements of Austria Mikro Systeme International AG as well as of the subconsolidated financial statements of South African Micro-Electronic Systems (Pty) Ltd. (SAMES) and Thesys Gesellschaft für Mikroelektronik mbH.

Last year's comparable figures are only available for the AG, as the acquisitions of SAMES and Thesys were realized in the 2nd half of 1995.

The consolidated net income for the first 6 months of 1996 amounting to 50.2 MATS comprises of the result of the AMS-AG (102.3 MATS), the results according the participation in SAMES LTD (51 % of -64.9 MATS = -33.1 MATS) and Thesys GMBH (51,25% of -83.9 MATS =-43.0 MATS), consolidation gains of 4.1 MATS as well as income from a release (19.8 MATS) of the negative differences resulting from the initial capital consolidation (97.1 MATS), which were disclosed as provisions

BALANCE sheet as per June 30, 1996

	AMS-AG		AMS-Group Consolidated	
	30.6.1996 (1000 ATS)	31.12.1995 (1000 ATS)	30.6.1996 (1000 ATS)	31.12.1995 (1000 ATS)
ASSETS				
A. FIXED ASSETS	1,444,727	1,444,613	1,936,030	1,915,074
B. CURRENT ASSETS	1,384,900	1,206,676	1,786,101	1,855,747
C. PREPAID EXPENSES AND ACCRUED INCOME	5,317	2,135	22,298	11,037
TOTAL ASSETS	**2,834,944**	**2,653,424**	**3,744,429**	**3,781,858**
LIABILITIES & EQUITY				
A. EQUITY	1,436,491	1,370,157	2,018,728[2]	2,093,015[2]
B. UNTAXED RESERVES[3]	145,556	145,556	0	0
C. SUBSIDIES	10,738	11,278	64,887	73,378
D. PROVISIONS	291,283	242,928	407,806	399,455
E. LIABILITIES	943,319	877,012	1,245,451	1,208,799
F. DEFERRED INCOME	7,557	6,493	7,557	7,211
TOTAL LIABILITIES	**2,834,944**	**2,653,424**	**3,744,429**	**3,781,858**

[2] Including adjustments for minority interests.

[3] The untaxed reserves in the amount of 203 MATS separately disclosed in the individual financial statements are shown in the consolidated statements under equity according to § 253(3) Austrian Commercial Code (HGB).

for restructuring costs at the time of acquisition. The results of the subsidiaries were obtained with turnovers at Thesys of 270.1 MATS and SAMES of 87.6 MATS (including intra group sales).

The Outlook

As stated in the first quarter results, the AMS Group cannot disengage totally from the market pattern which will continue to be determined by worldwide overcapacities during 1996. The overall decline seen in the first half of the year has not bottomed out.

The new designs, the measures taken at SAMES and Thesys and the transition strategy should facilitate the expansion of the customer base and improve the market position. As SAMES and Thesys are being gradually transformed into becoming predominantly ASICs suppliers, they should be less affected by the market weakness encountered by the mass producers of chips. This should result in price stability and long-term improvement in margins in the coming years, as has been demonstrated by Austria Mikro Systeme in the past.

Conclusion

In these difficult market circumstances, and as we integrate SAMES and Thesys into the Group, we are grateful for your continued support and also extend our thanks to our business partners and particularly to our employees who are responsible for the success of the Group's development.

Managing Board of Directors

1997: More process technologies with more frequent departures of Austria Mikro Systeme Multi-Product Wafer Train ™

Austria Mikro Systeme International AG announces its new 1997 Multi-Product Wafer (MPW) Train Service Schedule for the 0.6 µm, 0.8 µm, 1.2 µm and 2 µm, in CMOS and 0.8 µm and 1.2 µm BiCMOS processes with a total of 24 runs. This capability, also known as shared silicon technology, allows the parallel processing of several devices on one wafer. Austria Mikro Systeme groups devices with compatible processes on a wafer and receives a tape input from the customer and delivers packaged parts. The company is believed to be one of the only semiconductor facilities in Europe currently handling and providing full in-house services for Multi-Product Wafer-Projects.

The benefits of MPW Train Service for customers is that circuit development charges are reduced by up to 50% due to reduced mask shop and fabrication costs. Span times are also kept at a minimum. Furthermore, MPWs allow at a very little extra cost the parallel study of design options which lowers the risk of redesign; the customer can evaluate the performance of several design options at once without lengthening development times.

Participation is guaranteed provided customer's data input arrives on time. The practical implementation of MPW runs at Austria Mikro Systeme has succeeded in the recent past due to significant efforts initiated in data preparation, mask making and assembly and the coordination of these activites. Austria Mikro Systeme successful installation of a MPW service was made possible because of the company's highly flexible and integrated facility which provides the necessary in-house mask making, data preparation, wafer fabrication, assembly and test.

For the "Wafer Train" schedules please contact your local sales office or Austria Mikro Systeme, Corporate Communications, Schloss Premstatten, 8141 Unterpremstätten, Austria

This text is available on the Internet Address: http://www.ams.co.at

News from Solid State Technology

July 1996

Sicilian volcano fab is only part of ST's aggressive expansion

SGS-Thomson Microelectronics (ST) of St. Genis, France, is now in the process of ramping up its new 0.35-micron, 8-inch fab in Catania, Sicily (Italy). By the end of the year, the semiconductor company expects to be producing 4-Mbit and 16-Mbit flash memories at the rate of 1000 wafers/week, despite the M5 fab's location at the base of an active volcano.

The project is only one of several new fabs and fab expansions under way at the company which is moving assertively to maintain its fabrication expertise as it sees rising revenues and profits (see table).

Catania is located at the base of Mount Etna, one of the few remaining active volcanoes in Europe. The mountain has had several eruptions within the last few years, and smoke issues constantly from its summit crater. Thus, the entire area is prone to seismic disturbances, and building the fab posed a major challenge.

*SGS-Thomson selected financial data (millions of US$)**

	1993	1994	1995
Revenues	2037	2645	3554
Net earnings	160.1	362.5	526.5
R&D	270.9	338.3	440.3
Capital expenditures	445.9	779.7	1,002

*Years ending Dec. 31

To ensure a vibration-free environment, the site of the new fab was the subject of extensive geological surveys before the building foundations were laid. The building's supporting structure is provided by 520 concrete pillars, tested with loads in excess of 2000 tons and driven 32 m into the ground. The new building is made up of three separate parts. The first part is a four-story building dedicated entirely to services for the Class 1 laboratory The second and largest block complies with the stringent vibration speafication required for sub-micron production.

The fab is completely isolated from adjacent buildings by flexible couplings. The floors and the walls of the underground areas are also separated from the pillar: supporting the laboratory by means of flexible couplings. Furthermore, all rotary motors are mounted on anti-vibration springs and the fluid speed in the facility's pipes is low in order to reduce vibrations. These measures were intended to give a level of vibration less than 3.15 microns/sec at a frequency between 4 and 100 Hz, complying with Class E specifications; early results indicate that even these requirements were surpassed.

The first floor houses the air-conditioning equipment, while the second floor contains the services for the equipment installed in the cleanroom. Meissner & Wurst of Stuttgart, Germany, was responsible for delivering and installing the cleanroom equipment. The air is changed 450 times/hour and 4,240,000 m^3 of air are recycled every hour while 202,000 m^3 of air is newly introduced. Air speed is 0.45m / sec, while temperature is $21 \pm 0.25^{o}C$ with a relative humidity of $40 \pm 1.5\%$. The maximum noise is 60 dBa and the power consumption is 22 MVA, about the same as an Italian town with 25,000 inhabitants.

The Class 1 laboratory is situated on the third floor. The sophisticated equipment will be installed in this area, and the fab might even be ready for 300-mm equipment. "For us, 300 mm is more an equipment problem than a building problem," says Pasquale Pistorio, the president and CEO of ST.

The third and tallest building is separated from the second building by flexible couplings. In the underground basement are the cloakrooms and services. The ground floor contains a reception area, where personnel must change into special shoes. On the first floor there is a Class 10 changing room of about 500 m^2. Above this there is the EWS department with an area of about 600 m^2 in Class 10. The fifth floor is dedicated to CAD/CAM and data processing and design, while the top floor is occupied by offices. In total the working area will be 15,950 m^2. Of this, 3500 m^2 is Class 1 cleanroom areas and 1800 m^2 are reserved for CAD, design and offices.

The first steppers were in place by the end of January Three Canon 3000i4 steppers have been installed, but 20 steppers of this type are on order. The first 200-mm wafer handling took place on Feb. 22, and plans call for production of about 50 developmental wafers /week by August. For September, ST's schedule calls for 100 wafer starts/week with a first output of 40 wafers/week. Target production for October, November and December is 400, 800, and 1000 wafer starts/week, respectively with 90, 340, and 680 wafers leaving the fab each week

The building capacity is 25,000 to 30,000 wafers/month, which might be reached in about three years, says Pistorio. He added that the Catania fab can be extended to 0.18micron geometries.

ST has been active in Catania since the early 1960s, and seems to be very happy with its decision to build the M5 fab in Sicily. Pistorio, a native of the area, noted, "The cost of engineering is very good. An engineer with three years of working experience costs us US$30,000 per year. This is higher than in Singapore, but it is still very good."

ST will not rest on its laurels when the Catania fab is completed. The firm is engaged in heavy capacity expansion and is making long-range plans for two additional fabs to come online late in the decade.

"One will be in Europe and one outside Europe," says Pistorio. "These plants will come to work in 1999 or later;" he explains, saying that they will use 200 mm wafers. Capacity has not been determined.

"Our objective is to be ready. And then we can accelerate or delay our plans to build a new fab. We have the concept of a modular capacity growth," said Pistorio. "We try to optimize three parameters of the decision: Access to the market, existence of know-how and competitiveness, which includes cost of labor and cost of energy."

The *Singapore Business Times* reported that ST, which already operates several facilities in Singapore, would build its non-European fab there, and rumors to that effect were circulating at Semicon/Singapore. Pistorio declined to comment.

In 1994, ST's 8-inch fab in Crolles, France, went into operation and in 1995 the company's Phoenix, AZ, fab started to ramp up. As well as the Catania plant, expansion work is under way at the fab in Agrate, Italy which is expected to be ready for operation in 1997. The new Agrate line will process 5000 200-mm wafer starts/week.

In late summer ground-brealang ceremonies for a 200-mm fab will take place. Heavy construction machinery is already on site in Rousset, France (close to Nice and Marseilles), where a 200-mm fab is being built for production in 1998.

Last year ST invested about $1 billion in new facilities, and Pistorio added, "We'll spend about the same amount this year." As ST has been reporting excellent sales within the last two fiscal years and also had its best quarter ever in 1Q96, it is likely that the company will spend even more on investments in the future.

Environmental research planned at new center

A new partnership between the National Science Foundation (NSF) and the Semiconductor Research Corp. *(SRC)* will produce a $10 million research center for Environmentally Benign Semiconductor Manufacturing.

The Center will be housed at the University of Arizona, and will be headed by Professor Farhang Shadman of the Department of Chemical and Environmental Engineering. Engineers and scientists from Arizona, the Massachusetts Institute of Technology, Stanford University, and the University of California Berkeley will work together to address the semiconductor industry's needs for a more environmentally friendly high-performance manufacturing process.

The center's funding is equally cooperative. NSF and SRC are each committing $1 million/year for five years, with $750,000 in start-up funds coming from Sematech.

The semiconductor industry is concerned about developing environmentally conscious high-performance manufacturing processes. Examples include reducing the large amount of ultrapure water needed to rinse and clean wafers, and minimizing the amount of energy required by wafer fabs. Another concern is the search for safe solvent alternatives to glycol ethers, used as a cleaning solvent.

The Industry's hope is that the center's students will become engineers capable of integrating environmentally conscious concepts up-front in the design of manufacturing processes. The center will work in partnership with semiconductor firms that will contribute to strategic plannig of research programs. Firms will interact with faculty and students in research and provide opportunities for student interns to learn the manufacturing process first-hand.

Donald L. Wollesen, director of technology and reliability engineering at Advanced Micro Devices, noted that students at the center will work on vital research and have the opportunity to network across technical disciplines. He added that graduates will have the experience of a well-rounded education and will be able to influence the future direction of the semiconductor Industry.

IZOBRAŽEVANJE O VAKUUMSKI TEHNIKI

Vse uporabnike vakuumske tehnike obveščamo, da so v letu 1996 predvideni naslednji strokovno izobraževalni tečaji:

VZDRŽEVANJE VAKUUMSKIH NAPRAV - 15. in 16. oktober 1996

Pod tem naslovom se obravnava predvsem tematika, ki jo srečujemo v tehniki grobega vakuuma. To je: delovanje, vzdrževanje in popravila rotacijskih črpalk, pregled in uporaba različnih črpalk, ventilov in drugih elementov, meritve vakuuma, hermetičnost in odkrivanje netesnosti v vakuumskih sistemih, materiali za popravila, tehnike čiščenja in spajanja; skupno 20 šolskih ur, od tega tretjina praktičnih prikazov in vaj.

Cena tečaja je **30.000 SIT**. Vsak tečajnik bo prejel tudi brošuro "Osnove vakuumske tehnike za vzdrževalce naprav" in potrdilo o opravljenem tečaju.

OSNOVE VAKUUMSKE TEHNIKE - 26.- 28. november 1996

Pri tem tečaju je večji poudarek na teoretičnem razumevanju snovi. Obravnavana so vsa, že prej omenjena področja in poleg tega še: pomen in razvoj vakuumske tehnike, fizikalne osnove, črpalke za visoki vakuum, tankoplastne in druge vakuumske tehnologije, čisti postopki, analize površin ter doziranje, čiščenje in preiskave plinov - skupno 26 šolskih ur z vajami in ogledom Inštituta.

Cena tečaja je **28.000 SIT**. Udeleženci prejmejo zbornik predavanj "Osnove vakuumske tehnike" in potrdilo o opravljenem tečaju.

Oba tečaja se pričneta ob 8.00 uri v knjižnici Inštituta za elektroniko in vakuumsko tehniko, Teslova 30, Ljubljana.

Prosimo interesente, da se informativno javijo čimprej, za dokončno potrdilo udeležbe pa velja kopija položnice o plačilu - najkasneje tri dni pred pričetkom tečaja na naslov:

Društvo za vakuumsko tehniko Slovenije,
Teslova 30
1111 Ljubljana

(štev. žiro računa: 50101-678-52240).

Prijave sprejema organizacijski odbor (Koller, Spruk, Mozetič, Nemanič), ki daje tudi vse dodatne informacije (tel. 061 126 45 84).

IN MEMORIAM Janko Colnar

Janko Colnar, 1921-1996

V začetku avgusta leta 1996 je v petinsedemdesetem letu starosti nenadoma preminil Janko Colnar.

Dolga leta je bil novinar glasila ISKRA, po upokojitvi leta 1984 pa je začel s tehničnim urejevanjem glasila "Informacije SSESD", oz. med leti 1986 in 1995 revije "Informacije MIDEM".

Janka Colnarja se bomo spominjali kot vestnega in požrtvovalnega sodelavca.

Uredniški odbor Informacije MIDEM

KOLEDAR PRIREDITEV

OCTOBER

02.10.-04.10.1996
ISSM'96 - 5th INTERNATIONAL SYMPOSIUM ON SEMICONDUCTOR MANUFACTURING
Tokyo, Japan
Info.: fax 81/4623-05572

06.10.-11.10.1996
SYMPOSIUM ON THIN FILM TRANSISTOR TECHNOLOGIES
San Antonio, TX, USA
Info.: +1 914 945 1144

07.10.-11.10.1996
SODOBNA ELEKTRONIKA '96
Ljubljana, Slovenija
Info.: + 386 61 17 35 385

09.-10.10.1996
EUROBOT '96 - 1st EUROMICRO WORKSHOP ON MOBILE ROBOTS
Kaiserslauten, Germany
Info.: +39 30 3715453

09.10.-10.10.1996
TEST '96
Birmingham, England
Info.: +44 171 837 8727

10.10.-11.10.1996
ISEP '96 - 5. MEDNARODNI SIMPOZIJ O ELEKTRONIKI V PROMETU
Ljubljana, Slovenija
Info.: +386 61 13 13 149

14.10.-18.10.1996
FLAT PANEL DISPLAYS TOPICAL CONFERENCE
Philadelphia, PA, USA
Info.: +212 248 0200

20.10.-25.10.1996
INTERNATIONAL TEST CONFERENCE '96
Washington DC, USA
Info.: +1 814 941 4666

NOVEMBER

03.11.1996
3rd EUROPIAN CONFERENCE ON MICROLECTRONICS AND THE ENVIRONMENT
London, England
Info.: +44 181 743 3106

04.11.-08.11.1996
INTERNATIONAL SYMPOSIUM ON THE INDUSTRIAL APPLICATIONS OF THE MOSSBAUER EFFECT
Johannesburg, South Africa
Info.: + 2711 716 4053

06.11.-08.11.1996
9th INTERNATIONAL SYMPOSIUM ON SYSTEM SYNTHESIS
La Jolla, CA, USA
Info.: +1 909 787 4710

11.11.-14.11.1996
SILITECH PRAGUE '96
Prague, Czech Republic
Info.: PO Box 45,170 01 Prague

12.11.1996
OXIDATION AND ISOLATION IN SEMICONDUCTOR TECHNOLOGY
Dresden, Germany
Info.: +49 89 90474 0

12.11.-13.11.1996
MEPTECH Micro Electronics Packaging Technology Symposium
Santa Clara, CA, USA
Info.: +1 415 390 8575

12.11.-14.11.1996
7th ANNUAL ADVANCED SEMICONDUCTOR MANUFACTURING CONFERENCE AND WORKSHOP
Cambridge, MA, USA
Info.: +1 415 940 6903

12.11.-15.11.1996
ELECTRONICA '96-17th INTERNATIONAL TRADE FAIR FOR COMPONENTS AND ASSEMBLIES IN ELECTRONICS
Munich, Germany
Info.: +49 89 51070

18.11.-20.11.1996
2nd INTERNATIONAL CONFERENCE ON THE SCIENCE AND TECHNOLOGY OF DISPLAY PHOSPHORS
San Diego, CA, USA
Info.: +1 212 620 3377

20.11.-21.11.1996
INSTRUMENTATION
Southampton, England
Info.: + 44 171 417 7400

DECEMBER

02.12.-06.12.1996
FALL MEETING OF THE MATERIALS RESEARCH SOCIETY IN CONJUCTION WITH ICEM'96
Boston, MA, USA
Info.: +1 412 367 3003

08.12.-11.12.1996
1996 IEEE INTERNATIONAL ELECTRON DEVICES MEETING (IEDM)
San Francisco, CA, USA
Info.: +1 301 527 0900

09.12.-10.12.1996
13th ANNUAL FLAT INFORMATION DISPLAYS CONFERENCE
San Jose, CA, USA
Info.: +1 408 448 4440

NAVODILA AVTORJEM

Informacije MIDEM je znanstveno-strokovno-društvena publikacija Strokovnega društva za mikroelektroniko, elektronske sestavne dele in materiale - MIDEM. Časopis objavlja prispevke do-mačih in tujih avtorjev, še posebej članov MIDEM, s področja mikroelektronike, elektron-skih sestavnih delov in materialov, ki so lahko:

izvirni znanstveni članki, predhodna sporočila, pregledni članki, razprave z znanstvenih in strokovnih posvetovanj in strokovni članki.

Članki bodo recenzirani.

Časopis objavlja tudi novice iz stroke, vesti iz delovnih organizacij, inštitutov in fakultet, ob-vestila o akcijah društva MIDEM in njegovih članov ter druge relevantne prispevke.

Strokovni prispevki morajo biti pripravljeni na naslednji način

1. Naslov dela, imena in priimki avtorjev brez titul.
2. Ključne besede in povzetek (največ 250 besed).
3. Naslov dela v angleščini.
4. Ključne besede v angleščini (Key words) in podaljšani povzetek (Extended Ab-stract) v angleščini.
5. Uvod, glavni del, zaključek, zahvale, do-datki in literatura.
6. Imena in priimki avtorjev, titule in naslovi delovnih organizacij, v katerih so zapo-sleni ter tel./Fax/Email podatki.

Ostala splošna navodila

1. V članku je potrebno uporabljati SI sistem enot oz. v oklepaju navesti alternativne enote.
2. Risbe je potrebno izdelati s tušem na pavs ali belem papirju. Širina risb naj bo do 7.5 oz.15 cm. Vsaka risba, tabela ali foto-grafija naj ima številko in podnapis, ki označuje njeno vsebino. Risb, tabel in fotografij ni potrebno lepiti med tekst, am-pak jih je potrebno ločeno priložiti članku. V tekstu je potrebno označiti mesto, kjer jih je potrebno vstaviti.
3. Delo je lahko napisano in bo objavljeno v kateremkoli bivšem jugoslovanskem jezi-ku v latinici in v angleščini.

Uredniški odbor ne bo sprejel strokovnih člankov, ki ne bodo poslani v dveh izvodih.

Avtorji, ki pripravljajo besedilo v urejevalnikih besedil, lahko pošljejo zapis datoteke na disketi (5.25" /1.2 MB/ ali 3.5" /1.44 MB/) v formatih ASCII, wordstar (3.4, 4.0), wordper-fect, word, ker bo besedilo oblikovano v pro-gramu Ventura 5.0. Grafične datoteke so lahko v formatu TIFF, PCX, GEM ali HPL, SLD (Auto-CAD).

Avtorji so v celoti odgovorni za vsebino objav-ljenega sestavka. Rokopisov ne vračamo.

Rokopise pošljite na naslov

Uredništvo Informacije MIDEM
Elektrotehniška zveza Slovenije
Dunajska 10, 61000 Ljubljana

UPUTE AUTORIMA

Informacije MIDEM je znanstveno-stručno-društvena publikacija Stručnog dnrštva za mikroelektroniku, elektronske sestavne dije-love i materijale - MIDEM. Časopis objavljuje priloge domačih i stranih autora, naročito čla-nova MIDEM, s područja mikroelektronike, elektronskih sastavnih dijelova in materijala koji mogu biti:

izvomi znanstveni članci, predhodna priop-čenja, pregledni članci, izlaganja sa znanstve-nih i stručnih skupova i stručni članci.

Članci će biti recenzirani.

Časopis također objavljuje novosti iz struke, obavijesti iz radnih organizacija, instituta i fakulteta, obavijesti o akcijama društva MIDEM i njegovih članova i druge relevantne obavije-sti.

Stručni članci moraju biti pripremljeni kako slijedi

1. Naslov članka, imena i prezimena autora bez titula.
2. Ključne riječi i sažetak (najviše 250 riječi).
3. Naslov članka na engleskom jeziku.
4. Ključne riječi na engleskom jeziku (Key Words) i produženi sažetak (Extended Abstract) na engleskom jeziku.
5. Uvod, glavni dio, zaključni dio, zahvale, dodaci i literatura.
6. Imena i prezimena autora, titule i naslovi institucija u kojima su zaposleni. sa tel/Fax/Email podacima.

Ostale opšte upute

1. U prilogu treba upotrebljavati SI sistem jedinica od. u zagradi navesti alternativne jedinice.
2. Crteže treba izraditi tušem na pausu ili bijelom papiru. Širina crteža neka bude do 7.5 odnosno 15 cm. Svaki crtež, tablica ili fotogfafija treba imati broj i naziv koji označuje njen sadržaj. Crteže, tabele i fotografije nije potrebno lijepiti u tekst, već ih priložti odvojeno, a u tekstu samo naznačiti mjesto gdje dolaze.
3. Rad može biti pisan i biti će objavljen na bilo kojem od bivših jugoslavenskih jezika u latinici i na engleskom jeziku.

Autori mogu poslati radove na disketama (5.25" /1.2 MB/ ili 3.5" /1.44 MB/) u formatima tekst procesora ASCII, wordstar (3.4. i 4.0), word, wordperfect pošto će biti tekst dalje obraden u Venturi 5.0. Grafičke datoteke mogu biti u formatu TIFF, PCX, GEM ili HPL, SLD (AutoCAD).

Urednički odbor će odbiti sve radove koji neče biti poslani u dva primjerka.

Za sadržaj članaka autori odgovaraju u pot-punosti. Rukopisi se ne vračaju.

Rukopise šaljite na adresu:

Uredništvo Informacije MIDEM
Elektrotehniška zveza Slovenije
Dunajska 10, 61000 Ljubljana
Slovenija

INFORMATION FOR CONTRIBUTORS

Informacije MIDEM is professional-scientific-social publication of Professional Society for Microelectronics, Electronic Components and Materials. In the Journal contributions of do-mestic and foreign authors, especially mem-bers of MIDEM, are published covering field of microelectronics, electronic components and materials. These contributions may be:

original scientific papers, preliminary commu-nications, reviews, conference papers and professional papers.

All manuscripts are subject to reviews.

Scientific news, news from the companies, institutes and universities, reports on actions of MIDEM Society and its members as well as other relevant contributions are also welcome. Each contribution should include the following specific components:

1. Title of the paper and authors' names.
2. Key Words and Abstract (not more than 250 words).
3. Introduction, main text, conclusion, ac-knowledgements, appendix and refer-ences.
4. Authors' names, titles and complete com-pany or institution address including Tel./Fax/Email.

General information

1. Authors should use SI units and provide alternative units in parentheses wherever necessary.
2. Illustrations should be in black on white or tracing paper. Their width should be up to 7.5 or 15 cm. Each illustration, table or photograph should be numbered and with legend added. Illustrations, tables and photographs are not to be placed into the text but added separately. Hower, their position in the text should be dearly marked.
3. Contributions may be written and will be published in any former Yugoslav lan-guage and in English.

Authors may send their files on formatted disk-ettes (5.25" /1.2 MB/ or 3.5" /1.44 MB/) in ASCII, WordStar (3.4 or 4.0), Word, WordPer-fect as text will be formatted in Ventura 5.0. Graphics may be in TIFF, PCX, GEM or HPL, SLD (AutoCAD) formats.

Papers will not be accepted unless two copies are received.

Authors are fully responsible for the content of the paper. Manuscripts are not returned.

Contributions are to be sent to the address:

Uredništvo Informacije MIDEM
Elektrotehniška zveza Slovenije
Dunajska 10, 61000 Ljubljana,
Slovenia